B-BAND GALAXY COUNTS AS A FUNCTION OF MORPHOLOGICAL TYPE

by

Seth H. Cohen

A Dissertation Presented in Partial Fulfillment
of the Requirements for the Degree
Doctor of Philosophy

ARIZONA STATE UNIVERSITY

May 2003

B-BAND GALAXY COUNTS AS A FUNCTION OF

MORPHOLOGICAL TYPE

by

Seth H. Cohen

has been approved

May 2003

APPROVED:

_____, Chair

_____

_____

_____

_____

Supervisory Committee

ACCEPTED:

_____

Department Chair

_____

Dean, Graduate College

ABSTRACT

In the past decade, the Hubble Space Telescope (HST) has provided spectacular images of the most distant galaxies. This dissertation provides a foundation for understanding the nature of these faint galaxies. Historically, attempts to model the faint galaxy number counts have suggested that the luminosities of galaxies evolve over cosmic time, with the caveat that the models also underpredicted the bright end of the counts. This "normalization problem," as it became known, is investigated here.

The distribution of morphological types (ellipticals, spirals, irregulars) in the deepest HST fields indicated that, in contrast to the local Universe, the majority of the faintest galaxies are irregulars. This led to speculation that this normalization problem was type-dependent. The first part of this dissertation is a large HST survey aimed at addressing this issue. The results of this thirty field survey suggested that the normalization problem was larger for the irregulars and that these galaxies also showed the strongest signature of luminosity evolution. It was also clear that more data was needed to firmly draw detailed conclusions.

The second part of the dissertation utilizes data from ground-based telescopes and is complementary to the HST work. This data allowed the galaxy counts as a function of morphological type to be extended to brighter flux levels, where the galaxies being studied are far enough away so that they are outside the local large-scale structure, but at low enough redshifts such that the effects of evolution will

be minimized. The data, along with newly computed models, indicated that there really was not a normalization problem at all. This allowed for a simple study of the luminosity evolution of the faintest galaxies as seen by *HST*. The indication is that all types are evolving, with the irregulars showing the strongest amount of evolution. This claim is strengthened by the understanding of the normalization problem, or lack thereof, given in this dissertation. The study concludes with the exciting prospects for improving both the models and the data for this type of research with upcoming *HST* surveys.

This dissertation is dedicated to my mother, Yvonne Cohen, for her unconditional love and support.

ACKNOWLEDGEMENTS

First and foremost, I thank my parents, Fred and Yvonne Cohen, for supporting me along the way. I thank my brother, Dan Cohen, for helping to set up the computer on which most of this dissertation was written. I also appreciate the support from the rest of my family over the years.

I thank my advisor, Rogier Windhorst, for pushing me to do my best and teaching me about the way astronomy is really done. Stephen Odewahn really served as a secondary advisor to me. He taught me many of the technical details of how to study galaxies the right way and was a pleasure to work with. I began my first research project and taught with Susan Wyckoff, who also gave me a new perspective on science education.

I thank my whole committee for doing their part to make this process worthwhile. They are R. Windhost, S. Odewahn, S. Wyckoff, R. Chamberlin, and R. Acharya, who put off his retirement, partly to see me finish.

I gratefully thank my fellow graduate students who provided both emotional support and taught me many of the important skills that I learned along the way. In no particular order, they are Catrina Hamilton, Carl Covatto, Brian Moore, Sam Pascarelle, Roger Rouse, Haojing Yan, Jason Aufdenberg, Karen Vanlandingham, Greg Schwarz, Lisa Will, Heidi Van Tassell, Julie Lorentzen, Violet Taylor, Luis Echevarria, Kevin Healy and Claudia Chiarenza.

Besides those already mentioned, I enjoyed working with many other excellent

astronomers along the way, including Simon Driver, Bill Keel, Ian Waddington, Paul Scowen, and Rolf Jansen.

I also thank Arizona State University and the Department of Physics and Astronomy for their hospitality during my ten year journey through this process.

Finally, I would also like to thank the ASU NASA Space Grant for providing me with a Graduate Research Fellowship over the course of many semesters. This research was also funded by NASA grants GO.5985.01.94A, GO.6609.01.95A, AR.6385.01.95A, AR.7534.02.96A & AR.9528.01A (to RAW & SCO) from STScI, which is operated by AURA, Inc., under NASA contract NAS5-26555.

TABLE OF CONTENTS

CHAPTER Page

PART III: On The Normalization Problem of the Faint Galaxy Counts

PART IV: Conclusions

LIST OF TABLES

LIST OF FIGURES

PART I

BACKGROUND AND METHODOLOGY

CHAPTER 1

Overview

A brief historical overview of the study of galaxy morphology and galaxy counts is presented. This is followed by a description of the the problem to be addressed, mainly the understanding of the faint galaxy counts as a function of morphological type. A summary of the major parts of the data analysis and methodology is also given.

CHAPTER 2

Introduction

Upon the discovery of any patterns in nature, there is the natural tendency to develop some classification system in order to characterize what has been discovered and to relate it to other known patterns or physical laws. This is also true for galaxies, which were discovered because they appeared different than stars in early observations of the sky. Galaxies were originally referred to as "nebulae," due to their clould-like and fuzzy appearance. In fact, even after Hubble (1922) discovered that M31 (the Andromeda Galaxy) was external to the Milky Way, he still used the term nebulae to refer to what today would be called galaxies. These fuzzy blobs showed great variation in their appearance (later termed morphology) and apparent brightness. The two simplest observational tests to perform are to count the number of each type of galaxy, or to try and determine the distribution of apparent brightnesses and then see what trends appear in this data. This basic exercise is the foundation of the work presented here. Galaxies are classified according to their visual appearance and then counted as a function of this morphological type and apparent brightness.

2.1 Morphological Galaxy Classification

The images of galaxies are perhaps some of the most beautiful and intriguing astronomical images that exist. Some appear smooth and elliptical in shape, while others appear to have beautiful spiral structure of several varieties. Still others appear to lack either of these characteristics. Many classification schemes have been developed over the years. The most well known of these is now known as the Hubble classification scheme and is described in Hubble (1936). Here we adopt the Revised Hubble System (RHS; de Vaucouleurs 1959), which is an extension Hubble's original scheme that was meant to incorporate more of the details seen in the galaxies, such as rings and the degree of spiral structure, and whether or not the galaxy had a visible bar. As these classification schemes are fairly well-known, we refer the reader to these two references for more details. An important point to note is that what people commonly refer to as the Hubble type (*i.e.*, E, Sa, Sb, Sc, Sd, Irr) forms the "stage" axis of the RHS. The other two axes of the RHS are called the "family" and "variety," and indicate the presence, or lack thereof, of bars or rings, respectively.

2.2 Galaxy Counts and the Faint Blue Galaxy Problem

In the many years since their discovery, galaxies have been studied in great detail both individually and as a population as a whole. A fundamental advance in this field was the discovery that their distances could be measured based on the shifts of

their spectral lines (called redshifts), now known to be due to the expansion of the Universe. Once their distance is known, this fact can be combined with their apparent magnitude (*i.e.*, brightness) to determine their intrinsic luminosity. In Euclidean space, the apparent brightness of an object varies as the inverse square of its distance from the observer. In an expanding universe, however, the relation between apparent brightness and distance is slightly more complicated.

This led to several redshift surveys, where hundreds (and later thousands) of galaxies were selected from photographic catalogs, usually from blue sensitive emulsions, and their redshifts were measured with spectrometers on large optical telescopes. Perhaps one of the most comprehensive (*i.e.*, largest) and important redshift surveys was the Center for Astrophysics Redshift Survey, which showed that nearby galaxies are not randomly distributed in space, but rather are grouped in clusters and filaments (Davis et al. 1982; de Lapparent, Geller, & Huchra 1986). Once the distances and luminosities of the galaxies are known, one can compute the luminosity function (LF) of the galaxies. This is simply a measure of the number of galaxies per unit luminosity per unit volume.

As the size and quality of the telescopes and the imaging instruments increased, so did the power to observe faint galaxies. Whereas the galaxies in the aforementioned redshift surveys may be as faint as $B \lesssim 15 - 16$ mag, in the mid 1980's galaxies were observed as faint as $B = 27$ mag (*e.g.*, Tyson 1988) using charge coupled devices (CCD's) as detector. From this data, faint B-band galaxy counts were computed. At

some distance (and hence faint flux level), there should be no or few galaxies seen because the Universe is not old enough for the typical stars that constitute a galaxy to have formed. There is also the problem that, if there are too many faint galaxies, the integrated sky brightness of the Universe would be infinitely bright (Olber's paradox). Therefore, attempts were made to model the observed galaxy number counts using what was known about the nearby Universe. Could a model of this variety show that these distant galaxies were similar to the ones we observe nearby, or is there a fundamental difference? How do the various types of galaxies form, and do they all evolve in the same way as one another, if at all?

The basic method of modeling the faint counts is to use the measured local LF to describe the luminosity distribution at every redshift, combine this with a mathematical description of the Universe's geometry, and integrate this over redshift to get the predicted distribution of galaxies in apparent magnitude. The results of this, along with the simplest assumptions, showed that there was an excess in the observed galaxy counts over the model predictions for all magnitudes fainter than $B \gtrsim 20-22$ mag. As these observations were generally performed at blue wavelengths, this issue became known as the faint blue galaxy (FBG) problem and the excess counts over the models is known as the FBG excess. And so began the industry of trying to explain this apparent difference between the relative numbers of observed local and distant galaxies. Was this FBG excess simply due to luminosity evolution? Were galaxies merging more often in the past? Was there some bias in the local LF, because we

happen to live in an underdense region of the Universe? Could the FBG excess all be due to selection effects in the determination of the local LF? Comprehensive reviews of the FBG population are given by Koo & Kron (1992) and Ellis (1997).

2.3 Toward a Solution

Fundamental advances were made when the redshifts of these faint galaxies were measured. Somewhat surprisingly, the faint blue galaxies were not at as high a redshift as one would expect. In fact, at $B \simeq 24 - 25$ mag, the median redshift is only $z \simeq 0.6 - 0.7$ (Koo & Kron 1992). Broadhurst et al. (1988) used a redshift survey to show that simple luminosity evolution alone cannnot explain the excess, and that many of the spectra of these FBG's showed evidence of strong star-formation, which lead to the conclusion that the steep slope in the faint counts was due to lower luminosity galaxies undergoing brief bursts of star-formation. More details of these types of studies are given in the introduction to Part II.

The next important breakthrough came with the Hubble Space Telescope (HST) with its subarcsecond resolution. Typically, turbulence in the atmosphere (called seeing) limits the resolution of ground-based observations to approximately $1''.0$ FWHM. The *HST* observations showed that the median sizes of the faintest $B \lesssim 25$ mag galaxies were about $0''.2 - 0''.3$ (Driver, Windhorst & Griffiths 1995). This made HST the only way to study the morphology of the faintest galaxies. The number of papers published on faint galaxy morphology are far too many to list, but this has been one

of the main uses of this telescope (e.g., Driver et al. 1995a; Glazebrook et al. 1995; Abraham et al. 1996a; Odewahn et al. 1996; Ratnatunga, Griffiths & Ostrander 1999, etc). The important result found with *HST* is that the galaxies responsible for the FBG excess were of late or peculiar type (Driver et al. 1995a; Driver, Windhorst & Griffiths 1995; Glazebrook et al. 1995). These authors showed that the counts are in excess of the *non-evolving* LF model predictions, regardless of adopted cosmology, with the caveat that the local luminosity function has to be (arbitrarily) renormalized by a factor of up to 2 at a flux level of $b_J = 18$ mag.

It is this renormalization issue that is investigated in the following body of work. In particular, we use data from various sources to investigate whether this renormalization is a function of galaxy type. We provide the first galaxy counts with morphological information near the normalization point at $b_J \simeq 18$ mag, which puts a firm constraint on the issue, if it is really an issue at all. We build on the work of Odewahn et al. (1996), who investigated the application of artificial neural networks on galaxy classifications in the northern Hubble Deep Field (HDF-N), and in the deep HST field surrounding the weak radio galaxy 53W002. Among other things,this work showed that the area covered by these extremely deep surveys was insufficient to provide statistically significant galaxy counts for $B \lesssim 22 - 23$ mag. Here, we first present the results and analysis of the HST B-band Parallel Survey, which extended the galaxy counts as a function of morphological type, and when combined with the deeper surveys, covered the flux range of $19 \lesssim b_J \lesssim 27$ mag. This data

is then combined with ground-based data from several sources, along with our own visual classifications. The total set shows the B-band galaxy counts as a function of morphological type over the range $15 \lesssim b_J \lesssim 27$ mag, which allows the normalization problem to be firmly addressed.

CHAPTER 3

Data Reduction Methods

This section is an explanation of the major data reduction steps that were necessary to process the data in this work. All the work was begun from fully reduced and calibrated digital images.

3.1 HST WFPC2 Image Stacking

Data from the *HST WFPC2* is delivered as biased subtracted and flat-fielded images with known photometric zeropoints. Each exposure is littered with cosmic rays (CR's) due to the telescope being above the Earth's atmosphere. The atmosphere shields ground-based observations from most of these CR's. The observer is then left to either use existing tools or develop their own to remove these CR's in a statistical way. The method is based on the fact that successive exposures of the same patch of sky should not have CR hits at the same pixel locations, since these are random events. For four or more exposures, a simple clipping algorithm is usually sufficient to remove these. For fewer exposures, it is less straightforward, as the seemingly small probabilty for multiple exposures to be hit by a CR at the same pixel is countered by the fact that there are a large number of CR's.

The algorithm used here was developed for this data in collaboration with S.

Pascarelle (see also Pascarelle, Windhorst & Keel 1998). It is called *stcombine* and was written using the Interactive Data Language (IDL), along the IDL Astronomy User's Library (Landsman 1993). The basic steps are as follows. First of all, each WFPC2 observation consists of data from four individual CCD's, and we refer to these as chips. One of the chips, called the Planetary Camera chip or PC1, has twice the spatial pixel sampling of the other three Wide-Field chips (WF2, WF3, WF4). Each of the chips is handled separately. The combination of successive images of the same patch of sky is called "stacking." The process requires that one has already used the measured centroids of bright and compact objects to spatially register the images.

First, all of the images to be stacked are scaled to the average exposure time, which is a multiplicative operation because CCD's are detectors with responses that are linear in time. Next, the sky is determined for each image. The sky is simply the most frequently occuring occuring DN value, also known as the mode. It is crucial to properly determine this value, since it is easily corrupted by the CR's we are trying to remove, as well as by the objects of interest, both of which cause the distribution of pixel values to be skewed towards the positive DN side. The mode is determined by computing the histogram of all the pixel-values, and then fitting a polynomial to a range of values near the median. The location of this peak of the fitted polynomial is then taken as the mode, which we call the "sky" or sky-background. After the sky is determined from each image, a constant is subtracted so that all images will

have the same sky. This is an additive correction, because the differing sky is due to a combination of varying Zodiacal background or light reflected from the Earth's limb. In fact, the data used here was often taken during Continuous Viewing Zone (CVZ) orbits, during which *HST* necessarily points nearer to the Earth's limb than during a typical *HST* exposure. The benefit of using CVZ orbits is that they have the longest possible exposure times. After making this background correction, the skies were remeasured to verify that the process was properly executed.

The next step is to repair pixels that have anomalously low values, either due to bad pixels or CCD charge traps. These pixels were located by subtracting the image from a 3×3 pixel median smoothed version of itself. All pixel locations in the difference image that differed by more than 3.5σ of the local sky in the original image were replaced by a median of the eight surrounding pixels. The σ used here is computed on a pixel by pixel bases from:

$$\sigma = \sqrt{DN \times g + RN^2 + DK \times t}/g \tag{3.1}$$

where DN is the number of ADU in a given pixel, $g = 7.0\ e^-/ADU$ is the WFPC2 detector gain, $RN = 5.3\ e^-$ is the WFPC2 read-noise, $DK = 0.0033\ e^-/sec$ is the WFPC2 dark current rate, and t is the exposure time in seconds.

After these three initial steps are completed, the images are ready to be stacked in order to clean out the CR's. For N registered images, the IDL routine performs the following operations at *each* pixel (x,y) location *separately*. It creates a list of N

pixel values which is then sorted from the lowest to the highest value for each pixel. A Poisson noise model based on the known CCD characteristics, using the above equation, is then used to determine which pixel values should and should not be included in the average. Starting with the *lowest* value of each pixel, each successive value is checked to see if it is within 2.5 σ of the current average value. This way, higher pixel values that are likely due to cosmic rays are rejected (at the 2.5 σ level). This process is then repeated for each pixel. This rejection algorithm will fail for the two orbit cases when a pixel is hit by a CR in *both* images, which we measured to occur about 0.3% of the time, or for about ~ 2000 pixels that were affected by CR's in both full-orbit WFPC2 CCD exposures.

3.2 Selecting and Measuring Galaxies from Images

With perhaps the exception of the deepest *HST* surveys, our goal was to study the brighter galaxies from each of the particular surveys incorporated into this work, as we were most interested in galaxies for which a reliable morphological classification is possible. This means that our selection criteria are somewhat on the conservative side. Objects are selected by how much they standout relative to the background. No matter what algorithm is applied, this is necessarily based on surface brightness, which is the astronomical term for flux per unit area. This, and, in general, all object selection is therefore biased by the selection criteria that are used, as below some level objects will be missed. This must be accounted for in any subsequent analysis.

All our objects were selected from the digital images using a freely available software package called *SExtractor* (Bertin & Arnouts 1996). In all the surveys studied here, with one exception, two important parameters dictated the selection of objects (stars and galaxies). The first requirement was that the objects must be 2.5σ above the local sky-background, where sigma is the measured local *RMS* variation of the background. The second value that is specified is the minimum number of connected pixels that also satisfy the first requirement. This minimum number of pixels was different for the different surveys, because it should depend on both the pixel scale and the number of individual pixels per resolution element (or FWHM). For the B-band Parallel Survey, where there were some remnant CR's, this was taken to be large enough so as to minimize false detections. Following this, we made a second cut to prune out objects that were too small by selecting a minimum area requirement to make it into the final catalog. Note that this minimum number is a different criteria than the minimum number of connected pixels. An object may have enough pixels above the threshold to be intially selected, but there are more pixels out in the wings of the objects that are measured, but that are less than 2.5σ above the sky. In other words, there is a measurement threshold that is lower than the detection threshold. For the *HST* data, this was set to the area of the minimum number of connected pixels used for object detection, and for the ground-based surveys it was set to the approximate area of a circle with a diameter equal to the FWHM of the measured seeing disk.

Once a catalog of this type is determined, our own in house software, *LMORPHO* (or its predecessor *MORPHO*; Odewahn et al. 1996, 2002; Cohen et al. 2003), was used to perform the final photometry of the objects. The first step is to visually inspect the catalog by displaying the outer isophotes of the galaxies on an image display tool on the computer screen. This allowed for improper centering or deblending to be corrected manually, and even to add missed objects or remove objects that were clearly image defects. It is extremely important to emphasize that this is a crucial step no matter what type of data was involved. It was clearly necessary for both the *HST* data (with $0\farcs05$ FWHM in the B-band), as well as the $1\farcs5$ FWHM ground-based data. This is because no deblending algorithm can work perfectly on all scales, and because "clumpy" objects are not always detected properly. Also, the diffraction spikes, wings, and ghost images around bright stars, as well as saturated pixels and image edges, will also cause missed or corrupted detections.

Once the position and shape information for each object is verified or corrected, individual sub-images are cut for each object that we wish to measure with our code. These are called "stamps" because they resemble postage stamps with the image of a single object in their centers. These stamps are then passed through the photometry subroutine of *LMORPHO*, which measures a vast array of galaxy photometric parameters, such as the azimuthally averaged radial surface-brightness profile, several types of magnitudes, sizes and light concentration indices. The photometry routine uses the *SExtractor* parameters as a starting point for the centroid, position angle,

ellipticity, and magnitude determinations, but iteratively redetermines these with its own algorithms. Afterwards, the user can graphically inspect each measurement to verify that the program did not get confused by other nearby objects that happened to be in that stamp. An improvement was made to this in early 2002, where all the objects on each stamp were flagged in a separate file for each stamp, and the number of objects that had to be manually repaired at this later step was decreased by an order of magnitude. Note that the extra objects remained on the stamp, but their locations and sizes were given to the *LMORPHO* photometry program, so that it could essentially ignore them. This will allow for possibly more sophisticated algorithms, such as simultaneously fitting each potentially contaminating object and subtracting them from the image, to be applied to the stamps in the future. For the record, the *LMORPHO* magnitude that we used here is called "magTOTell_G," which is the magnitude measure in an elliptical aperture that is optimally determined, based on the signal-to-noise ratio of the local sky.

3.3 Automated Galaxy Classification

In order to provide a systematic and quantitative measure of a galaxy's morphology, a machine based classifier was used in our HST work. A method such as this is meant to avoid the inherent bias of human classifiers, and therefore provides as objective a classification as possible. We employed an artificial neural network (ANN) classifier, based on parameters measured from the galaxy's elliptically averaged radial

surface brightness profile. The mathematical description of the method is given by Odewahn et al. (2002) and will not be reproduced here, because we used it as an established tool, and the current document is not a plausibility study of this tool, but rather an application of it. A thorough discussion of galaxy classification methods is also given by Bazell (2000).

Schematically, the way the ANN works is based on a set of known inputs (here SB-profile parameters) and their desired outputs (here a galaxy T–type). This is known as a training set. The training set here was created by the mean types that four human classifiers assigned to a set of a few hundred galaxies that they classified visually from HST images. The mean type was used so as to remove any biases or accidental errors of the individual classifiers. This training set is then used to train or teach the ANN to assign the proper output for a given input vector. The specific ANN's employed here (Odewahn et al. 1996; Cohen et al. 2003) assign a galaxy stage value on the 16-step Revised Hubble System. The typical errors are $2-3$ steps (Odewahn et al. 1996), and therefore the results were binned down to three general morphological classes. This is also about the same error expected from human classifiers (*e.g.*, Naim et al. 1995), but it is much more efficient to have the computer assign a type for a large number of objects, than for a person to look at every galaxy individually. The resulting T–types are in the range $-7 \leq T < -0.5$ for objects designated as "E/S0" galaxies, $-0.5 \leq T < 5.5$ for "Sabc" galaxies, and $5.5 \leq T < 12$ for "Sd/Irr" galaxies. We also interchangeably refer to these as early-,

mid-, and late-types or ellipticals, spirals, and irregulars, respectively.

There are three important points to make here about this application of neural network galaxy classification. The first is that it is fully *quantitative* and systematic (ie., reproducible), but it is also inherently non-linear. This last fact differentiates it from simple linear cuts in a single or a series of two dimensional parameter spaces (cf., Abraham et al. 1996a,b) or bulge-disk decomposition (Marleau & Simard 1998), which is model dependent. All of these methods produce similar quality results, but are fundamentally different. Secondly, this is a one dimensional technique and therefore not a true measure of the galaxy morphology, which is a description of the two-dimensional appearance of a galaxy. A first step towards a 2–D approach was provided by Odewahn et al. (2002), who used novel mathematical techniques to create ANN inputs for finding bars in galaxies. Lastly, some have questioned the usefulness of using Hubble types at all. This is justified here, as it is the simplest thing to measure and, for nearby galaxies, Hubble types have been shown to correlate strongly and smoothly with, for example, color, gas content, and rotational velocity (Roberts & Haynes 1994). In an ideal world, one would rather measure these physical quantities directly, but this becomes increasingly difficult for fainter objects. In the absence of such spectrally dependent measurements, we chose a morphological analysis, with the implicit assumptions that these correlations potentially exist over cosmic time.

PART II

The *HST WFPC2 B*–Band Parallel Survey

CHAPTER 4

Overview

We present the results of the Hubble Space Telescope B–Band Parallel Survey (BBPS). It covers 0.0370 square degrees and consists of 31 shallow (4–6 orbit), randomly selected high latitude HST WFPC2 parallel fields with images taken in both the B (F450W) and I (F814W) filters. The goal of this survey is to morphologically classify the galaxies in a homogeneous manner and study galaxy properties as a function of type and B–band magnitude for $18 \lesssim b_J \lesssim 23.5$ mag. The full sample contains 1800 galaxies, 370 of which are brighter than the formal statistical completeness limit of $b_J \lesssim 23.5$ mag. The galaxies are selected from the B–band images and classified using an artificial neural network (ANN) galaxy classifier on the higher S/N I–band images. These provide (more) reliable types for $I \lesssim 24$ mag (or $b_J \lesssim 26$ mag), since these I–band classifications are less subject to the uncertain redshifted rest-frame UV morphology. The ANN classification depends on the shape of the surface brightness profile, but not on color. These results are combined with similar (deeper) studies in the Hubble Deep Field and the deep WFPC2 field surrounding the radio galaxy 53W002, for which galaxies have been classified to $b_J \lesssim 27$ mag.

The galaxy counts for the combined B–band selected samples show adequate statistics for a range $19 \lesssim b_J \lesssim 27$ mag, and are in good agreement with other studies

in the flux range where they overlap, while showing improved statistics at the bright end. The galaxies are subdivided into 3 morphological classes: early-types (E/S0), mid-types (Sabc) and late-types (Sd/Irr), and the B–band counts are presented for each class, as well as the total counts. The faint end of the counts is dominated by the irregular galaxies, which have a steep count slope of $d\log N/dm \approx 0.4$. These type dependent counts are compared to models based on local luminosity functions which include the effects of the cosmological constant, Ω_Λ. The whole BBPS sample, along with the two deeper fields, is used to delineate the general trends of effective radius and (B–I) color as function of both morphological type and apparent magnitude for $18 \lesssim b_J \lesssim 27$ mag. These properties are discussed in the context of recent redshift surveys. A possible explanation for the combined results is given in terms of the effects of Ω_Λ on the evolution of the merger rate in a hierarchical scenario.

CHAPTER 5

Introduction

Over the last 20 years, the galaxy counts conducted in the blue passband showed a remarkable excess of faint galaxies relative to model predictions. This excess is known as the faint blue galaxy (FBG) problem (see reviews by e.g., Koo & Kron 1992; Ellis 1997). Attempts to model the counts and color-distributions of these faint blue galaxies led to the conclusion that galaxies were more luminous and bluer in the recent past. In order to better understand the field galaxy population, faint galaxy redshift surveys were conducted which showed that standard luminosity evolution alone cannot account for the excess of FBG's (e.g., Broadhurst et al. 1988). Many of the faint galaxy spectra show evidence for strong star-formation, which led to the conclusion that the steep slope of the number counts is produced by lower luminosity galaxies undergoing short bursts of star-formation (Broadhurst et al. 1988).

More recently, many ground-based redshift surveys have been conducted to faint limits in order to further study this issue. The Canada-France Redshift Survey (hereafter CFRS; Lilly et al. 1995a) contains 591 galaxies brighter than $I_{AB} \lesssim 22.5$ mag. They have studied the redshifts, emission line strengths and ground based photometric properties. With this data, Lilly et al. (1995b) showed that the evolution in the luminosity function (LF) out to $z < 1$ was greater for the bluer galaxies than for the

redder ones (presumed to represent late and early morphological types, respectively). Recently, this work has been extended to include HST based morphology (Brinchmann et al. 1998; Lilly et al. 1998; Schade et al. 1999; Le Fèvre et al. 1999), as we will use for a larger number of field galaxies in this paper. The Canadian Network for Observational Cosmology cluster redshift survey (Yee, Ellingson & Carlberg 1996) aimed at studying galaxy clusters in the range $0.2 < z < 0.55$, and was complete for *field* galaxies with $z < 0.3$. This work has been extended to include more galaxies (Yee et al. 2000). For a better measurement of the local galaxy luminosity function, the 2dF Galaxy Redshift Survey will provide spectra and redshifts for 250,000 galaxies to a limit of $b_J = 19.45$ mag (herafter 2dFGRS; Colless et al. 2001). Within several years, the Sloan Digital Sky Survey will provide redshifts for $\sim 2 \times 10^6$ field galaxies to r'=18.0 mag or $b_J \lesssim 19$ mag (hereafter SDSS; Gunn et al. 1998; Blanton et al. 2001). These surveys provide very significant spectroscopic coverage of relatively nearby galaxies. However, as we will show in this paper, the median scale-lengths of galaxies at $b_J \gtrsim 19$ mag is $r_e \lesssim 1\farcs0$, and rapidly decreases at fainter magnitudes, so that reliable morphological information for faint galaxies ($b_J \gtrsim 19 - 20$ mag) over wide fields is beyond the capabilities of ground-based facilities and has to be done from space.

The advent of high resolution space-based optical imaging opened the door for studying the sub-arcsecond properties of many types of astronomical objects (e.g., Driver et al. 1995a; Glazebrook et al. 1995; Abraham et al. 1996a; Odewahn et al.

1996, etc). In particular, the Hubble Space Telescope (HST) has proven very useful for studying the properties of faint, as well as distant galaxies. Most notably the Northern Hubble Deep Field (HDF–N, Williams et al. 1996) provided deep ($I \lesssim 29$ mag) imaging of a single field in the $UBVI$ filters at a resolution of better than $0\farcs1$ (actually $\sim 0\farcs06$ FWHM after *drizzling*). There have been many studies of faint galaxy morphology from this data set (e.g., Odewahn et al. 1996; Abraham et al. 1996b; van den Bergh et al. 1996; Driver et al. 1998; Marleau & Simard 1998). The HST Medium Deep Survey (MDS) covered a much larger area of sky, but to a lesser depth, and took advantage of HST's parallel observing mode to image many fields in mostly V and I (e.g., Ratnatunga, Griffiths & Ostrander 1999). This large data set has produced many studies (e.g., Driver, Windhorst & Griffiths 1995; Abraham et al. 1996a; Im et al. 1996; Roche et al. 1996; Im et al. 1999), including one that utilized the small fraction of the MDS data that was observed in the B–band (Roche et al. 1997).

The HST data allowed for the morphological properties of these faint field galaxies to be studied. One of the main discoveries was that most of the FBG excess is due to galaxies of irregular or peculiar types (Driver et al. 1995a; Driver, Windhorst & Griffiths 1995; Glazebrook et al. 1995). These authors showed that the counts are in excess of the *non-evolving* LF model predictions, regardless of adopted cosmology, with the caveat that the local luminosity function has to be (arbitrarily) re-normalized by a factor of up to 2 at a flux level of $b_j = 18$ mag. The justification

for this re-normalization is typically given as either due to: (1) local inhomogeneity (Marzke et al. 1994; Zucca et al. 1997); (2) photometric scale errors (Metcalfe, Fong & Shanks 1995); (3) rapid recent evolution in the galaxy population (Maddox et al. 1990); and/or (4) the probability that local surveys are biased against late-type low-SB galaxies in selection for spectroscopic follow-up. Nevertheless, it remains an unsatisfactory situation that an ad hoc correction is required to reconcile the local measures of the luminosity function of galaxies with galaxy counts as bright as $b_J = 19$ mags. For more details on this issue, see discussions in Driver, Windhorst & Griffiths (1995) and Marzke et al. (1998). It is therefore crucial to have good statistics, *with morphology* at this brighter flux level in the blue filter to attempt to explain, or perhaps even rule out, this apparently necessary normalization factor.

Further work on the evolutionary model predictions for faint field galaxies has produced conflicting results. Without being able to fully cover the literature on this topic here, we will try to present the flavor of the problem. The bright HDF–N galaxies were used to model what the distribution and appearance of the fainter HDF–N galaxies should look like assuming no-evolution (Bouwens, Broadhurst & Silk 1998a), as well as assuming different types/amounts of evolution (Bouwens, Broadhurst & Silk 1998b). Assuming that the 30 brightest HDF–N galaxies are a fair representation of the thousands of fainter ones, they showed that the no-evolution models could not simulate the observed properties of the population of the fainter galaxies (Bouwens, Broadhurst & Silk 1998a). It was then shown that pure luminosity evolution (PLE) models

fit the galaxy counts, but not the galaxy size distribution, and that dwarf augmented populations would not fit the counts (see also Babul & Ferguson 1996; Ferguson & Babul 1998). A model that does fit the data was that of "mass-conserving" density evolution (Bouwens, Broadhurst & Silk 1998b). These results should be viewed with caution, since the HDF–N was selected to be devoid of bright objects (Williams et al. 1996), which, compounded by the fact that galaxies are known to cluster, would logically lead to a general deficit of low- to intermediate-redshift galaxies in this field. Kauffmann, Charlot & White (1996) used the ground-based CFRS colors and redshifts to predict which galaxies are of early-types, and then showed that more than the standard amount of passive evolution was required by the data. It should be noted that the use of colors to determine morphology of distant galaxies was shown to be problematic within the same data set, when the HST morphologies were added, and no evolution of the space density of ellipticals was observed (Schade et al. 1999). Another study showed that in an open universe, the counts (in the Ub_Jr_kIK bands) and color and redshift distributions could be reasonably explained by pure luminosity evolution, but that number and luminosity evolution (NLE) would be required in an $\Omega = 1$ universe (Pozzetti, Bruzual & Zamorani 1996). In contrast, it was shown that PLE models that fit the number counts and redshift distributions cannot fit the observed $(B - K)$ color distribution regardless of chosen cosmology (He & Zhang 1998). This was due to the fact that all galaxies with $(B - K) > 5.5$ mag must be ellipticals, and the PLE models do not match the observed redshift distribution for

these red galaxies. These authors showed that number luminosity evolution better matched all the data that was considered (He & Zhang 1998). The luminosity functions of elliptical galaxies out to $z < 1.2$, with morphologies determined from the HST-MDS, were constructed and showed 1 ± 0.5 mag of luminosity evolution, and argued against strong number density evolution (Im et al. 1996). Therefore, it is reasonable to say that the issue of the amount or type (luminosity, density or some combination thereof) of evolution is not a solved problem, and is further compounded by our poor understanding of the LF normalization factor mentioned above.

Traditionally, galaxies have been classified visually by eye. The large number of galaxies that are observed today necessitated the development of automated, computer-based classification methods. Odewahn et al. (1996) used artificial neural network (ANN) classification in a seven-dimensional photometric parameter space to estimate galaxy stage values in the revised Hubble classification system (de Vaucouleurs 1959). Abraham et al. (1996a) used linear relationships between two parameters, asymmetry and central concentration. Marleau and Simard (1998) used a 2-dimensional bulge-disk decomposition to compare the ratio of bulge-to-total light to the types of Abraham et al. (1996a) and of van den Bergh et al. (1996). Though the results for a given galaxy may differ for any of these methods, the overall qualitative results are in reasonably good agreement.

Where do all these faint galaxy studies leave us? Currently, these HST surveys have yielded rather poor statistics for galaxy morphology in the magnitude range $b_J \simeq$

$18 - 24$ mag. Since the correspnding median scale-lengths of faint galaxies are $r_e \simeq 1''.0 - 0''.5$ in this magnitude range (see § 8.2 and figures below), we cannot get reliable galaxy morphology $b_J \simeq 18 - 24$ mag over wide fields from the ground. Hence, there remains a need for better statistics *and* good HST morphologies in the magnitude range of $18 \lesssim b_J \lesssim 24$ mag, where the earlier surveys have provided little statistics. Since the number of galaxies observed at a given magnitude is roughly proportional to the area surveyed, and since there are more faint galaxies than bright ones, ultra-deep surveys like the HDF–N and the field surrounding the weak radio galaxy 53W002 (Odewahn et al. 1996) have provided important information on galaxies fainter than $b_J \gtrsim 23$ mag. However, the statistics get increasingly sparse for brighter galaxies. The goals, therefore, of this paper are to survey a large number of HST fields in the B and I filters over a wide area to a lesser depth, and to study the properties of these brighter galaxies as a function of observed B–band brightness. This will help to fill in this new, but essential portion of parameter space and aid in the understanding of the faintest galaxies observed today.

The HST observations are described in § 6 and the data reduction and catalog generation are outlined in § 7. The results of this paper are presented in § 8 and discussed in § 9 in terms of other recent work in the field. We summarize the paper in § 10. For clarification of nomenclature, we refer to the observed radius of a galaxy containing half of the observed light as the effective radius (r_e), and this is discussed in § 8.2. Since the two deeper fields, HDF–N and 53W002, are essentially complete

past our classification limit at $b_J \lesssim 27$ mag (Odewahn et al. 1996), we shall group them together and refer to them as the B–band Deep Survey (BBDS), while the 31 shallower fields will be referred to as the B–band Parallel Survey (BBPS). We adopt $H_o = 65\ km\ s^{-1}\ Mpc^{-1}$ and a flat ($\Omega_M = 0.3, \Omega_\Lambda = 0.7$) cosmology throughout, except where otherwise noted.

CHAPTER 6

Observations

All data for this survey were taken with the Hubble Space Telescope using the Wide-Field and Planetary Camera 2 (WFPC2) in parallel mode during Cycles 6–7. Fields were randomly selected with the criteria that they be at high Galactic latitude ($\mid b^{II} \mid \geq 30^{\circ}$) and that they contain no bright SAO stars, RC3 galaxies or known Abell galaxy clusters. The data set consists of 31 fields, all selected to have low Galactic extinction, $A_B \leq 0.4$ mag (Burstein & Heiles 1982). The data are summarized in Table 6.1. Note that fields bb025 and bb026 were not used in the final analysis because they contained single I–band exposures that were inadequate for this survey.

Table 6.1: BBPS Data Summary

Field Name[1]	α_{2000} ($h\ m\ s$)	δ_{2000} ($^\circ\ '\ ''$)	$l^{(II)}$ (deg)	$b^{(II)}$ (deg)	A_B[2] (mag)	F450W[3,4]	F814W[3,4]	SB(b_J,lim)[5]	$b_{J,lim}$[6] (mag)	I_{lim}[5] (mag)
bb001[7]	12:50:11.981	+31:24:53.96	126.46593	+85.704507	0.025	11200(4)	5100(2)	24.6	24.75	23.75
bb002	01:07:13.836	+32:21:15.98	126.80099	−30.400644	0.169	4400(2)	5600(2)	24.1	24.25	24.25
bb003	00:20:13.606	+28:36:18.54	114.68943	−33.765055	0.125	4600(2)	5600(2)	24.2	24.75	23.75
bb004[7]	12:34:35.321	+07:44:52.51	290.51752	+70.212661	0.005	11200(4)	5500(2)	24.1	24.75	23.25
bb005	23:19:50.369	+08:05:59.64	87.49011	−48.367645	0.153	5600(2)	5600(2)	24.3	24.75	24.25
bb006	11:17:43.549	+44:18:09.89	164.38333	+64.541796	0.000	4800(2)	10500(3)	24.0	24.75	24.75
bb007	23:25:06.940	−12:15:02.39	65.03796	−64.892020	0.073	11600(4)	5800(2)	24.5	25.25	24.25
bb008	22:56:55.450	−36:35:17.19	4.40599	−64.031413	0.000	1900(2)	7500(3)	23.5	24.25	23.75
bb009	10:02:24.069	+28:50:05.65	200.15747	+52.838381	0.057	5600(2)	8400(3)	24.3	24.75	24.75
bb010	11:17:29.177	+18:12:37.26	230.40198	+66.615733	0.000	3500(2)	5400(2)	23.8	24.25	23.75
bb011	13:13:30.877	−19:26:31.27	310.07117	+43.123824	0.213	8400(3)	4100(2)	24.2	24.75	23.25
bb012	01:09:56.803	−02:27:02.22	133.89849	−64.930090	0.141	5600(2)	4700(2)	24.2	24.75	23.75
bb013	21:51:04.643	+28:43:48.64	81.76111	−19.377477	0.369	6000(2)	4200(2)	24.3	24.25	23.25
bb014	01:10:01.312	−02:24:28.94	133.92383	−64.882760	0.141	11200(4)	5500(2)	24.4	24.75	23.75
bb015[7]	12:36:12.756	+12:35:01.77	288.41154	+75.024854	0.125	7300(3)	2900(2)	24.2	24.75	23.75
bb016[7]	12:31:16.915	+12:28:06.02	284.09600	+74.600629	0.085	5600(2)	5600(2)	24.2	24.25	23.75
bb017	10:04:52.212	+05:14:59.54	234.22682	+44.750990	0.001	5400(2)	4600(2)	24.2	24.75	24.25
bb018[7]	12:25:31.456	+12:57:52.96	278.48442	+74.593150	0.109	7500(3)	2100(2)	24.3	24.75	23.25
bb019[7]	13:21:41.828	+28:53:29.83	49.48354	+83.094088	0.005	10900(4)	5400(2)	24.5	25.25	24.25
bb020	01:10:00.052	−02:27:30.75	133.93187	−64.933420	0.141	8400(3)	5000(2)	24.1	24.75	23.25
bb021	12:19:35.983	+47:23:10.10	137.96173	+68.801852	0.000	5800(2)	4500(2)	24.4	24.75	23.75
bb022	10:34:54.818	+39:45:57.58	180.01970	+59.085801	0.000	7700(3)	2800(2)	24.4	24.75	23.75
bb023	00:18:27.140	+16:21:16.09	111.55027	−45.787178	0.065	8400(3)	4700(2)	24.2	24.75	23.25
bb024[7]	12:23:29.779	+15:51:21.40	271.60958	+76.996802	0.037	5400(2)	5400(2)	24.3	24.75	23.75
bb025	21:07:32.081	−05:22:23.81	44.61967	−32.581289	0.241	2900(2)	700(1)	23.8	···	···
bb026	16:36:34.801	+82:34:11.34	115.71923	+31.066578	0.293	3200(2)	900(1)	24.0	···	···
bb027	10:24:38.286	+47:04:36.35	168.23496	+55.070087	0.000	5600(2)	3000(4)	24.3	24.75	23.75
bb028	14:17:43.542	+52:23:20.91	96.23854	+60.034761	0.000	6200(2)	4100(2)	24.5	25.25	23.75
bb029[7]	12:56:53.243	+22:06:43.94	317.08991	+84.833774	0.125	6000(2)	4300(2)	24.3	24.75	24.25
bb030	00:49:18.900	−27:52:42.31	334.92501	−89.114023	0.025	12200(4)	5600(2)	24.6	24.75	23.75
bb031	00:49:18.664	−27:52:03.10	335.35253	−89.122747	0.025	9900(3)	5800(2)	24.5	24.75	24.25

[1]These are the field names listed in the order the data was received. The original data can be obtained from the HST Archive search form.
[2]Galactic absorption A_B (in mag) from Burstein & Heiles (1982)
[3]Total integration times in seconds (number of exposures).
[4]There is a total of about 151 Parallel HST orbits in this data set.
[5]SB(b_J,lim) is the limiting surface brightness in b_J *mag arcsec*$^{-2}$ for a given field averaged over the 3 WF detectors.
[6]Center of faintest complete 0.5-mag bin in the total galaxy counts (50% complete).
[7]Field is in or near the Coma or Virgo superclusters (see §7.6 and §7.7 for details).

For each field, images were taken in both F450W (the WFPC2 B–band) and F814W (the WFPC2 I–band) with a longer exposure time in B due to the approximate 20% lower sensitivity at that wavelength (see Table 8 of Holtzman et al. 1995). Combined with the expected relative colors of the faint field galaxies compared to the Zodiacal sky, the total survey efficiency in F814W is $\gtrsim 2\times$ better than in F450W. Therefore, we took 2–4 orbits in B and two orbits in I. The reason for using both filters is to select the galaxies from the B–band images, where the HST resolution improves deblending over ground-based data, and therefore provides the most reliable object selection and photometry. The I–band images (which corresponds to the rest-frame B-band) have significantly higher S/N, and therefore provide the best possible source of morphological classifications, as well as provide color information over a wider color baseline than the standard V–I color (F606W–F814W) that has traditionally been used in most WFPC2 studies. The two sets of images coupled with a future redshift survey will also allow us to do a study of the rest-frame color gradients in the brighter galaxies. The total area of the BBPS survey, including the PC exposures, is approximately 0.0370 square degrees. The WF(PC) data have a $0\farcs0996(0\farcs0455)$ spatial sampling and a limiting magnitude of $b_J \lesssim 23.5$ mag (the approximate 90% completeness limit for compact objects), as discussed in § 8.1.

CHAPTER 7

Data Reduction

7.1 Image Stacking

All images were registered using the centroids of manually selected compact and bright objects, with the centroids being determined from the IRAF task *imcentroid*. Since the detectors are fixed relative to each other, shifts were determined for each of the 4 WFPC2 CCDs, and then averaged together to get the optimal offset for each set of exposures in a given field. These offsets were rounded off to whole numbers and only integer shifts were applied, so as not to introduce additional numerical noise into the data (*cf.* Ratnatunga, Griffiths & Ostrander 1999). Due to the nature of parallel observing with HST, a set dither pattern cannot be chosen by the parallel observers, and so the method employed here produces the most self-consistent data set. The appropriate shifts were then applied taking into account the different chip orientations and the finer sampling of the PC.

Since most fields were two orbit cases, it was necessary to improve upon existing cosmic ray (CR) rejection algorithms, which were optimized for use with $N \geq 5$ images (e.g., Windhorst, Franklin & Neuschaefer 1994). All image stacks were created using a customized IDL routine which was specially developed for this project. This routine was also used for the low light-level images in the F410M filter of Pascarelle,

Windhorst & Keel (1998). Images through different filters were handled separately to ensure that our final morphological classifications were as color-independent as possible. The reason for developing this new routine was the need to accurately reject CRs over a few (2–4) independent exposures, while assuring at high reliability that the science image itself would not be corrupted by the algorithm.

For N registered images, the IDL routine performs the following operations at *each* pixel (x,y) location *separately*. It creates a list of N pixel values which is then sorted from the lowest to the highest value. The following Poisson noise model based on the known CCD characteristics is then used to determine which pixel values should and should not be included in the average:

$$\sigma_{x,y} = \sqrt{DN_{x,y} * g + RN^2 + DK * t}/g \tag{7.1}$$

where $DN_{x,y}$ is the number of ADU in pixel (x,y), $g = 7.0\ e^-/ADU$ is the WFPC2 detector gain, $RN = 5.3e^-$ is the read-noise, $DK = 0.0033e^-/sec$ is the dark current rate and t is the exposure time in seconds. Starting with the *lowest* pixel value, each successive value is checked to see if it is within 2.5 σ of the current average value. This way, higher pixel values that are likely due to cosmic rays are rejected (at the 2.5 σ level). This process is then repeated for each pixel. This rejection algorithm will fail for the two orbit cases when a pixel is hit by a CR in *both* images, which we measured to occur about 0.3% of the time, or for about $\sim$ 2000 pixels that were affected by CR's in both full-orbit WFPC2 CCD exposures. This number is in excellent agreement with

an extrapolation of the values given in the *WFPC2 Instrument Handbook* [1] (Biretta et al. 2000). These left-over CR's cause problems with automated image extraction, because they would be counted as objects and possibly classified as faint galaxies, which would contaminate the sample.

In order to deal with this problem, we checked for cases of "double hits" by subtracting a 3×3 pixel median-smoothed image from each original image, and compared this difference image to the difference image for the other orbital exposures. This way, all "double hits" were located and interpolated over by substituting the median of the 8 surrounding pixels. The result was a much cleaner looking image, but this process also unavoidably generated holes in the centers of bright, centrally-concentrated objects (stars and early-type galaxies). Since these holes would obviously contaminate the photometry of the bright galaxies we are interested in, we opted to use the cleaner but non-photometric images *for the object selection only.* Once the object positions were found, all analysis was performed on the images that still contained the "double hit" CR's, but that had objects that were uncorrupted in their central regions.

7.2 Object Extraction

All image detection was done using the SExtractor version 1.0a (Bertin & Arnouts 1996) object finding software package. Each WFPC2 WFC (or PC) image is convolved with a 7×7 (or 9×9) convolution mask of a Gaussian kernel with a FWHM of 3 (or

[1] Updates to the WFPC2 Instrument Handbook can be found on the world wide web at: http://www.stsci.edu/instruments/wfpc2/wfpc2_top.html

5) pixels. Then all objects with at least 8 contiguous pixels that are 2.5 σ above the local sky-background (as determined by SExtractor) are extracted, and their location, size, and magnitude are written to a file. The mean isophotal 2.5σ detection limits for each field are listed in Table 6.1. Averaged over all fields, this surface brightness ("SB") detection limit corresponds to SB(b_J)$\simeq$ 24.2$\pm$0.2 (22.8$\pm$0.2) mag arcsec^{-2} for the WF (PC) detectors. The 1σ SB sensitivity limits for 53W002 field of Windhorst, Pascarelle & Keel (1998) are SB(b_J)$\simeq$27.5 mag arcsec^{-2} and SB(I)$\simeq$26.7 mag arcsec^{-2} , and these numbers are about $\sim$1.5 mag fainter for the HDF-N (Odewahn et al. 1996).

For each detected object, a smaller sub-image is then cut whose size is determined by the SExtractor image parameters. The subsequent image analysis is done on these individual object images (i.e. all surface photometry and morphological classification), using the MORPHO package of Odewahn et al. (1996, 1997).

Once the sub-images are extracted, all objects are visually inspected to determine whether they are true detections, as well as to determine if SExtractor over-did the deblending of neighboring objects. The latter was especially a problem for the brighter spiral and irregular galaxies that had several peaks in their 2–dimensional brightness distributions, and is a general problem for other object finding algorithms as well (see e.g. Valdes 1982; Neuschaefer & Windhorst 1995). The number of objects that had to be re-extracted by hand was relatively small, about 10 per field. The number of separate objects that were close enough to overlap was also small, but SExtractor generally did an excellent job of deblending these, although we emphasize that any

deblending process is, by definition, somewhat arbitrary. The photometry of these blended objects is addressed below.

7.3 Surface Photometry

Photometric zero-points were taken from Tables 9 and 10 of Holtzman et al. (1995). In the visual–red, these have not changed much during the lifetime of WFPC2 (Biretta et al. 2000). We used the "synthetic" WFPC2 zero-points (Vega-based), which means that the F450W magnitudes are equivalent to b_J[2], and the F814W magnitudes are the same as the ground-based I magnitudes. This is to allow optimal comparison to previous ground-based galaxy B-band counts, which were primarily done in the b_J filter (or a filter that easily transforms to b_J). For completeness, we used zeropoints of $ZP_{F450W} = 21.929$ mag and $ZP_{F814W} = 21.676$ mag for b_J and I, respectively, for a count of 1 DN per second of exposure time.

In order to accurately derive light-profiles and compute total magnitudes, a good determination of the sky-background must be made. For each field and filter, sky-values are determined for each of the four WFPC2 CCD's using the following technique. The CCD is divided into 16 squares of 101×101 pixels each. Next, a sky-value and sky-sigma are determined for each square by fitting a "tilted plane" (*cf.* Neuschaefer & Windhorst 1995) to that area, after rejecting all real objects that

[2]Kron (1980) gives the transformation from standard to photographic B magnitudes as $B - b_J = 0.23(B - V)$ and, using Holtzman et al. (1985) Table 10, we derive $B - F450W = 0.23(B - V)$, which shows that the synthetic WFPC2 F450W system is the same as the photographic b_J system.

were found at the $\geq 2\sigma$ above the local sky level. The reason for not fitting a more complicated surface is that the images are sufficiently flat-fielded over $\sim$ 100 pixel scales, so that mostly linear sky gradients are left, if any. Residual sky gradients could be due to, *e.g.*, the telescope pointing too close to the Earth's limb, which is not always controllable when scheduling parallel observations. This could produce a simple mono-directional linear gradient in the WFPC2 sky, although this was not often observed. The median of the 16 sky-box values was then used to determine the final sky-value and sky-sigma. These values were found to agree with the global *BACKGROUND* and *RMS* values determined by SExtractor to within 2%.

Since the Zodiacal sky at moderate to high Ecliptic latitudes is about SB(b_J)$\approx$23.8–24.1 mag arcsec^{-2} and SB(I)$\approx$22.15–22.45 mag arcsec^{-2} (Windhorst, Keel & Pascarelle 1998), a 2% error in the sky-subtraction becomes the dominant factor at surface brightness levels SB(b_J)$\approx$28.0–28.3 mag arcsec^{-2} or SB(I)$\approx$26.4–26.7 mag arcsec^{-2} , at which level this sky-subtraction error equals $\sim$100% of the galaxy SB-profile signal. In the noisier BBPS images, we cannot push the galaxy SB-profiles this faint, but for the two BBDS fields this is one reason why we do not push the galaxy classifications (see § 8.1) fainter than total fluxes of $b_J = 27.0$ mag (or $I = 25.5$ mag). This is because at these total flux levels, the median galaxy scale-lengths are $r_e = 0\farcs2 - 0\farcs3$ (see § 8.2), so that the sky-subtraction errors in the average SB-value out to r_e are of order 10–20%. This is the maximum acceptable error in SB-profile parameters to allow reliable ANN classifications, which are based on the galaxy SB-profile and

other parameters (see § 7.5). Fainter than $b_J \gtrsim 27$ mag, ANN galaxy classifications are mainly unreliable due to a lack of a good training set (Odewahn et al. 1996), which would be necessarily based on the abilities to assign eyeball classifications as well as accurately measure the light profiles of these galaxies, both of which become increasingly suspect fainter than this flux level, for reasons stated above. The issue of uncertain resdshifted UV-morphology could also play a role here and is further discussed in § 7.7.2. Given that $b_J \simeq 27.0$ mag is *also* the limit due to the sky background subtraction (at these wavelengths), there is little hope of reliable classification for fainter galaxies with HST, *even with improved resolution and/or deeper images.*

All surface photometry was performed on each sub-image, using these sky-values, with the MORPHO package as described in Odewahn et al. (1996, 1997). Since each sub-image to be analyzed has to contain a single object, the analysis on crowded areas was done as follows. If two objects were too close together, two sub-images were generated, each with *one* of the two objects replaced by the local sky value, as interpolated from surrounding unaffected sky areas. The size and shape of the "blanked" out region was an ellipse based on the SExtractor values for position, size, axis ratio and position angle. This way, when the isophotal ellipses were fit to determine the light-profile, the target object was minimally affected by its neighbor. Since the total magnitude is determined from the integrated light-profile, this was the most reliable way to handle proximate objects, while reducing the effects of crowding on the other measured object parameters. Note that because the ANN classification

is based on individual object light-profile based parameters (§ 7.5), and simultaneous light-profile fitting on *more* than one object is very difficult to do (Schmidtke et al. 1997), this seemed to be the most robust way to get an accurate ANN class for every object, even if close neighbors were present.

7.4 Catalog Generation

Once the images in both the B and I filters are processed and cataloged, the B and I object lists are cross-matched by pixel location. For each object in the B–band catalog, the I–band catalog is searched using a search radius of 3 effective radii. The effective radius r_e used here is the half-light radius as measured from the B–band image. With this search criteria, about 70% of the objects in the B–band catalog have I–band counterparts, while more than 95% of the I–band catalog have B–band counterparts. A manual check of the images showed that almost all the unmatched B–band catalog objects were not real galaxies, but likely image defects, noise spikes or remaining cosmic rays left in the B–band images. We thresholded at 2.5σ so as not to exclude any real objects, at the expense of making false detections which would get thrown out in cross-matching. Since the I–band images are of higher quality and go deeper, despite their generally shorter exposures, it is doubtful that very blue objects were excluded through this selection process. However, this matching procedure could select against extremely red objects, which we must bear in mind during the interpretation (§ 8 and 9).

7.5 Morphological Galaxy Classification

Galaxy types are assigned to all objects using an automated artificial neural network (ANN) pattern classifier that is based on the *shape* of the object light-profile. Galaxy types, or hereafter T–types, were designated on the 16 step revised Hubble system (de Vaucouleurs 1959). This classification scheme was chosen because T–types have been shown to correlate well with physical properties in nearby galaxies (Roberts & Haynes 1994) and the available data used to produce our galaxy count models are segregated in the same way. Since the typical machine classification error in type is 2–3 steps (Odewahn et al. 1996), types were rebinned into three broad intervals, that each span a much larger range than the ANN classification error (E/S0, Sabc, Sd/Irr). This classification error results from noise in the profile-parameters of the faint objects (as discussed in § 7.3), and from inconsistencies between experienced classifiers, who visually classified a limited number of galaxies in the "training set" that is used to train the ANN before it is run on a much larger sample. To the extent possible, the personal offsets and biases between these expert classifiers were removed (*cf.* Odewahn et al. 1996, 2002) before constructing the final training set, thereby reducing systematics in the ANN classifications (although not yet proving that these classifications are necessarily correct). The ANN's used here are the rest-frame networks developed in Odewahn et al. (1996), which were trained on the HDF–N galaxies that had published redshifts at that time. The redshifts are required

to know the rest-frame wavelength in which each galaxy in the $UBVI$ training set was actually observed. T–types are in the range $-7 \leq T < -0.5$ for objects designated as "E/S0," $-0.5 \leq T < 5.5$ as "Sabc", and $5.5 \leq T < 12$ as "Sd/Irr".

We note that the ANN's of Odewahn et al. (1996) always produces an answer, *i.e.*, based on the actual galaxy SB-profile parameters, it forces a classification in one of these three T-type intervals, no matter how faint or how low-SB the object is. That is, we deliberately sacrifice classification accuracy to get 100% completeness in the classifications, so that no objects remain unclassified. The corollary of this is, of course, that beyond a certain flux and SB limit, the classifications become increasingly unreliable due to the lack of an adequate training set. The lack of an adequate training set at these faint flux levels is due to a combination of insufficient S/N and resolution for a human classifier to assign a reliable type, as well as a poor understanding of the rest-frame UV morphology for the higher redshift objects where this is a potential issue. As discussed in § 7.3, we believe that this limit occurs in the two BBDS fields at total fluxes of approximately $b_J = 27.0$ mag ($I = 25.5$ mag). We will show in § 8.1 that the shallower BBPS fields produce consistent classifications close to their completeness limit of $b_J \simeq 23.5$ mag in the flux range of overlap with the two BBDS fields ($22.5 \lesssim b_J \lesssim 24.0$ mag), where the classification of the latter objects are robust, since they have much higher S/N at the same flux level.

Using the suitably trained neural networks, galaxy types were generated from both the B–band and I–band images, as described below. However, for a variety of reasons,

all types used in this paper are based on those ANN-values assigned from the I–band images. First, the I–band images are superior to the B–band ones due to the larger overall sensitivity and the much darker Zodiacal sky background at that wavelength, even for the bluest detectable field galaxies. The second reason is bandpass shifting. The median redshift of the fainter galaxies at $b_J \leq 25$ mag is $z \simeq 0.6 - 0.7$ (Koo & Kron 1992; Ellis 1997). Therefore, the light observed in the I–band was emitted in approximately the B–band where morphology of local galaxies has been well studied, and a good training set for the ANN exists. Analogously, the light observed in the B–band is emitted in the rest frame near-UV, where systematic studies of nearby objects have only recently been done (*cf.* Giavalisco et al. 1996; Burg et al. 1997; Kuchinski et al. 2001; Marcum et al. 2001; Windhorst et al. 2002). The issue of uncertain rest-frame UV morphology and its effect on the galaxy counts as a function of type is further discussed in § 7.7.2. For the BBPS, the use of I–band classifications allows us to take advantage of bandpass shifting instead of being hampered by it. Thirdly, the effects of the k-corrections are smaller at this longer wavelength. Finally, the HST images are closer to being properly sampled in the I–band, compared to the B–band, allowing for better classifications.

We classified all these galaxies from their I–band images, but using an ANN defined at a shorter wavelength which is closest to the rest-frame wavelength sampled by the I-band for that particular object. These rest-frame ANN's were constructed from the HST $UBVI$ images in the HDF–N for objects with spectroscopic redshifts ($z \lesssim 1$).

The details of this classification method and the use of rest-frame ANN's are given in Odewahn et al. (1996, 1997) and references therein. For this project, seven parameters are used as input to the ANN which then produces a type. These parameters are all based on the object's azimuthally averaged radial surface- brightness profile and are:

1. the SB at the radius containing 25% of the total light;
2. the SB at the radius containing 75% of the total light;
3. the mean SB within the effective (half-light) radius;
4. the mean SB within an isophotal radius ($SB(I) = 24.5 mag\ arcsec^{-2}$);
5. the slope of a linear fit to the profile in $r^{1/4}$ space;
6. the intercept of a linear fit to the profile in $r^{1/4}$ space; and
7. the axial ratio (b/a) of the outer isophote.

It is important to note that in the ANN classifications, color is not used *at all* and that the effective radius is not used *directly*. Fig. 7.1 shows that this indirect use of effective radius does result in a loose correlation of r_e with type in any given I–band magnitude slice. It is also important to reiterate that no bulge-to-disk decomposition or model profile-fitting is used. This particular choice of the 7 ANN parameters is somewhat arbitrary. Different sets of structural parameters were tested (Odewahn et al. 1996) and produced similar classifications to within the errors quoted above.

As discussed in Odewahn et al. (1996), the classification limit in the two BBDS fields is $b_J \lesssim 27$ mag (or $I \lesssim 25.5$ mag). At fainter flux levels, human classification becomes increasingly unreliable. As illustrated in § 8 (Figures 3–7), it is interesting to notice that the ANN classifications appear reasonable, even a magnitude or so fainter than the visual classification limit of the training sets.

These classifications are reasonable because the parameters that are not used in the classifications (color and effective radius) follow the type-dependent trends for galaxies at cosmological distances that one would expect from the known properties of local galaxies (see discussions in § 8.2 and § 8.3). However, this is not proof that these classifications are therefore correct, and two things are required to verify these classifications beyond the currently stated limits: higher resolution images of these galaxies and a better mid-UV training set for the ANN (see § 7.7.2). For the brighter BBPS sample, the B–band data is too noisy near its completeness limit to believe the classifications from the B–band images alone. This is another reason for classifying in the I–band images, which go $\approx 0.5 - 1.0$ magnitudes deeper even for blue galaxies, and therefore have a higher signal-to-noise ratio. Therefore, all BBPS fields have reliable classifications to their respective B–band detection limits listed in Table 6.1, and the two BBDS fields have reliable classifications to $b_J \lesssim 27$ mag (ie. $I \lesssim 25$ mag).

7.6 Star-Galaxy Separation

The issue of star-galaxy separation is an important one, especially in a survey of this nature where the goal is to count different types of objects, including the most compact ones. The star-galaxy separation for the BBPS was initially performed using a linear division in a single 2–D photometric parameter space. The effective radius, r_e forms the Y axis. The X axis is formed with the ($MORPHO$) "C42" parameter. This is a concentration index formed by the ratio of the size of the "total aperture" to the 50% flux aperture (i.e. the number of effective radii inside the total aperture). Both apertures have an elliptical shape defined by the median ellipticity of the ellipse fits to the lower SB isophotes. The determination of the "total aperture" is a complex procedure, which finds the optimally sized aperture based on the local signal-to-noise ratio of the sky. An object is classified as a star if $C42 \geq 60.0$, or if it lies below the line $r_e = 0.010 * C42 - 0.095$. These values were determined using the F814W data from the HDF–N, the HDF–N flanking fields, the 53W002 field and the 6 earlier MDS fields from Driver, Windhorst & Griffiths (1995). They were plotted for several magnitude cuts using symbols to indicate the morphological types assigned in our past visual classification work. Bright objects with clear diffraction spikes were always visually classed as stars. These could erroneously include a few QSO's, if these were not otherwise recognized, *i.e.*, from their available spectra (*e.g.*, Pascarelle et al. 1996) or weak radio fluxes (Windhorst, Keel & Pascarelle 1998). By inspecting many

such plots, the best line that divided the stars and the E/S0 types was determined. At bright magnitudes (usually $I \leq 22$ mag for most BBPS fields), the parameter space always showed a fairly substantial segregation between stars and even compact, high SB galaxies (likely E/S0). Of course, as we go fainter, this division blurs due to increasing noise in the extracted r_e and C42 measurements. This separation limit is similar to the one found by Méndez & Guzmán (1998), who used a different method. Also, a visual inspection of the 40 objects with $b_J < 21$ mag and not classified as stars showed that this method failed for 12 bright ($b_J < 19$ mag) and saturated stars. These 12 stars were removed from the the final galaxy counts.

To demonstrate the success of this star-galaxy separation method, Fig. 7.1 shows the I–band magnitude versus effective radius relation for the BBPS objects, including those objects that were classified as stars. It is clear that to the BBPS I–band compact-object detection limit ($I \simeq 23.75$ mag), the stars easily separate out from most of the galaxies, except for an interesting group of objects, most of which were initially classified as "elliptical" galaxies, that are small ($\log(r_e'') \simeq -1$) and near the faint end of the sample ($I \simeq 22.0$ mag – these objects are plotted as pluses in Fig. 1). This raises the obvious and important question of whether or not these objects are misclassified stars.

In order to test this issue, the Galaxy Model of Bahcall & Soneira (1981) was used to predict the star-counts in these fields. The model was run for the (l^{II},b^{II}) coordinates of *each* of the 29 telescope pointings and the resulting predicted star

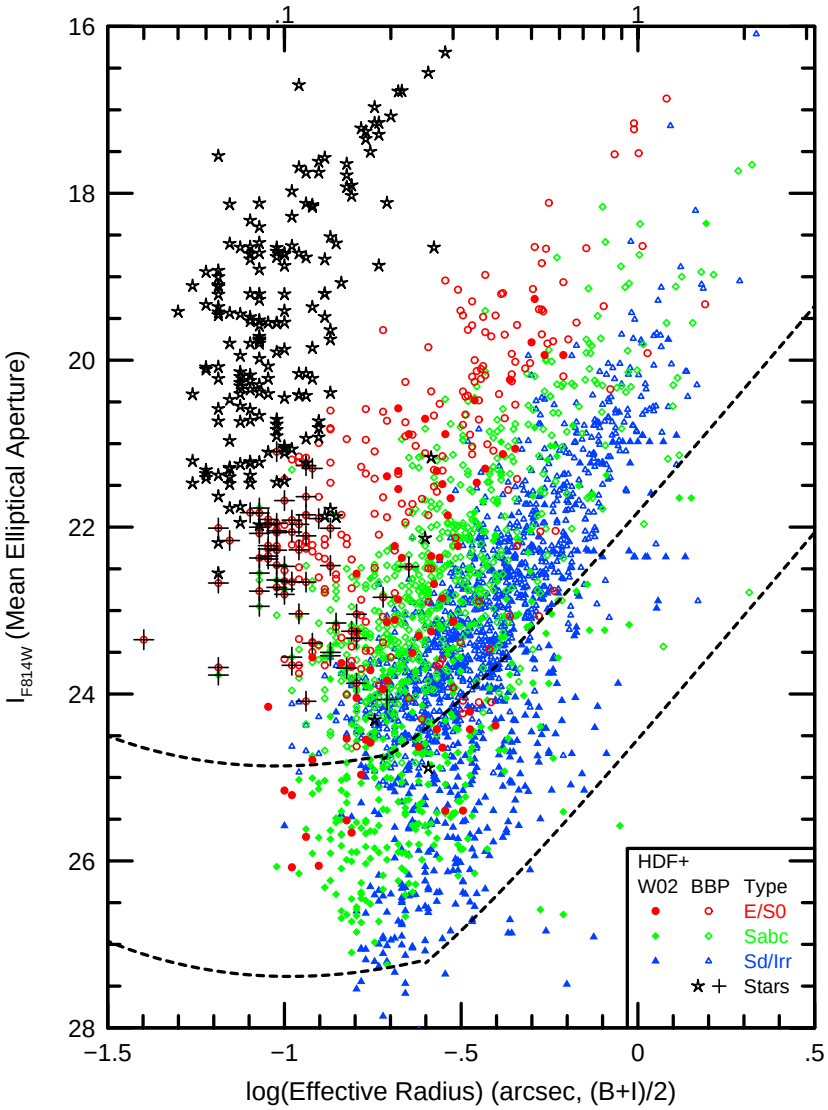

Figure 7.1: I–band magnitude vs. effective radius for the BBPS. This figure shows that misclassification between stars and galaxies occurs for $I \gtrsim 22$ mag. At this magnitude, a fraction of stars may be classified as early-type galaxies. Note that stars are only plotted for the BBPS fields and not for the two BBDS fields. The dashed lines indicate the approximate completeness limits for the BBPS and BBDS, as discussed in the text. The objects with pluses superposed were re-classified as "stars", and are likely globular clusters in the Virgo cluster, as explained in § 7.6. The scale indicated across the top is for r_e in arcseconds.

counts were *averaged* together. Fig. 7.2 shows the differential number counts in the B–band for all non-stellar objects, for the objects classified as stars, for the E/S0 galaxies only, as well as for the average Bahcall and Soneira model. The first issue to notice is that the average star count model matches the observed star counts very well. When compared to the star count model, it is clear that our first pass of the star counts (plotted as upwards arrows in Fig. 1) turn over at $b_J \geq 23.5$ mag due to a significant fraction of misclassifications and incompleteness, even before the galaxy counts noticeably turnover at $b_J \geq 24.5$ mag. It is therefore highly probable that some fainter stars have been misclassified as galaxies. These would have most likely been misclassified as centrally concentrated (and therefore elliptical) galaxies, as seen in Fig. 7.1. There is also a color selection effect, in that the fainter stars are expected to have redder colors and therefore may have escaped the blue selection limit. Note that, in order for an object to appear in our catalogs, and hence in Figs. 1–7, it had to be seen in *both* the B and I filters. The majority of the stars from the two deeper fields with $I \geq 22$ mag are too red [$(B-I) \geq 4$ mag] to have been selected in the BBPS sample. This is less of a problem for the galaxies because, as Fig. 8.5 shows, at $I \geq 22$ mag galaxies have (B–I) colors in the range of 1.0–2.5 mag. Fortunately, at this brightness level and at fainter flux levels, the galaxy counts are much higher than the predicted star counts (see Fig. 7.2), even for the early-type galaxies which have the shallowest counts slope (see also Fig. 8.1). Therefore, the likely contamination of the faint galaxy counts by misclassified stars is minimal and not significant. The

few missing bright ($b_J \lesssim 18$ mag) stars in Fig. 7.2 are due to the saturation problem mentioned above. These missing bright stars were obviously detected, but due to saturation, no reliable fluxes could be measured, so they are not plotted in Fig. 7.2.

Since the star-counts should go as deep as the total object counts, and Fig. 7.2 shows that our first-pass star counts (shown as upwards arrows) turns over before the galaxy counts, there must be some number of fainter stars that were not classified as such. Therefore, a second step in star-galaxy separation was applied to rectify this situation. The model star counts were used as a reference point to update the stellar classification for $b_J > 23$ mag. *Therefore, the resulting star counts can not and must not be used fainter than* $b_J > 23$ *mag to test any star count models.* This is not a problem here, since the goal of this study is to properly count the *galaxies* in order to compare to galaxy count models as a function of galaxy type. A diagonal line was drawn in the magnitude–$\log(r_e)$ parameter space, where both quantities are measured in the I-band. Note that Fig. 7.1 shows the effective radius (r_e) as an average over the values measured in the B and I bands, while all star-galaxy separation (and galaxy classification) was done exclusively on the I-band images. All objects to the left of this line were declared stars and all objects to the right were declared galaxies. This step did not change the classification of any previously determined stars. The process was iterated by trial and error until the observed star counts matched the predicted star counts up to the completeness limit of the total counts. The final star-galaxy separation line that was used is given by $I = -20.313 \times \log(r_e) + 6.188$. The objects

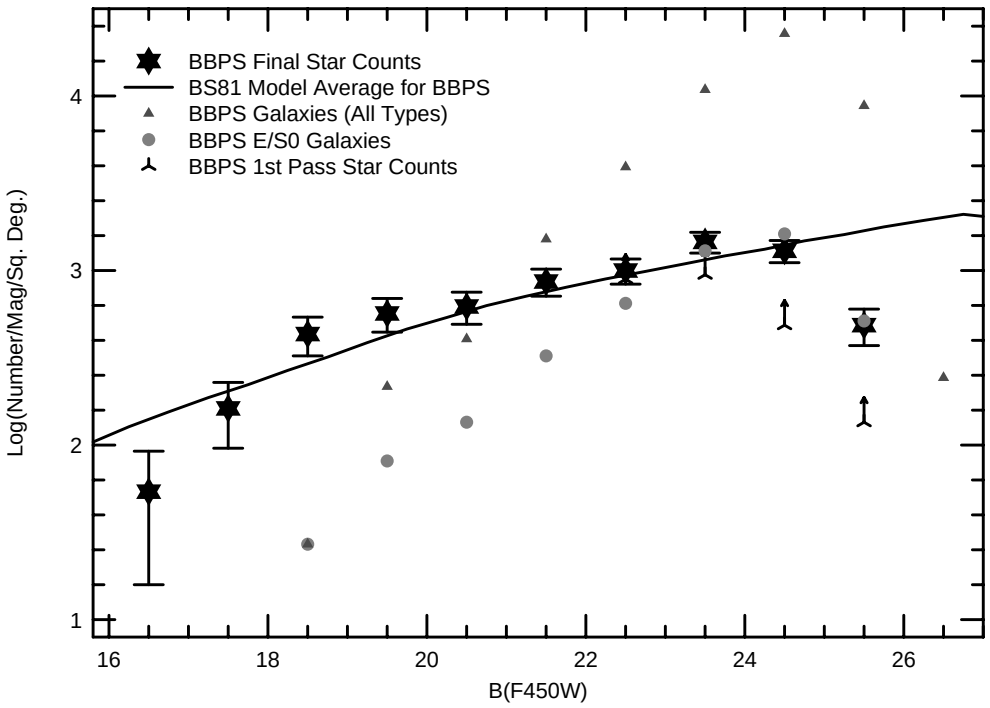

Figure 7.2: Differential star counts for the BBPS data. Objects initially classified as stars are shown as upward pointing arrows and the final star counts are shown as stars with error-bars (see § 7.6). The solid line shows the predicted star counts from the Bahcall & Soneira (1981) Galaxy model averaged over the Galactic coordinates of all 29 different HST parallel pointings. For comparison, the total counts for objects classified as galaxies (triangles) and those classified as E/S0's (circles) are also shown (see also Fig. 3). Note that to $b_J \lesssim 23.0$ mag, the initial star-galaxy separation is good. Beyond this limit, the galaxies begin to far outnumber the stars, so that a few misclassifications of stars will not substantially affect the results on faint galaxies. However, at $b_J \gtrsim 23$ mag, the star counts become less reliable.

that were re-classified as stars are shown as superposed pluses in Fig. 7.1, and it can be seen that the majority of them were originally classified as ellipticals.

However, for any reasonable application of this second pass at star-galaxy separation, the new star counts were always several sigma above the Bahcall and Soneira models (at the faint end) and so warranted further investigation. The colors of these faint centrally concentrated objects were examined and a significant number of them were grouped around $\langle(B-I)\rangle = 1.44 \pm 0.42$ mag and the majority of these came from 2 HST parallel fields in the Virgo Cluster, bb016 and bb018. Using the NASA/IPAC Extragalactic Database (NED), it was realized that field bb016 is only $8\farcm2$ away from M87. This well studied elliptical galaxy is known to have a large and extended globular cluster population (Harris 1986). If we designate all the compact objects in this field with the colors mentioned above as globular clusters in Virgo (loosely associated with M87), and compare the number that we find (N=19) to the surface density of these objects in Harris (1986), we get very reasonable agreement. The apparent magnitude of these objects, combined with the M87 distance, also argues that these have the expected luminosities of Virgo globular clusters. Inspection of the location of the bb018 field shows that it is situated between two bright Virgo ellipticals M84 ($8\farcm2$ away) and M86 ($9\farcm9$ away). It is therefore highly likely that the bb018 star-like objects (N=18) in this color range are globular clusters in the (overlapping) halos of both of these galaxies. The final corrected star counts, shown in Fig. 7.2, have these globular cluster candidates removed, and show that the updated star-galaxy separa-

tion has no noticeable effect on the total galaxy counts, but do impact on the counts of the faintest ellipticals, albeit minimally. In fact, given what is known about faint star counts (Flynn, Gould & Bahcall 1996), even if all faint stars were mis-classified as early-type galaxies, the E/S0 counts would be *at most* 10% too high in this flux range.

We emphasize that star-galaxy separation with HST is non-trivial, even at the relatively bright limit of $I \approx 22$ mag, because faint galaxies generally have small angular sizes (see § 8.2 and Fig. 8.4 below), and because objects other than stars and galaxies can sneak into the HST samples.

7.7 Galaxy Counts as a Function of Type

Objects classified as galaxies were counted in half-magnitude wide bins. The counts for each field were combined in the following way. The completeness limits in each field is different for both observational (mainly varying exposure times) and statistical reasons (*i.e.*, cosmic variance). First, the completeness limit for each field is determined from the flux level at which the total counts in that field turn over (cf. Neuschaefer & Windhorst 1995). All counts beyond the completeness limit are given a weight of zero while all counts brighter than this limit are given a weight of one. Therefore, no field contributes to any magnitude bin (in the combined counts) in which it is less than 90% complete. The center of the faintest bin that was used from each field is listed in the last column of Table 6.1. This ensures that the fainter

points are properly handled given the different exposure times. These weights are then used to keep track of the area that contributes to the counts in each bin. This results in some of the fainter bins having a smaller effective area than the brighter bins, as indicated in Table 8.1. This is not a problem because there are many more faint objects and hence the statistics in the faint bins are not compromised. Below we discuss two possible sources of contamination, other than the stars already mentioned in § 7.6.

7.7.1 Local Large Scale Structure

Some of the parallel fields had coordinates that placed them in or near the edge of the Coma or Virgo superclusters (as indicated in Table 6.1). In order to test whether there was any excess of bright galaxies from these superclusters, the counts were compared for the cluster and non-cluster fields. For fainter flux levels, the counts from the cluster fields were within the 3σ field-to-field variance of the mean of the non-cluster field counts. The only statistically significant contaminants were two galaxies from bb019 ($b_J = 17.08, 17.22$ mag) and one from bb001 ($b_J = 17.97$ mag), which are in the Coma supercluster. This was the *primary* HST target which may, therefore, have biased the bright galaxy sample in the WFPC2 parallels we are studying here. This a valid and well known concern in HST parallels (*cf.* Casertano et al. 1995), and the obvious remedy is to excise these excess bright galaxies from the sample. These three galaxies were therefore omitted from the final counts because

they are not representative of *field* galaxies in general, given that the primary HST target was biased towards these clusters.

Also the brightest galaxy in the survey ($b_J = 16.99$ mag) was excluded from the counts because it is part of the NGC 383 group, which was also the primary target of that particular HST acquisition. This galaxy is an elliptical that appears to be interacting with a fainter spiral galaxy, and it was only noticed because the ANN assigned a much later type. A careful inspection shows that this galaxy contains a significant disk structure with low level spiral arms which explains why it was incorrectly classified. Therefore, there was only one true "field" galaxy found in this survey brighter than $b_J \lesssim 19$ mag.

To let the readers judge our line of reasoning for themselves, we plot the three bright data points based on these four galaxies in the total counts (upper left panel in Fig. 3), but plot their detected surface density as *upper limits*, since the true field galaxy count at these flux levels ($16.5 \lesssim b_J \lesssim 18.0$ mag) must be lower than the count that we observe in these few not-so-random parallel fields. This is important for the discussion of the counts in § 8 and 9.

7.7.2 Misclassification Trends due to the Uncertain Rest-frame UV

The mid-UV (2500-2900$\mathring{A}$) images of nearby galaxies available thus far (Windhorst et al. 2002) suggest that it is more likely to misclassify true ellipticals or early-type spirals in the rest-frame mid-UV as late type galaxies than the other way around.

This is because *truly* late-type galaxies are dominated by young and hot stars in filters from the mid-UV to the red, and so have to first order the same morphology and a rather small morphological k-correction. However, early-type galaxies (ellipticals and early-type spirals) can, *although do not have to* look dramatically different when one goes from the rest-frame mid-UV to the optical-red part of the spectrum. Hence, misclassifications due to the morphological k-correction will more likely move more ellipticals and early-type spirals into the late type/irregular category, rather than vice versa. Since all galaxies in the present study were classified from I-band images, this would only be relevant for galaxies with redshifts of $z \gtrsim 1.8$, which corresponds to the fainter part of our sample, as can be seen in the morphologically segregated redshift distributions of Driver et al. (1998). These redshift distributions show that significant numbers of $z \gtrsim 1.8$ galaxies are only present in fainter sample where the classifications become increasingly unreliable ($b_J \gtrsim 27.0$ mag) for reasons discussed in § 7.5. While this can perhaps explain part of the excess late-type/irregular galaxies at faint magnitudes as discussed below, it cannot explain all of the FBG excess, and it certainly cannot explain the apparent excess of early-mid types at $b_J \gtrsim 24$ mag relative to the best available models, as discussed below.

CHAPTER 8

Results

Here we present our results for the $\sim$ 1800 BBPS galaxies as a function of *measured* B-band brightness *and* ANN morphological type. The statistically complete sample is composed of $\sim$ 370 galaxies with $19 \lesssim b_J \lesssim 23.5$ mag.

8.1 The Morphological Galaxy Counts

The fundamental question we will address in this section is that of the galaxy counts as a function of morphological type at fluxes between the ultra-deep HST fields and what can be done from the ground. We will show that, in order to use galaxy counts as a function of morphological type to address issues of galaxy evolution, this intermediate flux range is crucial.

In Fig. 8.1, we show the BBPS galaxy counts as a function of morphological type. Also included for comparison are the deeper counts from the two BBDS fields (Odewahn et al. 1996). At the bright end ($b_J \lesssim 18$ mag), we include as upper limits the four galaxies, discussed in § 7.7.1, that were excluded from the sample due to their high probability of not being representative of field galaxies. Also plotted are the combined ground-based counts from the Millenium Galaxy Catalog (MGC; Liske et al. 2002), which is a wide-field B-band CCD survey covering 30 square degrees, which

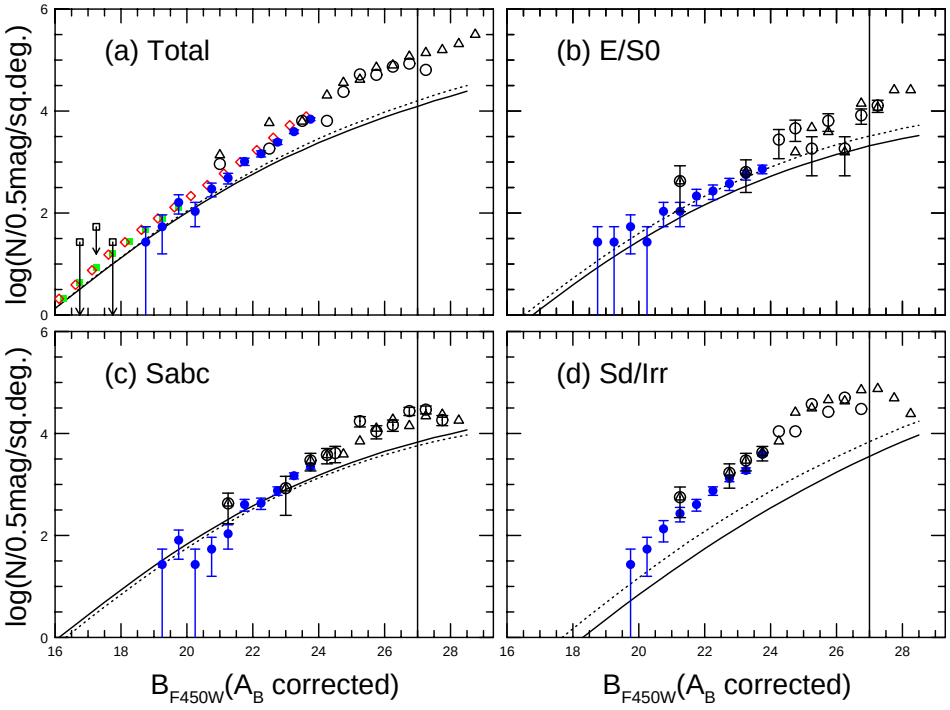

Figure 8.1: Differential B–band galaxy counts for all BBPS galaxies as a function of morphological type and b_J magnitude. The solid blue points represent the new BBPS data that cover $18 \lesssim b_J \lesssim 24$ mag. The open triangles (HDF–N) and open circles (53W002) represent the counts from the two deeper fields analyzed in the same way as the BBPS counts. The curves are predictions from local LF plus no-evolution models as described in Odewahn et al. (1996) and in Driver et al. (1995a). The models assume a cosmology with $(\Omega_M, \Omega_\Lambda)$ equal to $(0.3, 0.7)$. These non-evolving models use the type-dependent LF's of Marzke et al. (1994; dashed lines) or Marzke et al. (1998; solid lines). The open squares show the upper limits at the bright-end, as described in the text. The red diamonds are the total ground-based CCD counts from the Millenium Galaxy Catalog (Liske et al. 2002) and the green squares are from a first part of the SDSS (Yasuda et al. 2001). These SDSS and MGC total counts are perfectly consistent. The reliable classification limit in the BBDS is $b_J \lesssim 27$ mag, based upon the available training-sets and S/N in the images (see text and Odewahn et al. 1996).

Table 8.1: Differential b_J-band Galaxy Counts as a Function of Type

b_J lower[1]	b_J upper[1]	$\log_{10}(n)$ Total[2,3]	$\log_{10}(n)$ E/S0	$\log_{10}(n)$ Sabc	$\log_{10}(n)$ Sd/Irr	Effective Area (Square Degrees)
18.5	19.0	1.431	1.431	···	···	0.0370
19.0	19.5	1.732	1.431	1.431	···	0.0370
19.5	20.0	2.209	1.732	1.908	1.431	0.0370
20.0	20.5	2.033	1.431	1.431	1.732	0.0370
20.5	21.0	2.473	2.033	1.732	2.130	0.0370
21.0	21.5	2.687	2.033	2.033	2.431	0.0370
21.5	22.0	3.011	2.334	2.607	2.607	0.0370
22.0	22.5	3.164	2.431	2.635	2.878	0.0370
22.5	23.0	3.390	2.577	2.878	3.121	0.0370
23.0	23.5	3.596	2.753	3.172	3.276	0.0370
23.5	24.0	3.840	2.863	3.350	3.596	0.0370
24.0	24.5	4.006	2.857	3.556	3.764	0.0361
24.5	25.0	4.162	3.021	3.609	3.974	0.0295

[1]Lower and upper b_J-magnitude bounds of given bin
[2]All counts are $\log_{10}$(Number/sq. degree/0.5 mag)
[3]The $23 \lesssim b_J \lesssim 23.5$ mag bin is the faintest bin where the total counts are better than 90% complete.

we have analyzed using the same software allowing for the best direct comparison of our HST work to brighter ground-based data. For independent comparison, we also plot the transformed to the b_J-band counts from the SDSS Commissioning Data (Yasuda et al. 2001). Both sets of ground-based counts match up well with the HST counts. The BBPS number count data are tabulated in Table 8.1.

The galaxy counts for the three main morphological types in Fig. 8.1 now span a range of nearly 10 magnitudes ($18.5 \lesssim b_J \lesssim 28.5$ mag), of which about 8 magnitudes ($19 \lesssim b_J \lesssim 27$ mag) have decent statistics *and* reliable classifications. This is a major improvement in survey dynamic-range that could not have been achieved from the

ground, since reliable classifications are not possible for most galaxies in ground-based seeing for $b_J \gtrsim 19$ mag (see § 8.2). This also could not have been achieved from a few single deep HST fields, since these do not have sufficient statistics for $b_J \lesssim 24$ mag. Thus, the current combined HST morphological counts have the potential to set significant constraints on galaxy evolution models in the flux regime $19 \lesssim b_J \lesssim 27$ mag. This is especially important for $b_J \gtrsim 25.5$ mag, where routine spectroscopic measurements with 8–10 meter class telescopes becomes increasingly difficult and incomplete.

The *total* counts are remarkably continuous and smooth from $b_J \sim 18$ mag down to the formal HDF detection limit of $b_J \sim 29$ mag. In the flux range where both surveys have good statistics ($22 \lesssim b_J \lesssim 24$ mag), the type-dependent counts for the BBPS and BBDS samples show good continuity, adding confidence that the I–band classifications of the faint BBDS galaxies are consistent with the brighter counts.

For comparison with this new data, we plot in Fig. 8.1 models for the galaxy count models that are based on the local LF as a function of galaxy type, as described in Driver et al. (1995a), Driver, Windhorst & Griffiths (1995) and Driver et al. (1998). These model have been updated using the currently favored flat cosmology of $(\Omega_M, \Omega_\Lambda) = (0.3, 0.7)$ and more recent estimates of the local LF. The solid lines use the type-dependent LF's of Marzke et al. (1994; hereafter CfA) and the dashed line uses the more recent ones of Marzke et al. (1998; hereafter SSRS2). These are simple zero evolution models, which include only k-corrections with no explicit evolution in

luminosity, number density or color. The models in the upper left panel of Fig. 8.1 are the sums of those of the individual types in the other panels. *No* LF-normalization has been applied at the bright end. In fact, these new data show that such normalization is not needed, and that a global (*i.e.*, the same factor for all types) LF-normalization would cause the models to overpredict the observed counts for both the E/S0's and the Sabc's. Such an LF-normalization has been used in the past to help explain the excess of fainter galaxies (for a discussion, see Driver, Windhorst & Griffiths 1995; Marzke et al. 1998), but this is incompatible with the new data presented here.

Therefore, the current data argue against a blanket LF-normalization with the same amplitude for all types. This directly results from the fact that the new BBPS data yield both morphology *and* b_J-band magnitudes nearer to the normalization point ($b_J = 18 - 20$ mag) than previous studies did. The adopted cosmology, which allows for more volume at high redshifts than an Einstein–de Sitter ($\Omega = 1$) model, has little effect near the normalization point, but serves to bring the models *slightly* closer to the data at fainter fluxes (*e.g.*, the two models differ by a factor of ≈ 2 at $b_J \simeq 26$ mag). From the high dynamic range of the current survey it is now becoming clear that the FBG *excess* is almost entirely due to the late-type galaxies, which have the steepest slope at the bright end, and are the most numerous type at the faint end of the counts. In fact, we will argue that more than 90% of the FBG excess for $b_J \gtrsim 25$ mag is attributed to these late-types. The next question to address is how to explain this.

8.1.1 Evolution Models vs. Renormalization

As Fig. 8.1 shows, the local LF's with zero-evolution do not reproduce the observed galaxy counts as a function of type. Though this is most pronounced at the *faint* end, it is also true at the bright end, especially for the late-types. This difference between the local (*i.e.*, where the LF's have been measured) and the more distant Universe needs to be further investigated. One way to model this discrepancy would be through a normalization of the models, which is the equivalent of compensating for the possibility that the local present day Universe is either over- or under- dense in a particular type (or every type) of galaxy. Another way is to assume some type of evolution (*e.g.*, luminosity or number-density) in the galaxy populations at relatively low redshifts.

Under the assumption that the data do not justify an LF-normalization of the models, especially for the early-types, we include luminosity evolution as a first step to explain the galaxy excess at faint magnitudes. As described in Driver et al. (1995a), we assume that galaxy luminosities evolve as $L \propto (1+z)^{\beta}$, which is supported through the CFRS for early–mid type galaxies (Lilly et al. 1995b). As local references, we use the LF's of the SSRS2 (Marzke et al. 1998), which are the best available until the morphologically type-dependent LF's from the 2dFGRS and SDSS become available. Fig. 8.1 shows that using the CfA LF's leads to the same qualitative conclusions in the discussion that follows. The new evolutionary models are plotted in Fig. 8.2.

The $\beta = 0$ (no evolution) models are shown in black, $\beta = +1, +2, +3, etc$ (positive evolution) are shown in green and $\beta = -1, -2$ (negative evolution) are shown in red.

The no-evolution models ($\beta \simeq 0$) clearly provide reasonable fits to the BBPS data for both the E/S0 and Sabc for $b_J \lesssim 24$ mag. This implies that the majority of these types with $b_J \lesssim 23$ mag were in place by the redshift $z \sim 0.5$, which is the median redshift at this magnitude. There is an indication that models with a little more evolution may better describe the data, but a small type-dependent LF-normalization would also fit the data. From the bright-end to the limit of $b_J \lesssim 23-24$ mag, ellipticals are well fit by $\beta \simeq 1$ or a modest upward LF-normalization of +0.1 dex. Similarly, mid-type spirals are well fit by $\beta \simeq$1–2 or an upward LF-normalization of ∼0.1–0.2 dex for $b_J \lesssim 24$ mag. The CFRS has shown that giant early-mid–type galaxies underwent luminosity evolution with $\beta \simeq$1 since $z \lesssim 1$ (Lilly et al. 1995b), which further supports our suggestion that a significant upward LF-normalization of the early–mid types is not warranted.

As has been noted in the past (Driver et al. 1995a), the late-types are clearly in excess of the no-evolution models over the full flux range shown here. In fact, even the most rapidly evolving model ($\beta = +5$), under-predicts the faint Sd/Irr counts at $b_J \gtrsim 24$ mag. The best model for the total galaxy counts is the sum of this rapid evolution model for the late-types plus the no-evolution models for the earlier types ($\beta = 0$), and is shown in green in the upper left panel of Fig. 8.2. This model follows the observed total counts to the flux level $b_J \lesssim 22 - 23$ mag, fainter than which the

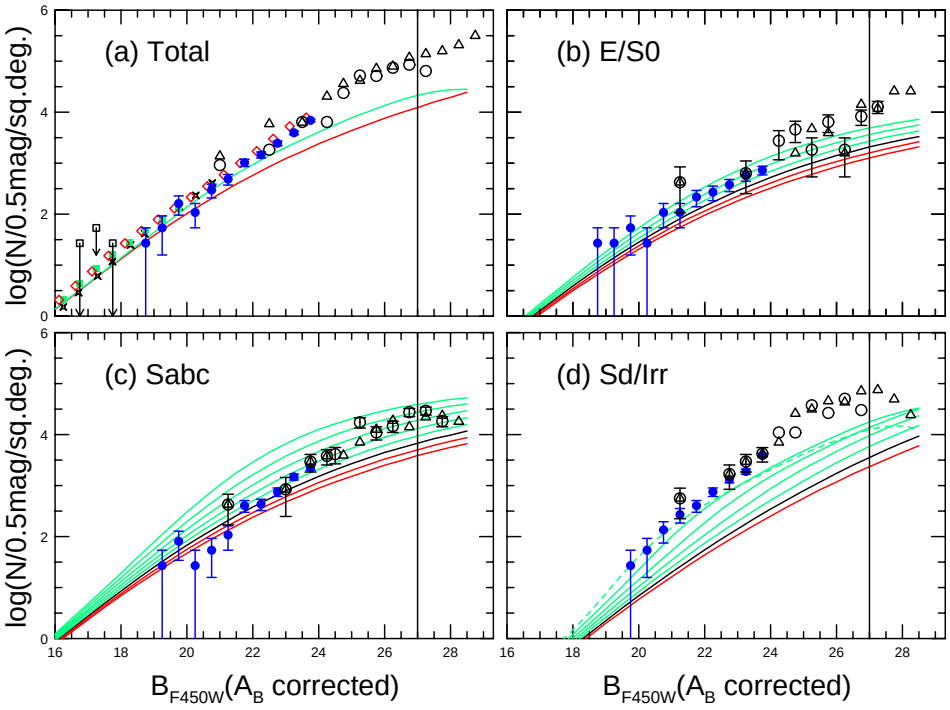

Figure 8.2: Evolutionary models for the differential B–band galaxy counts as a function of morphological type and b_J magnitude. The solid blue points represent the new BBPS data that cover $18 \lesssim b_J \lesssim 24$ mag. All plotted data symbols are the same as in Fig. 8.1. These models use the LF's of Marzke et al. (1998), and assume galaxy evolution in the form of $L \propto (1+z)^{\beta}$. The no-evolution ($\beta = 0$) models are shown as solid black lines, positively evolving models with $\beta = +1, +2, +3, +4, +5$ as green lines, and negatively evolving model with $\beta = -1, -2$ as red lines. In panel (a), the red line is for $\beta = 0$ for all types, and the green line is for $\beta = 0$ for the E/S0 and Sabc galaxies and $\beta = +5$ for the Sd/Irr population. Clearly the Sd/Irr counts in panel (d) are well above any reasonable model for $b_J \gtrsim 23$ mag, and this is causing most of the *excess* of the total counts in panel (a).

late-type irregulars cause the biggest discrepancy. If one wanted to completely fit the *total* galaxy counts with a no-evolution ($\beta = 0$) model, one would have to normalize the late-type LF by a factor of $\approx 4 - 5$, and such a large LF-normalization factor would be difficult to explain in any case as a deficit of galaxies in local surveys or inhomogeneties in local large-scale structure. A combination of luminosity evolution and LF-normalization is also a possibilty to fit the late-type counts over the full flux range presented here, but better statistics for $b_J \lesssim 20$ mag are required for a stronger statement to be made in this regard.

In order to illustrate that the FBG *excess* is dominated by late-types, we consider two extreme cases. First, if one assumes that the zero-evolution, zero-renormalization models are correct, then the excess of the data over the models for $25 \lesssim b_J \lesssim 26$ mag is composed of approximately 95% Sd/Irr's. In the other extreme, where the E/S0's and Sabc's are modeled by zero-evolution, zero-renormalization and the late-types are renormalized a factor of 10 (an upper limit for illustrative purposes), then the FBG excess in the same magnitude range is only slightly reduced to 93% late-types. In other words, assuming that the models and classifications are reasonable, both the faint counts and the FBG excess over the model predictions are dominated by late-types.

One caveat that should be mentioned is that the morphological LF's from the SSRS2 are separated by type (E/S0, Sabcd, Irr/Pec) differently than our data where we place the Sd's in the late-type category. Assuming an upper-limit of Sd galaxies

comprising 25% of all spirals, this would argue for lowering the models for mid-types by this much and raising the late-type models by a similar amount. This is too small an effect to be seen in the current data, but ultimately it is an issue that should be resolved. Another possible explanation for the excess of late-types is that they were somehow excluded from the local surveys, many of which were based on photographic data which have inherent low surface-brightness selection issues. In fact, if one examines the data for the late-type LF (*i.e.*, Marzke et al. 1998), it is seen that there are far fewer of this type of galaxy, relative to the other types, in each luminosity bin. This means that whether the lower SB galaxies exist and were undetected or don't exist at all, the late-type LF is necessarily the least well determined of the three. This potentially could be resolved with a new determination of the local LF's from more modern data such as SDSS and 2dFGRS, although careful attention must be paid to not select against these late-type galaxies which is clearly a difficult problem to avoid.

It is also readily apparent from Fig. 8.2 that none of the models fit beyond $b_J \gtrsim 24$ mag. This probably implies that we are seeing the epochs where galaxy evolution is more dramatic and not well described by our model. Merging and hence number density evolution probably play a major role in this regime and our models are therefore most likely too simplistic. The issue of merging and the effects of the Λ are further discussed in § 9.4.

The new BBPS data shown here make it very clear that the issues of renormaliza-

tion versus evolution cannot be disentangled without a statistical sample of galaxies with morphological types that extend to even brighter magnitudes. The steep slope of the late-type counts at the brighter end ($b_J \lesssim 20$ mag) indicates that filling this portion of parameter space should provide a large step forward in modelling the galaxy counts. Once this is done, different evolutionary scenarios can be modelled and tested. Also, questions of merging and/or morphological evolution should be further investigated, but this requires the redshifts to be known (*cf.* Le Fèvre et al. 1999). Unfortunately, the bright-end of the counts cannot be filled in by HST, because the surface density of bright galaxies is too low to efficiently use the small HST field-of-view. We will show in § 10 that ground based efforts it $b_J = 19 - 20$ mag are limited by atmospheric seeing, but is still plausible with the large CCD surveys that are now being conducted, as long as the best seeing ($FWHM \lesssim 1\farcs0$) images are used.

8.2 The Magnitude–Effective Radius Relation

The apparent effective radii of galaxies in the BBPS are shown in Fig. 8.3 as a function of B-band brightness and ANN type. Plotted is the half-light or effective radius (r_e), averaged over the two pass-bands, versus B-magnitude. This is the radius of the galaxy containing half the light, with no assumption about the shape or type of profile. It is determined from integration of the light-profile. The dark short-dashed lines represent the approximate detection limits for the exposure depths in

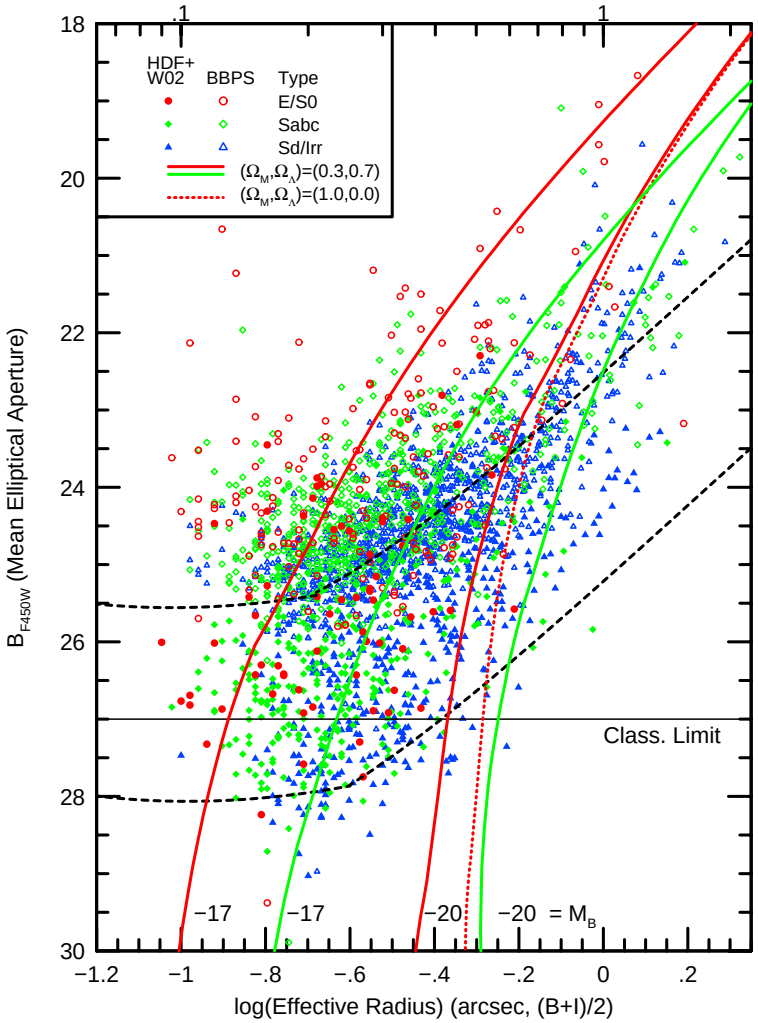

Figure 8.3: B–band magnitude–effective radius relation for galaxies in BBPS and BBDS data sets. The thick dashed lines represent the approximate completeness limits for the deep and shallower surveys as described in the text. The lines that are almost vertical at the faint end from Odewahn et al. (1996) show the expected b_J–r_e relation for redshifted RC3 galaxies of a given absolute magnitude and assumed cosmology, as indicated. Objects below the horizontal line at $b_J = 27$ mag are beyond the reliable classification limit of the BBDS. The scale across the top indicates r_e in arcseconds. The quantity r_e plotted here is the average of the individual effective radii measured from the light profiles in the B and I pass-bands. The r_e values are generally similar between the B and I filters, so yielding a better measure of r_e.

the two surveys. The detection limit for smaller, unresolved objects was modeled as a simple Gaussian source convolved with the SExtractor convolution mask. The limit for the more extended objects was modeled by an exponential disk. The fact that the object detection is based on surface-brightness (*i.e.*, a minimum number of pixels above a specified threshold) makes it readily apparent that bright extended objects could be missed by automatic detection procedures. This is further discussed below. The colored lines that are almost vertical at the faint end give the expectations for a local galaxy of a given absolute magnitude, morphological type and intrinsic effective radius (as determined by a type-dependent relation between absolute magnitude and size from the RC3) that is redshifted back to higher z. These are the same models used in Odewahn et al. (1996), except that here we used the $\Omega_M = 0.3, \Omega_\Lambda = 0.7$ and $H_o = 65$ km/s/Mpc cosmology.

The general trend in Fig. 8.3 is that the brighter objects appear larger, even given the plotted completeness limits. More interestingly is that there are separate, although overlapping, size distributions for the different morphological types. This is shown in more detail in the histograms of Fig. 8.4. It is important to emphasize that size information was not *directly* used in classifying the galaxies. As seen in these histograms, the general trend is that, at a given flux level, E/S0 galaxies are the smallest in size while the Sd/Irr class contains the larger galaxies. The arrows represent the observed medians of the distributions for the BBPS (thin arrow, solid line) and for the BBDS (thick arrows, dashed line). In rows where both data sets

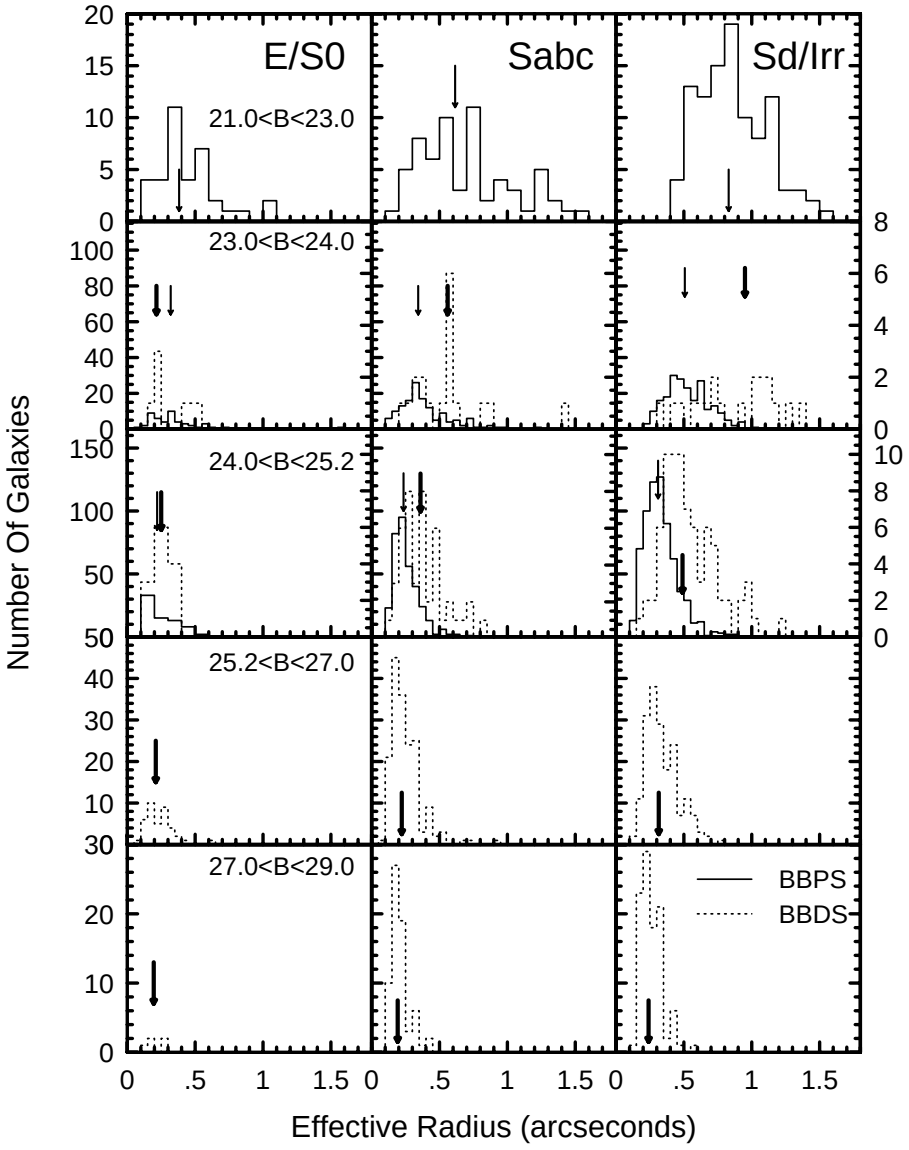

Figure 8.4: Distributions of galaxy sizes as a function of B–band brightness and I–band morphological type. The arrows indicate the median effective radii for the given distributions. The solid histograms and thin arrows are for the BBPS (using the number scale plotted on the left), and the dotted lines and thick arrows are the BBDS (using the scale on the right). In the second and third rows ($23 \lesssim b_J \lesssim 25.2$ mag), the BBDS data has been scaled up by the ratio of the areas of the two data-sets for comparison purposes. The completeness of the histograms as a function of flux and size is discussed in the text.

are shown, the BBDS histograms have been multiplied by the ratio of the areas of the two data sets, while the actual BBDS numbers are shown on the right axes. In all cases, the BBDS medians are (somewhat) larger than the BBPS medians. The fact that the BBDS and BBPS medians do not match in the second and third rows is due to the fact that the detection limit results from the different surface-brightness completeness thresholds in the two types of surveys, which reach rather different depths. The BBPS limit shown in Fig. 8.3 shows that a galaxy with $b_J \approx 24.5$ mag and $r_e \gtrsim 0\farcs8$ would escape detection in the BBPS, but would easily be seen in the BBDS catalogs. Therefore, in rows 2 and 3 of Fig. 8.4, the BBPS median effective radii are *lower* limits, while the BBDS medians are more realistic, but suffer from small number statistics. The bottom two rows of the histograms come from the BBDS alone and suffer from similar SB-selection problems as the BBPS has at brighter levels. In general, the main result is that at a given brightness level, the early-type galaxies appear smaller than the mid-type galaxies which appear smaller than the irregulars, and that fainter galaxies in general appear smaller than brighter ones. All this can be qualitatively seen in Fig. 5 — bearing in mind the respective SB-completeness limits of the different samples — and quantitatively in Fig. 6.

The trend for the two samples is the same to the completeness limit of the BBPS sample ($b_J \lesssim 23.5$ mag). The two BBDS fields are also included because they go deeper (formally $b_J \lesssim 27.5$ mag for 53W002 and $b_J \lesssim 29.0$ mag for HDF–N, see (Odewahn et al. 1996)), and because there are enough galaxies past $b_J \gtrsim 24.5$ mag

to make the comparison. The reason that the BBDS samples in Figs. 5–7 do not appear to go as deep in as they did in Odewahn et al. (1996) is that these deep survey fields were re-analyzed in an identical way to the BBPS, in order to make the optimal comparisons in the flux range where both surveys overlap. This includes the requirement that, because of the limited number of parallel orbits available, an object had to be detected in *both* the B and the I-band filters in order to be declared real. The middle panels ($23 \lesssim b_J \lesssim 25.2$ mag) for the three types clearly show that the larger BBPS objects are missing at this flux level, which is due to the stated surface brightness detection limits. The fact that the medians in the third row for the BBDS are larger than for the BBPS in the second row clearly illustrates that the completeness limit is a function of size as well as brightness, i.e. a surface brightness limit.

This surface brightness limit is very important because galaxy morphology is correlated with surface brightness. The later-types are more extended than the early-types at a given magnitude, and therefore are of lower surface brightness. This would imply that the galaxy counts from the BBPS could be underestimated for the later-types for $b_J \gtrsim 23$ mag. It is not clear whether this is actually the case in the galaxy counts of Fig. 8.1. Although the BBPS counts are slightly lower at this flux level than in the deeper fields, which also have a better SB threshold, the difference is not much larger than what we have seen from field-to-field variations. A careful examination of Fig. 8.3 shows that a small, but not insignificant number of $b_J \lesssim 23.5$ mag lower

surface-brightness (large r_e) galaxies from the deeper fields would be missed in the BBPS due to the different SB-thresholds *and* these are mostly later-typed galaxies. Though only about a 10% effect at $b_J \approx 23.5$ mag, it quickly becomes a larger problem as one goes to fainter fluxes. Therefore, the surface brightness selection criteria, which was implemented by specifying a certain area above a threshold in SExtractor, could cause later-types to be omitted, but that appears to be a minor effect for $b_J \lesssim 23.5$ mag in the BBPS. However, this is an important issue and the surface brightness–morphology correlation must be considered when detecting objects in this manner. Though presented here in the context of our $b_J \gtrsim 19$ mag HST data, this issue is equally important for both past and new local galaxy surveys, which need to be careful not to select against late-type galaxies.

8.3 The Color–Magnitude Diagram

Fig. 8.5 shows the (B–I) color–magnitude diagram for this data. The two BBDS fields were (re-)analyzed in exactly the same way as the 29 BBPS fields to allow optimal comparison. It is important to re-emphasize that the color was *not* an input parameter for the ANN classifier. Colors were measured in matched and registered elliptical apertures whose sizes and shapes were determined from the B-band images. For any given type, there is no tight correlation of color and magnitude that might be expected if one were observing a uniform population at different redshifts, suggesting that we are seeing a scatter which is cosmic in origin.

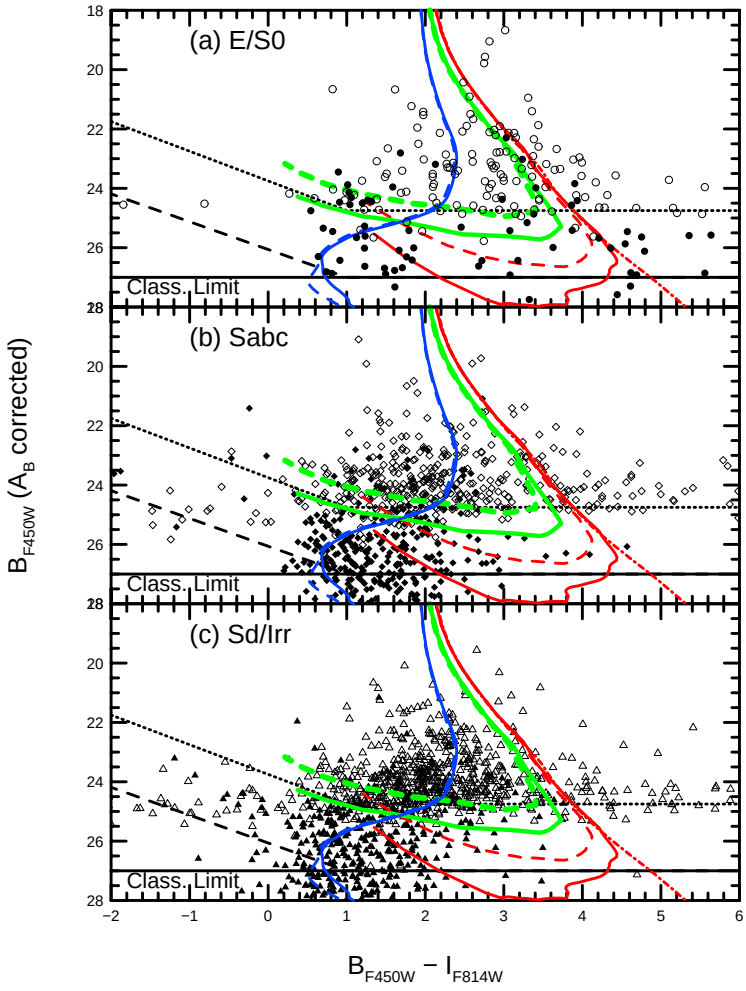

Figure 8.5: The B vs. $(B-I)$ color magnitude diagram as a function of galaxy type. Each of the three different morphological ANN types are plotted in different panels as indicated. Both the two BBDS (solid symbols) and 31 BBPS (open symbols) fields were measured in exactly the same way for consistency. The slanted and horizontal black lines indicate the B–band and I–band 50% detection limits, respectively. The solid black line at $b_J = 27$ mag indicates the I–band classification limit (as limited by the uncertain rest-frame near-UV morphology and S/N considerations). The models are plotted for a $M_B = -20.7$ mag galaxy that is either 14 Gyr old (solid) or 13 Gyr old (dashed). The non-evolving model is plotted as a red dot-dashed line. The red, green and blue lines are meant to be representative of E/S0, Sabc and Sd/Irr galaxies, respectively, although they are not neccessarily unique. More details of the models can be found in the text.

In general, the B vs. $(B-I)$ color–magnitude diagram shows that the reddest galaxies are E/S0's while the bluest ones are Sd/Irr's, with the Sabc's filling in the broad part middle of this range. However, there is also a fraction of red galaxies that are classified as "late-types." These could either be misclassifications, or possibly galaxies with *some* star-formation that is reddened by dust.

There are also some very blue galaxies that have been classified as ellipticals, as also noted by Driver, Windhorst & Griffiths (1995), who used $(V-I)$ colors. This could result from several factors. First, they could be misclassified objects. This is unlikely at brighter flux levels, unless the profile is contaminated by a neighboring galaxy, because ellipticals are so compact, which causes the S/N in the light profile to be rather good. Secondly, some of these, especially the brighter ones, may be misclassified and/or possibly saturated stars. Visual inspection shows this to be unmistakably true only for the few bluest outliers. The third possibility is that some of the "elliptical" galaxies have an additional and significantly younger stellar population. This could be indicative of a burst of recent star-formation, as is seen in Compact Narrow Emission Line Galaxies (CNELGS;*cf.* Koo et al. 1995). A fourth possibility, is that these objects, especially those with a small measured r_e, could have a significant AGN component. Lastly, this could be similar to the recent evidence against the traditional single burst model for star-formation in elliptical galaxies (*cf.* Glazebrook et al. 1998; Jimenez et al. 1999). This would require significant ongoing star-formation (possibly induced by a recent minor merger), while the light-profile of

the product had already sufficiently settled into an $r^{1/4}$-like profile.

To test these conjectures we have adapted the models of Windhorst et al. (1994), which were based on those of Windhorst et al. (1985) and and Kron, Koo & Windhorst (1985), for our filter set and cosmology. In each panel of Fig. 8.5, we have plotted these models for $M_B = -20.7$ mag which is approximately L^* for this cosmology. The solid lines are for ages (*i.e.*, last major epoch of star formation) of 14 Gyr, the dashed lines are for 13 Gyr and the dot-dashed line is a non-evolving model. The red lines are 1-Gyr early-burst or C-models that would represent early forming E/S0's that form all of their stars during the first Gyr after formation begins. The green lines are passively evolving $\mu = 0.7$ models, where 70% of the mass forms into stars in the first Gyr with an exponentially declining SFR and is representative for the mid-type Sabc's. The blue lines are actively evolving $\mu = 0.4$ models, where only 40% of the mass forms into stars in the first Gyr, a reasonable approximation for Sd/Irr's. We plot all models for each morphological type to allow a comparison of the morphologies with star formation histories.

Note that some galaxies appear "redder" than the red/green upper envelope model. Another way to look at this is that they are instead more luminous than the $M_B = -20.7$ mag models plotted. Had one plotted instead the brighter $M_B = -21.7$ mag models, or an even brighter model like $M_B = -22.2$ mag, these objects would also have been represented by these upper-envelope models (*i.e.*, the models would simply shift upward/brighter by -1.0 or -1.5 mag). The same is true for the blue model

representing the late-type objects — they do in general explain the observed blue objects rather well except for the few very blue objects seen at $(B-I) \lesssim 0.0$ mag. Those would generally require later star formation than is present in the $\mu = 0.4$ model, have a weak AGN component and/or possibly have larger photometric errors.

Therefore the observed spread in color present in the data is roughly represented by a reasonable range of plotted models (the C-models through the $\mu = 0.4$ models), except for the very reddest and bluest objects. The former can be explained by assuming $M_B = -21.7$ mag to $M_B = -22.2$ mag, the latter by assuming a more constant star formation scenario (perhaps $\mu = 0.1 - 0.2$).

CHAPTER 9

Discussion

Here we discuss the properties of the three morphological types as seen in the present BBPS data and compare it to other studies. The discussion will focus on the brighter BBPS galaxies, since that is the main subject of the present paper.

9.1 E/S0's

Adding the brighter elliptical counts from the BBPS does not substantially change the conclusion of Odewahn et al. (1996) that these counts can be modeled rather well by the no-evolution predictions for $b_J \lesssim 25$ mag. The new data strengthens this conclusion and also argues against re-normalizing the models of the E/S0 galaxy counts, although there is the hint that these galaxies may be undergoing some evolution at the faint end ($b_J \gtrsim 24$ mag). As discussed in § 5, the issue of evolution of the ellipticals, which in principle should be the simplest to study, is far from settled. It is clear that the high resolution of HST is needed to select a sample of field ellipticals, and that redshifts for all objects are also needed. This was done for 46 galaxies from the CFRS/LDSS (Schade et al. 1999), which showed that field ellipticals are not composed entirely of old stellar populations, but were largely in place since $z \simeq 1$ and therefore support the view of an early formation epoch with occasional, more recent

episodes of star-formation.

Though the reddest galaxies at a given magnitude are generally of early-type, Fig. 8.5 shows that there is a broad range of colors for galaxies of elliptical morphologies. The same conclusion was reached by the CFRS/LDSS, who computed rest-frame $(U-B)$ from the observed $(V-I)$ using the measured redshifts. As previously mentioned, the bluer ellipticals could be similar to the CNELGs (i.e. compact and blue), which are thought to be distant analogs of local HII galaxies as well as progenitors of today's spheroidal galaxies (Koo et al. 1995).

The size distribution in Fig. 8.4 shows the well known fact that the ellipticals are the most compact galaxies of all Hubble types. The average effective radius for $b_J \lesssim 24$ mag is $r_e \simeq 0\farcs35$. It was also shown in Fig. 8.4 that their effective radii increase with brightness.

Overall, these results are somewhat contrary to the view that *all* ellipticals are just old fossil galaxies, which all formed at the same time, whose stellar populations are simply passively evolving or are well understood. While this seems true in the local Universe, the evidence is mounting against old red ellipticals at higher redshift, where there seems to be a larger color scatter for all types than is seen locally at the same rest-frame wavelengths. Even in high redshift cluster studies (e.g. at $z = 0.83$; van Dokkum et al. 2000), there are cluster galaxies with redder colors that are not of elliptical morphology. Therefore, it is dangerously uncertain to use a *single* color for high redshift galaxies as an indicator of morphological type. However,

it may still be possible to determine types by using multiple colors which means that the galaxy spectrum is being sampled in more than two places across the SED, assuming that the spectra of the objects are well understood. Given that there seems to be some discrepancy between the properties of the local and distant elliptical galaxies, a comprehensive comparison of their SED's seems warranted in order to further investigate the situation.

9.2 Sabc's

The counts of the BBPS spirals also do not seem to require a large amount of luminosity evolution nor a renormalization to fit the models based on local LF's. There are far more spirals than ellipticals, but the numbers of mid- and late-types are about the same for a given magnitude. The sizes of the spirals are larger than the early-types and they have a median of $r_e \simeq 0\farcs41$ at $b_J \lesssim 24$ mag. It is important to re-iterate that a comparison of the deeper BBDS sample and the BBPS in a flux range where they overlap shows how the surface-brightness selection biases the sample *against* the larger galaxies at a given magnitude. This is a result of defining the object detection limit as a minimum area above some threshold SB. This is seen in Fig. 8.4, where the higher signal-to-noise BBDS fields have a larger fraction of larger mid- and late-type galaxies than the BBPS for $b_J \gtrsim 23$ mag. Lilly et al. (1998) showed that the distribution of the physical sizes of larger ($\alpha^{-1} > 3.2$ kpc) disk galaxies is roughly constant for $z \lesssim 1$. However, a study of the HDF–N disk galaxy sizes showed

an excess (in relation to a CDM model prediction) of faint ($M_B > -19$ mag) disk galaxies with smaller sizes ($R_d < 2$ kpc) seen from $z \lesssim 3$ even down to $z \sim 0.5$ (Giallongo et al. 2000). It is clear that the issue of size evolution and the growth of disks in spirals is far from settled, and the significant number of BBPS spirals found in the current work will allow further spectroscopic studies to elucidate the physical properties of these objects.

The observed colors of the spirals show a similar distribution to the irregulars. The spiral distribution is also broad, but the median is bluer than that of the early-types — $(B-I)_{med} = 2.8$ mag for E/S0 versus $(B-I)_{med} = 2.1$ mag for Sabc for $b_J \lesssim 24$ mag. This large dispersion in color is likely due to an intrinsic difference in the galaxies, and not entirely to bandpass-shifting. This is apparent in the redshift dependence of the $(B-I)$ color given by Roche et al. (1997), which shows that the dispersion in color expected for a given type is small for $z \lesssim 1$, especially for the later-types. A large dispersion in the rest-frame $(U-V)$ colors was also shown to exist in the disk dominated galaxies of the CFRS/LDSS with only a weak dependence on redshift (Lilly et al. 1998).

9.3 Sd/Irr's

The counts of galaxies beyond $b_J \gtrsim 24.5$ mag are dominated by the later-types. An examination of the counts of the brighter BBPS galaxies shows that somewhat brighter than $b_J \simeq 22$ mag, the counts become dominated by spirals. It will be

very important to carry out this study to even brighter magnitudes ($b_J \lesssim 19$ mag — with HST or from the ground in the best possible seeing) to see exactly where this crossover occurs. This will be very near the region where the count models are normalized ($b_j \approx 18$ mag), which makes it all the more important to understand the LF normalization as a function of galaxy type.

The Sd/Irr's are generally more extended than the spirals and ellipticals and, by definition, have a less regular appearance. At $b_J \lesssim 24$ mag, their median size is $r_e \simeq 0\farcs61$ and the SB selection effect mentioned above is therefore even more important here. The color distribution is very similar to the spirals. In fact, the bright spirals seem very similar to the bright late-types in terms of number counts, colors and sizes. However, given that they are classified differently by the ANN, they have differently shaped azimuthallty averaged light profiles. These Sd/Irr light profiles are similar to those of galaxies that have been visually classified as late-types (i.e. the training set of Odewahn et al. (1996)). The ANN types used here are based on a system that does not have a merger class. Mergers are most effectively studied by combining the high resolution imaging with measured redshifts (Le Fèvre et al. 1999) to rule out chance superpositions of pairs. Hence, without redshift information for all 1800 BBPS galaxies to $b_J = 24.5$ mag, we will defer studies of the pair-fraction and merger rate until spectroscopic or good photometric redshifts become available.

9.4 A Possible Explanation for the Excess of All Types at $b_J \gtrsim 24$ mag

Perhaps our most curious result is that none of our new models fit the observed galaxy counts as a function of type at flux levels fainter than $b_J \gtrsim 24$ mag (Fig. 8.2). This is despite the fact that these models now contain the latest Λ-dominated cosmology and the best available local LF as a function of type. For all galaxies, there appears to be a significant excess for $24 \lesssim b_J \lesssim 27$ mag, which corresponds to a range in median redshift of approximately $z_{med} \simeq 0.5$ to $z_{med} \simeq 1-2$. This excess amounts to up to a factor 3–4 for the early–mid types, and up to a factor of 6–10 for the late types with respect to the local LF plus the best fit luminosity evolution model for $b_J \lesssim 24$ mag (*i.e.*, $\beta = 1$ for early–mid types and $\beta = 5$ for late types). This appears to be a robust result, since the model galaxy counts as a function of type approximately fit the brightest available data points, which are now around $b_J \simeq 19-20$ mag.

In this section we suggest a possible explanation for this, namely that we are witnessing a global and type-dependent excess of galaxies of *all* types at $b_J \gtrsim 24$ mag, where the median redshift is $z_{med} \gtrsim 0.5$ — with a larger excess for the late types — and explore possible physical causes for this excess.

Together with the small galaxy sizes (Figs. 8.3 – 8.4) seen at faint magnitudes, this excess suggests that faint galaxies may be more numerous and smaller at $z \simeq 1-2$

compared to the ones seen today. While the luminous disk galaxies seen at $z \lesssim 1$ have approximately the same size distribution as that seen today (Lilly et al. 1998), this may no longer be true for $z \gtrsim 1$. Hierarchical formation scenarios predict larger numbers of smaller objects in the epoch $z \simeq 1-2$ and beyond. Based on the redshift distribution as a function of morphological type, Driver et al. (1998) suggest that an excess of mid–late type galaxies is seen for $I \gtrsim 23$ mag ($b_J \gtrsim 24.5$ mag), especially in the redshift range $z \simeq 1-2$. They tentatively identified this epoch as the epoch of disk formation. If true, then both the intrinsically smaller disk galaxies at $z \gtrsim 1$, and the temporary end-products of the mergers (*i.e.*, the early-types), as well as the building blocks and mergers-in-progress with temporarily enhanced star-formation (*i.e.*, the late types/irregulars/peculiars) may all be enhanced in numbers past $z \gtrsim 1$, and also be smaller in size and mass.

Galaxy formation may have proceeded such that, in the redshift range $z \simeq 1-2$ and at higher redshifts, *both* the early- *and* mid- *and* late-types were present, but likely in proportions that *slowly* changed with cosmic time, and likely with considerable migration back and forth between galaxy classes. For example, mergers between two spiral disks, or between a spiral and an irregular would eventually result in a bulge dominated galaxy, but since star-formation is known to not be a very efficient process, not all gas would be used up during that merger, nor would that gas necessarily reach escape velocity, so the gas would eventually settle back as a bulge dominated galaxy with a newly re-formed disk (*e.g.*, Hibbard & van Gorkom 1996). Hence, the end-

product of a merger would temporarily be a bulge-dominated galaxy, but it could grow a disk back in the next few gigayears after the merger, and then look like a spiral galaxy until the next (major) merger occurred. Similarly, many luminous irregulars and peculiars may be the temporary stages when observing mergers in action before a system settles as a bulge-dominated or a disk-dominated galaxy (Barnes & Hernquist 1996), although a good fraction of the late types that we see may likely just be the numerous smaller galaxy building blocks from which the hierarchical merging started (Pascarelle et al. 1996). In conclusion, in the hierarchical scenario, there would be considerable migration back and forth between galaxy classes, and galaxies at high redshifts would be smaller and more numerous than those seen locally (Fig. 8.2), consistent with the excess seen for *all* types at $b_J \gtrsim 24$ mag (Fig. 8.2b– 8.2d).

The one remaining issue that begs an explanation is what physical mechanism could explain the larger numbers of *all* types at $b_J \gtrsim 24$ mag, or $z \gtrsim 0.5$–1.0? In hierarchical formation scenarios (Navarro, Frenk & White 1996, etc), bulges form relatively quickly in the epoch $z \simeq 3-5$ and mostly via major mergers. Disks form later in the epoch $z \simeq 1-2$, but more through the gradual (hierarchical) infall gas or minor mergers. These predicted scenarios can be seen in the morphological redshift distributions of Driver et al. (1998). The merger rate was higher in the past by $(1+z)^m$ where $m \simeq 2$–3 (*cf.* Burkey et al. 1994; Neuschaefer et al. 1997; Le Fèvre et al. 1999), but mostly so for $z \gtrsim 0.5$–1.0. For the currently accepted values of $\Omega_m \simeq 0.3$ and $\Lambda \simeq 0.7$, the Λ-driven acceleration starts dominating the expansion of

the Universe for the first time at $z \lesssim 1$. We hypothesize that — as a consequence — the galaxy merger rate gradually winds down in the epoch $z \simeq 0.5-1.0$. For instance, groups of smaller galaxies or sub-galactic units that were nearly virialized at $z \gtrsim 1$ will still virialize for $z \lesssim 1$, but groupings of such objects that were not even close to turn-around at $z \simeq 1$ will be still expanding with the Hubble flow at $z \simeq 0.5$, and probably forever do so in a Λ-dominated universe. At $z \lesssim 0.5$, these late-types would never do much further merging, but just fade away (*cf.* Ferguson & Babul 1998). The end-result is that one observes a slowly evolving Universe consisting of E/S0's and Sabc's for $z \lesssim 0.5$ (or $b_J \lesssim 24$ mag) — as we observe here in Fig. 8.2b – 8.2c — plus the relatively rapid dwindling-away of late-types for $z \lesssim 0.4$–0.5, explaining their steep counts for $b_J \lesssim 24$ mag (Fig. 8.2d). And one would observe a *vast* increase in numbers for all types at $z \gtrsim 0.5$ (or $b_J \gtrsim 24$ mag), and especially at $z \gtrsim 1$ (or $b_J \gtrsim 26$ mag), because most groupings of smaller objects had still plenty time to turn-around from the Hubble flow and overcome the effects of Λ at $z \gtrsim 1$. Since the merger rate was likely much higher at $z \gtrsim 0.5$–1.0 than at $z \sim 0$–0.4 (Le Fèvre et al. 1999), merging proceeded rapidly and successfully for $z \gtrsim 0.5$, and vastly reduced the galaxy numbers with time at $z \simeq 0.5$–1.0, so that larger numbers of *all* types are seen at $z \gtrsim 0.5 - 1.0$, with the largest increase for the late types.

In conclusion, the new BBPS data shown here makes it clear that the issues of LF-normalization versus evolution cannot be disentangled without a statistical sample of galaxies with morphological types that extend to even brighter magnitudes. The steep

slope of the late-type counts at the brighter end ($b_J \lesssim 20$ mag) indicates that filling this portion of parameter space should provide a large step forward in modeling the galaxy counts. Once this is done, different evolutionary scenarios can be modeled and tested. Also, questions of merging and/or morphological evolution should be further investigated with better statistics from larger surveys, with wider dynamic range, and through a systematic assessment of the effects from the uncertain rest-frame UV (Windhorst et al. 2002) on the classifications at the *faintest magnitudes*.

CHAPTER 10

Summary and Future Work

We have presented an HST survey that connects the extremely deep HST studies, such as the HDF–N ($24 \lesssim b_J \lesssim 29$ mag) and existing ground based studies such as the RC3 ($b_J \lesssim 17$ mag). For example, the Stromlo-APM Redshift Survey (Loveday et al. 1996) provided a catalog with morphological types for 1797 galaxies and is complete to $b_j = 17.15$ mag, although there is some question as to the reliability of these catalogs (Pozzetti, Bruzual & Zamorani 1996). Unfortunately, there is a relatively small amount of good morphological data available in the literature for a magnitude range of $17.15 \leq b_J \leq 19$ mag. The bright-end of the galaxy counts cannot be filled in by HST because the surface density of bright galaxies is too low to efficiently use the small HST field-of-view. Our expectation is that this flux range can be addressed from the ground with existing telescopes and larger area detectors in good seeing. The SDSS and other wide angle ground-based CCD surveys should soon provide this data. The key problem with these surveys will be in classifying the fainter ($b_J \gtrsim 19$ mag) galaxies from the ground due to seeing-related effects, since their median r_e values are $\lesssim 1''$ (see Fig. 8.3 here), and rapidly decrease towards fainter fluxes. Hence, the flux range $19 \lesssim b_J \lesssim 24$ mag must be studied with HST, which was the purpose of the current study.

Another important piece of missing information is the redshifts of the BBPS. Since the BBPS galaxies are brighter than $b_J \lesssim 25$ mag, this is a project that can be started on a 4 meter class telescope and finished on an 8–10 meter class telescope. Objects of known redshift (even if estimated through photometric redshifts) can, in principle, be more accurately classified, because one can more effectively correct for the effects of band-pass shifting, mentioned in § 7.5. The BBPS along with measured redshifts can provide a wealth of information when combined with the wealth of HDF–N redshifts which are now measured (Cohen et al. 2000). Given the photometric redshift distributions of Driver et al. (1998) for the HDF–N, it is clear that the majority of the galaxies at $b_J \lesssim 25$ mag studied in this paper are at $z \lesssim 1$. Therefore, in order to classify galaxies observed in the B–band, we need to know what local galaxies look like in the rest-frame U–band or at slightly shorter wavelengths (2500–3000$\mathring{A}$). Relatively recent studies of the near–UV morphology of nearby galaxies show some morphological differences as compared to the B-band (Giavalisco et al. 1996; Burg et al. 1997; Kuchinski et al. 2001; Marcum et al. 2001; Windhorst et al. 2002), but a full quantitative analysis of how this would affect the galaxy counts has yet to be performed. The I-band classifications used in the present paper largely avoid this issue, except for the relatively small number of higher redshift ($z \gtrsim 1.5$) galaxies whose classifications are therefore necessarily uncertain.

The use of artificial neural networks was previously shown to be effective in classifying a large number of galaxies in a quantitative and systematic (*i.e.*, reproducible)

way (Odewahn et al. 1996). This method, based almost solely on the shape of the measured light-profiles, has been applied to our much larger data set at brighter levels. The appeal of this method is that it uses a large number of photometric parameters, and that it is also "trained" based on human classifiers in an effort to categorize the actual appearance in a systematic, albeit non-linear way. Other automated techniques in use today can produce consistent results and provide other useful types of information, while also providing a good consistency check on the method used here. The next logical step is to see if the ANN method can be improved by using some of the 2–dimensional information in the images. The ultimate goal, which no published method to date has achieved for faint galaxies (including the one used in this paper), would be to quantitatively measure the true morphology in an automated way. This would involve distinguishing between more subtle features such as spiral arms, bars and rings, as well as differentiating between, for example, Sa and Sb, and tracing their behavior with redshift (see Odewahn et al. 2002).

In summary, the galaxy counts, size distribution, and $(B-I)$ color distributions seen in the deep HST studies are consistent with what we are now seeing with good statistics for the brighter BBPS galaxies. The *excess* of faint galaxies for $b_J \gtrsim$22–23 mag is dominated by the late-types (*cf.* Driver et al. 1995a; Driver, Windhorst & Griffiths 1995). There are relatively few early-type galaxies at faint magnitudes. Models indicate that either luminosity evolution or an extra dwarf population of late-types is needed to explain the counts of the later types. Redshift surveys suggest the

former, i.e. evolution through episodic starbursts. The new data and new models presented here do not support the need for re-normalizing the total galaxy count models at $b_J \simeq 18$ mag. While not ruling out this need, they show that if this re-normalization is necessary then it *must* be a function of galaxy morphology. Brighter objects appear larger with the broad trend of increasing apparent size as one goes from early to mid- to late-types. This appears to be true over a range of almost 10 magnitudes. There is no sharp size cutoff between types. In general, the early-types are redder, while the later types are bluer with the mid-types in between. Again, there is no simple way to differentiate types based on observed colors, especially with *only two bands*.

From the current study, we provided the first systematic b_J–band counts as a function of galaxy type to address the problem of normalizing the model galaxy counts, which use the known local LF's as a function of morphological type. The galaxy statistics at the bright end ($b_J \lesssim 19$ mag) are still rather poor. At $b_J \approx 18$ mag, the galaxy counts are approximately 100 galaxies per 0.5 mag per square degree. A single WFPC2 field is 0.0013 square degrees, which means that about ten fields are needed to see even one galaxy at random in this magnitude bin. This implies that a few hundred fields would be needed to have adequate bright end statistics. Therefore, larger area detectors are needed. We expect that we can study the magnitude range $16 \lesssim b_J \lesssim 19$ mag from the ground (S. H. Cohen, in preparation), but only in good seeing, as *e.g.*, using images from the NOAO Deep Wide-Field Survey (Jannuzi & Dey

1999), and soon also from the Millenium Galaxy Catalog (Liske et al. 2002), when classifications are added to it. This may be feasible because the effective radii at this magnitude are larger than the seeing disk in good seeing conditions (see § 8.2). The exact magnitude limit to which these classifications can be reliably pushed from the ground is not yet known, but our expectation is to get complete and reliabel classifications to $b_J \lesssim 18 - 19$ mag. This combined data set will provide better statistics at the bright end, which then can be used to more firmly address the normalization problem at $b_J = 18.0$ mag discussed earlier, and determine if the normalization factor is a function of galaxy type.

Some of the requirements to improve upon the interpetation of the faint galaxy counts in order to truly get a handle on issues of galaxy formation and evolution are as follows:

1. Brighter galaxy counts ($16 \lesssim b_J \lesssim 19 - 20$ mag) as a function of morphological type

2. A better handle on the morphological classification accuracy

3. Better statistics throughout

4. CCD-based type-dependent LF's classified using consistent methods

5. Consideration of surface brightness selection effects

6. Measured redshifts and better determined k-corrections

An important point to close on is that we have an incomplete understanding of the local and intermediate distance Universe. Our knowledge and interpretation of the distant high-z Universe will always be limited by this. The advent of bigger and better telescopes brings about the temptation to observe the fainter and more distant objects in the Universe. These studies still need to be complemented by those of more nearby objects, such as that which is presented here, in order to paint the complete picture.

This research was funded by NASA grants GO.5985.01.94A, GO.6609.01.95A, AR.6385.01.95A, & AR.7534.02.96A (to RAW & SCO) from STScI, which is operated by AURA, Inc., under NASA contract NAS5-26555. SHC would like to thank the ASU NASA Space Grant Graduate Fellowship. We also thank the STScI staff, and in particular Doug van Orsow, for their dedicated help in getting these parallel observations scheduled. We also like to thank Drs. J. Bahcall and D. Burstein for making their respective codes available to us. We also thank the anonymous referee for their useful suggestions, especially in regards to the completeness limits. This research has made use of the NASA/IPAC Extragalactic Database (NED) which is operated by the Jet Propulsion Laboratory, California Institute of Technology, under contract with the National Aeronautics and Space Administration.

PART III

On The Normalization Problem of the Faint Galaxy Counts

CHAPTER 11

Overview

We present a study of the b_J-band galaxy counts as a function of morphological type in an effort to fully understand the faint blue galaxy excess and the distribution of Hubble types seen in the deepest HST surveys. Bright ($b_J \lesssim 18$ mag) galaxy counts and classifications are determined from three recent deep and wide field ground-based surveys. These new counts are combined with the best available deeper HST counts ($19 \lesssim b_J \lesssim 27$ mag) and new models in order to study the possible need to renormalize the models at $b_J \approx 18$ mag. The combined data do not suggest that the counts of any of the morphological types need to be renormalized, because the models fit the bright data reasonably well. This result strengthens the conclusions that can be drawn on galaxy evolution. With the models anchored at the bright end, we show that the faintest counts suggest the same amount of evolution for all types ($\beta = 2$), with the Sd/Irr class perhaps requiring slightly stronger luminosity evolution than the earlier types.

CHAPTER 12

Introduction

In a previous paper (Cohen et al. 2003), we extended the deep HST galaxy counts as a function of morphological type from HST to the *brighter end* to cover the flux range $19 \lesssim b_J \lesssim 27$ mag, but concluded that the flux range of the data were still insufficient to vastly improve upon existing evolutionary studies. The most important result was that the models for the late-type (Sd-Irr) galaxies based on the best available local luminosity functions were too low to reproduce our counts, and based on this it appeared that the models, based on local luminosity functions (LF's), would need to be renormalized to fit the data. In fact, the data indicated normalizations for all types could have to be adjusted based on the data available at that time. We point out that resolving this issue is crucial to understand before evolution should be added to the models.

Here we extend the counts even further and study the different evolutionary models over the range $16 \lesssim b_J \lesssim 27$ mag. This new data is combined with new models to suggest that there may not be a "normalization problem," and so in this paper the question of galaxy evolution is discussed in terms of this new realization.

CHAPTER 13

Data

The data in this paper is gathered from many sources. The requirements for this study were galaxies which we could classify from their digital images and a way to measure their B-band magnitudes in order to obtain consistency with the homogeneous *HST* B-band dataset that covers the flux range of $19 \lesssim B \lesssim 27$ mag (Cohen et al. 2003).

13.1 HST data

In order to be as consistent as possible, we have reprocessed the data from the deepest HST fields, the Hubble Deep Field North and the 53W002 field (hereafter HDF–N and W02; Odewahn et al. 1996), in as similar a manner as possible as our more recent B-band Parallel Survey (hereafter BBPS; Cohen et al. 2003). In addition, we have processed the Hubble Deep Field South (HDF–S) in the same way. For comparison, we plot these new counts along with those published in Odewahn et al. (1996) in Fig. 13.1. The shallower HST B-band Parallel Survey data is described in Cohen et al. (2003). These combined HST datasets provided reliable counts as a function of galaxy type for $19 \lesssim b_J \lesssim 26$ mag, and also suggested that extending the bright counts would provide a better assessment of the normalization problem.

All the HST data has been B-band selected and classified with the I-band ANN classifier and processed in exactly the same way as the BBPS (Cohen et al. 2003). The resulting counts are shown in Fig. 13.1. In §14, we decribe how all these HST counts are combined using a weighted average that accounts for the different areas and depths of the various surveys. The BBPS covers $19 \lesssim b_J \lesssim 23-24$ mag, and the three deeper *HST* fields (HDF-N, HDF-S, 53W002) cover $23-24 \lesssim b_J \lesssim 26-27$ mag where the faint limit is due to incompleteness and our rather conservative object selection criteria. We restricted ourselves to 2.5σ detections above the local sky, since lower S/N detections are generally not classifiable. For source detection and photometry, many groups have produced counts that extend fainter than $b_J > 27$ mag (see e.g. Williams et al. 1996; Metcalfe et al. 1996; Odewahn et al. 1996). We also required a minimum number of contiguous pixels to be able to classify the galaxies, depending on whether the images were drizzled or not.

13.2 Ground-Based Data

To complement these HST studies with data at brighter flux levels, we gathered data from publicly available ground-based surveys and processed them in as uniform a manner as possible. These are data from the Millenium Galaxy Catalog (hereafter MGC; Liske et al. 2002), the NOAO Deep Wide Field Survey (NDWFS; Jannuzi & Dey 1999) and the Deep Lens Survey (DLS; Wittman et al. 2002). A list of the individual fields that were available from these three surveys are summarized

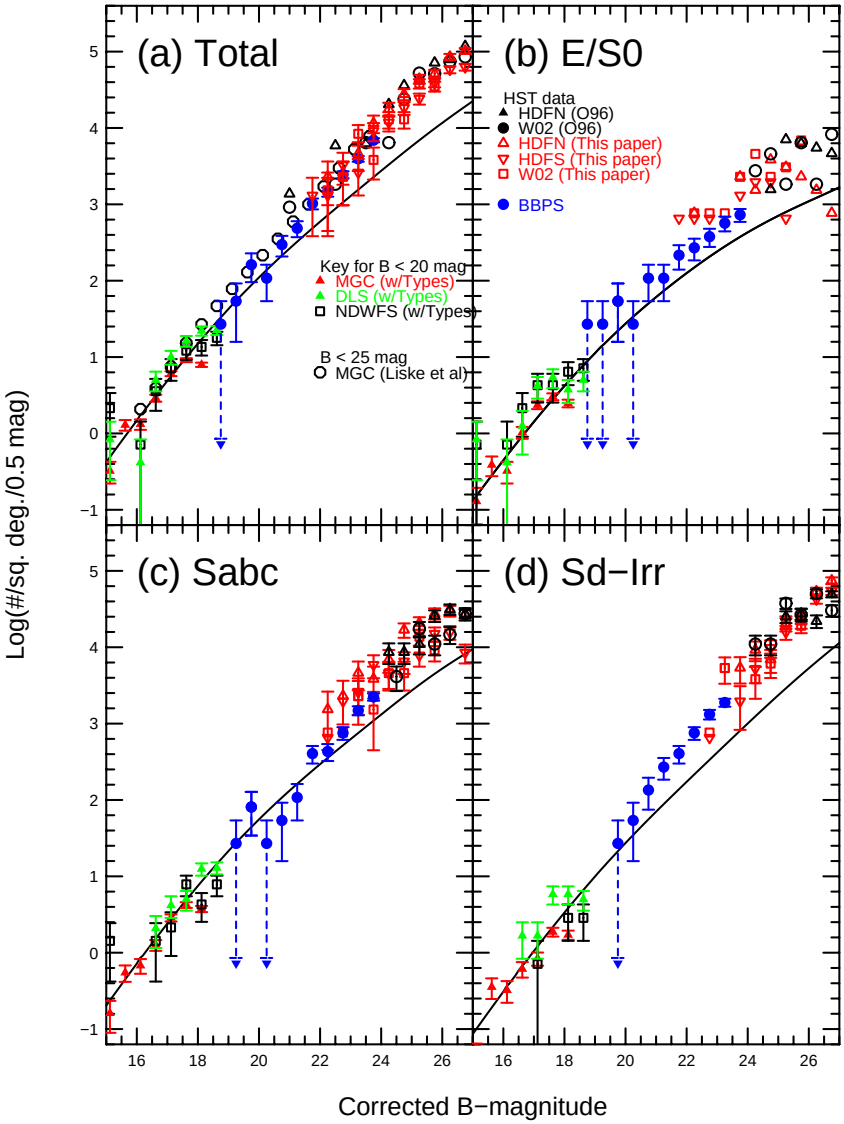

Figure 13.1: The combined galaxy counts as a function of morphological type and b_J-band magnitude for all surveys combined. Error bars are Poissonian. The solid lines are our no–evolution models.

Table 13.1: Ground Based Survey Fields

Field Name	α_{2000} (h m s)	δ_{2000} ($^\circ$ $'$ $''$)	$l^{(II)}$ (deg)	$b^{(II)}$ (deg)	FWHM (arcsec)
DLS_F1p22B	00:53:26.33	+12:33:22.44	123.6964724	−50.3124751	1.3
DLS_F2p11B	09:22:37.08	+30:39:59.74	195.4888782	+44.5646152	1.3
DLS_F2p12B	09:19:32.38	+30:39:59.74	195.3387117	+43.9114612	1.4
DLS_F4p11B	10:54:40.52	−04:19:59.74	256.5975773	+47.7558280	1.2
DLS_F4p21B	10:54:40.62	−04:59:59.74	257.2320898	+47.2452447	1.3
DLS_F4p22B	10:52:02.50	−05:00:11.80	256.4980642	+46.8204177	1.2
DLS_F4p33B	10:49:19.22	−05:39:08.34	256.3606383	+45.8870821	1.3
NDWFS_J1426+3531	14:26:00.80	+35:31:31.65	61.4272895	+68.1987337	1.2
NDWFS_J1426+3456	14:26:01.41	+34:56:31.67	59.9059621	+68.3509961	1.3
NDWFS_J1428+3531	14:28:52.82	+35:31:39.14	61.0142808	+67.6364473	1.5
NDWFS_J1428+3456	14:28:52.20	+34:56:39.10	59.5269775	+67.7850930	1.6
MGC	...	...	...	...	1.3

Note—The MGC data is along a 35 arcminute wide equatorial strip from $9^h58^m28^s$ to $14^h46^m45^s$ and has median seeing FWHM of $1\farcs25$.

in Table 13.1. The MGC covers the most area, while the DLS goes deeper and has slightly better seeing. The NDWFS lies somewhere in between. The three datasets are similar, but also different enough to provide good consistency checks, while covering slightly different regimes of parameter space in terms of seeing and depth. Table 13.2 summarizes the area coverage and reliable classification ranges for the three surveys. Though we refer to the data from these surveys by the official names of the surveys, we processed the calibrated images, measured the fluxes, and classified the galaxies ourselves.

The processing of this ground-based data will be described in a future paper, and here we present the main results for the B-band galaxy counts as a function of type for the flux range $15 \lesssim B \lesssim 27$ mag. For the ground-based data, all classifications are assigned by experienced human classifiers, as opposed to the ANN types used in the HST work. Automated classification of this type of ground-based data is a

Table 13.2: Properties of the Ground Based Surveys

Survey Name	Area (Sq. Deg.)	Range for Classification (b_J mags)
MGC	31.11	15.0–17.0
NDWFS	1.43	16.5–18.0
DLS	2.4	16.0–18.0
BBPS	0.0370	19.0–24.0
W002	0.0012	23.0–26.5
HDF-N	0.0015	23.0–27.0
HDF-S	0.0015	23.0–27.0

difficult problem due to varying seeing and overall image quality. Neural network classifiers that can robustly handle these issues are currently being developed (S. Odewahn, in preparation). All types are assigned on the 16-stage Revised Hubble System from digital images, where the human classifier has the ability to change the greyscale display levels to see as much detail of each galaxy as possible. The ability to classify a galaxy is limited by survey surface-brightness sensitivity and seeing, combined with the apparent size of the galaxy. In other words, it is not strictly a total magnitude limit. To this end, the classifiers agreed to only assign types to galaxies whose structure was clearly decernable. After classifications were assigned, we chose to cut off the counts where the classification fraction dropped below 75%. Therefore, completeness for this ground-based data is limited purely by classifiabilty. In fact, one could create reliable and complete galaxy catalogs for each of these datasets that go several magnitudes deeper than the classification completeness limits presented here. The NDWFS and DLS galaxies were visually classified by three of us (SHC,

SCO, RAW) and each galaxy was assigned a final type which was the mean of the three human classifiers. A comparison of the three classifiers with each other and the mean types showed that they all produced classifications with the expected (e.g. Naim et al. 1995; Odewahn et al. 1996) 1–2 stage RMS scatter. The MGC galaxies were only classified by one of us (SCO).

All magnitudes were converted to the WFPC2 F450W system. As described in Cohen et al. (2003), this Vega-based F450W magnitude is equivalent to the ground-based b_J magnitude. The ground-based data was generally calibrated to the standard Johnson B-band. Once these magnitudes were measured, the DIRBE/$IRAS$ dust maps were used to correct for foreground Galactic extinction (Schlegel, Finkbeiner & Davis 1998). Next, these were converted to b_J magnitudes, which amounts to subtracting 0.13 magnitudes from the standard B-band zeropoints that were distributed with the ground-based data (Liske et al. 2002; Cohen et al. 2003). Galaxy counts were then computed in 0.5 mag wide bins, as in Cohen et al. (2003), and presented in units of number per square degree per 0.5 magnitude. In Fig. 13.1, we present the galaxy counts as a function of type for the combination of the three ground based surveys, the 29 WPFC2 field B-band Parallel Survey, and for the three existing deep HST WFPC2 fields (HDF–N, HDF–S and 53W002). The data for the HDF–N and W02 fields from Odewahn et al. (1996) is also plotted for comparision.

CHAPTER 14

Combining the counts of many datasets

In Fig. 13.1, we show the galaxy counts as a function of type and B-band magnitude. All error bars are simple Poisson $sqrt(N)$ counting errors from the various individual data sets. This plot shows that the faint-end of the ground-based surveys just barely intersect with the bright-end of the HST counts. However, the three surveys agree well with one another, even though they are in different parts of the sky and cover different regimes in terms of seeing, depth and sky-coverage. It is also clear that the deepest HST fields show a large field-to-field variance, especially for the E/S0's. This can be easily understood given the small field of view of $2\farcm5$ ($\simeq 1.2$ Mpc at $z \simeq 0.5 - 3$) for each deep HST WFPC2 field. The issue of the faint E/S0 counts is further considered in § 17.

In order to be able to see the models on the plot and to incorporate this field-to-field variance in the error bars, we opted to combine all the HST data into a single set for each type. For each field, a faint limit is specified which is the completeness limit due to the 2.5σ detection threshold that was imposed due uncertainties in the classifiability of fainter galaxies. In order to deal with the regions where the deep single-field surveys overlap with the shallower multiple-field surveys, we have used

a weighted average, where the survey weights are derived from the total number of objects detected in that magnitude bin from that survey. For each 0.5 magnitude wide bin, the average number of galaxies per square degree, $\langle n \rangle$, is computed from:

$$\langle n \rangle = \frac{\sum_i N_i \sqrt{N_i}}{\sum_i A_i \sqrt{N_i}} \tag{14.1}$$

where N_i is the total number of objects in the given bin from survey i, and A_i is the area of survey i in square degrees.

This also allows for statistical error bars to be computed for the combined averaged counts. Differentiation of Equation 14.1 and a little algebra gives:

$$\Delta n = \frac{\sqrt{\sum_i N_i^2}}{\sum_i A_i \sqrt{N_i}} \tag{14.2}$$

The results are shown in Fig. 14.1, along with the no-evolution models described in § 15, where the error bars for the combined *HST* surveys are now given as the 2.5σ field-to-field uncertainties computed from Equation 14.2.

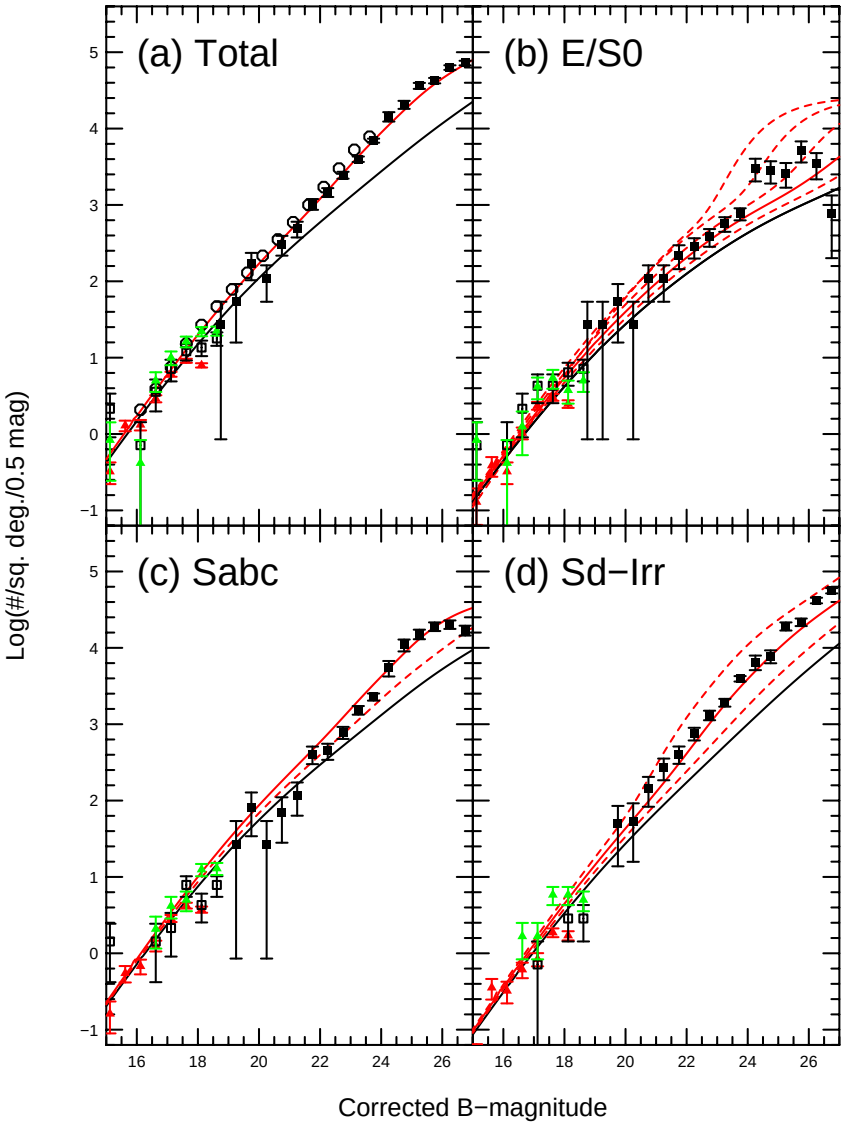

Figure 14.1: The combined galaxy counts as a function of morphological type and b_J-band magnitude with all the HST surveys combined. Error bars are representative of the 2.5σ field to field variance, and the curves are the models described in the text. The solid red lines indicate the best fitting $\beta = 2$ models.

CHAPTER 15

Galaxy Count Models

15.1 Basic Starting Point

The first assumption one needs to make is to adopt a cosmology and, based on the recent WMAP Microwave Background experiments (Spergel et al. 2003), we have chosen to use (H_o, Ω_M, Ω_Λ) = (0.71,0.27,0.73). Strictly speaking, H_o does not effect the models other than for the age of the template spectra used to compute the $k+e$ corrections. Once these numbers are chosen, simple numerical integration is used to compute the luminosity distance as a function of redshift, as well as the differential volume element, dV/dz (Gardner 1998).

Following the equations in Tinsley (1970), Poggiantti (1997) and Gardner (1998), the method involves using some luminosity function (LF; discussed in next section), which describes the number of galaxies per unit volume per unit luminosity in each redshift "shell" dz. In each shell, the product of the LF and dV/dz is evaluated and then these are numerically integrated over all redshift shells, from $z = 0$ to $z = z_F$, where z_F is the assumed galaxy formation redshift. Since luminosity is directly related to absolute magnitude, M, and since M is a function of apparent magnitude, m, and redshift, z, what actually is integrated is the number of galaxies per unit volume from each shell which will have an apparent magnitude of m.

The hidden details are all in how one computes $M(m, z)$, because this involves corrections to the apparent magnitude for both bandpass shifting, $k(z)$, and for the SED age of the galaxy at the redshift in question, $e(z)$. There are two bandpasses to consider here. First is the bandpass that the LF was measured in, which we shall refer to as the rest-frame band. The other bandpass is the one in which one is computing the observed number counts, which we shall refer to as the observed band. It is of the utmost importance to point out that the equations in the above references do not explicitly show that the zeropoints of these two photometric systems must be included in the computation. For example, if one computes an absolute magnitude in the B-band for a given apparent magnitude in the I-band, then $(B - I)$ for the zeropoints of the two bands must be *added* to the result. The formula we used is:

$$M_{rest} = m_{obs} - 5\log(D_L(z)) + 5 + ZP_0 - k(z, type) \tag{15.1}$$

where $D_L(z)$ is the luminosity distance in parsecs, as given by Carrol, Press & Turner (1990) and is a function of $(H_o, \Omega_m, \Omega_\Lambda)$, ZP_0 is the correction for the definition of the photometric systems defined as $ZP_0 = ZP_{rest} - ZP_{obs}$ in our system, and $k(z, type)$ is the k-correction described in the next section.

15.2 Evolutionary and K-corrections

In order to compute these, one has several options to choose which SED's are best suited for the task. For example, Poggiantti (1997) used SED's of various ages

and stellar populations based on their own spectral evolution models. Based on their success in photometric redshift estimates, we have opted to use SED's similar to those of Fernández-Soto, Lanzetta & Yahill (1999). These are a combination of empirical spectra of Coleman, Wu & Weedman (1980) and Kinney et al. (1996). The versions used here were compiled by H. Yan (private communication) for his own photometric redshift work. The definition of the K-correction is:

$$k(z, type) = 2.5 \log(1+z) + 2.5 \log \frac{\int_0^\infty F_{type}(\lambda) T_{rest}(\lambda) d\lambda}{\int_0^\infty F_{type}(\frac{\lambda}{1+z}) T_{obs}(\lambda) d\lambda} \tag{15.2}$$

where $F_{type}(\lambda)$ is the normalized SED of a given morphological type, $T_{rest}(\lambda)$ is the bandpass of the filter in which the LF was determined and $T_{obs}(\lambda)$ is the bandpass of the filter in which you are computing the number counts. Strictly speaking, $T(\lambda)$ should include contributions from all the telescope optics (CCD quantum efficiency, mirror reflectivity, etc), but this is not always done due to the complicated definitions of photometric systems, especially when going back and forth between photographic and CCD systems. The largest assumption in the computation of the k-correction is the choice of SED, because it is clear that distant galaxies of a given morphological type and redshift can have a spread in color (Schade et al. 1999; Cohen et al. 2003), and hence somewhat different SED's. Note that the integral in the denominator in the above equation is computed by integrating the flux of the *redshifted* spectrum through the observed filter. Computationally, though not very intuitively with this conventional notation, this is equivalent to multplying the wavelengths of the SED

by $(1+z)$ and then integrating the product of this shifted spectrum and the observed filter function of interest.

To implement this, we have evaluated Equation 15.2 for our SED's and bandpasses, but then fit two polynomials, $kcorr1(z, type)$ and $kcorr2(z, type)$, to the result for computational purposes. These polynomials have the form $k(z) = \sum_{i=0}^{N} A_i z^i$, and the coefficients, A_i, are tabulated in Table 15.1. These are to convert observed b_J apparent magnitudes to standard B absolute magnitudes. For $z < 1$, we determine $kcorr1(z, type)$, and for $z \geq 1.0$, we determine $kcorr2(z, type)$. The use of two polynomials provided much improved fits which is easily understood as the 4000 Å break passing through the optical bandpasses for $z > 1$. These polynomials are allowed to have any order and are chosen to have the best fit in the chi-squared sense. We also note that the k-corrections are only evaluated out to $z \leq 4.0$, because the templates run out of UV coverage in our optical filters for too high a redshift. These k-corrections computed from Eq. 15.2, as well as the polynomial fits, are shown in Fig. 15.1.

Table 15.1: K-correction Polynomial Coefficients

Order i	E/S0 $z<1$	E/S0 $1\le z\le 4$	Sbc $z<1$	Sbc $1\le z\le 4$	Irr $z<1$	Irr $1\le z\le 4$
0	−3.25478673E−01	−2.10692844E+01	−2.83728957E−03	1.59267693E+01	−2.83104539E−01	5.19813080E+01
1	3.70215774E+00	8.39608994E+01	1.49611616E+00	−1.43661453E+02	−3.66468549E−01	−2.11785568E+02
2	3.34093976E+00	−1.17891190E+02	1.15541811E+01	2.53332016E+02	7.17288733E+00	3.66919342E+02
3	−3.18163147E+01	8.89591751E+01	−8.15189362E+01	−2.47548767E+02	1.54622070E+02	−3.52914764E+02
4	3.18573120E+02	−3.84741364E+01	4.44692810E+02	1.46845734E+02	−2.01278137E+03	2.05975662E+02
−1.43265942E+09	9.52424335E+00	−1.46388501E+03	−5.40337677E+01	1.06600410E+04	-7.46733398E+01	
E+03	−1.25206792E+00	2.77145117E+03	1.20262470E+01	−3.18418125E+04	1.64195728E+01	
E+03	6.76676780E−02	−2.99998340E+03	−1.48000133E+00	5.85230508E+04	-2.00275683E+00	
E+03	···	1.73122009E+03	7.71845505E−02	−6.75750078E+04	1.03847034E−01	
E+02	···	−4.13282379E+02	···	4.78051602E+04	···	
···	···	···	···	−1.89315195E+04	···	
···	···	···	···	3.21171948E+03	···	

The astute reader will notice that the evolutionary correction has been omitted from the previous section. We have opted to not explicity evaluate it based on the SED's, because that would require many templates of different ages and a more complex computation. Instead, we chose to let the LF parameter L^* be a function of redshift in the sense that $L^*(z) = L^*(z=0) \times (1+z)^\beta$, and then compute the models for various values of β. This is similar to the approaches of Brown & Tinsley (1974), Driver, Windhorst & Griffiths (1995), and Driver et al. (1998), who, instead of L^*, allowed the luminosity of a given galaxy to be a function of redshift. In fact, both methods are mathematically equivalent.

15.3 Type-Dependent Luminosity Functions

We have chosen to use the type dependent LF's of the Marzke et al. (1998, hereafter SSRS2) as the best currently available ones. These have been measured in a filter that is equivalent to the B-band and are divided into E/S0's, spirals and irregulars. Our faint number counts are divided slightly differently, based on the ability to classify faint *HST* galaxies, where we have grouped the disk-dominated late-type spirals (Sd's) with the irregulars. Therefore, we must incorporate this difference into our models of the galaxy counts as a function of morphological type.

We need to then estimate what portion of the spiral ($1 \leq T \leq 9$) galaxies to remove from the model number counts that we are matching to our observed Sabc ($1 \leq T \leq 5$) counts. We computed this ratio as 0.23 for the RC3 (de Vaucouleurs et

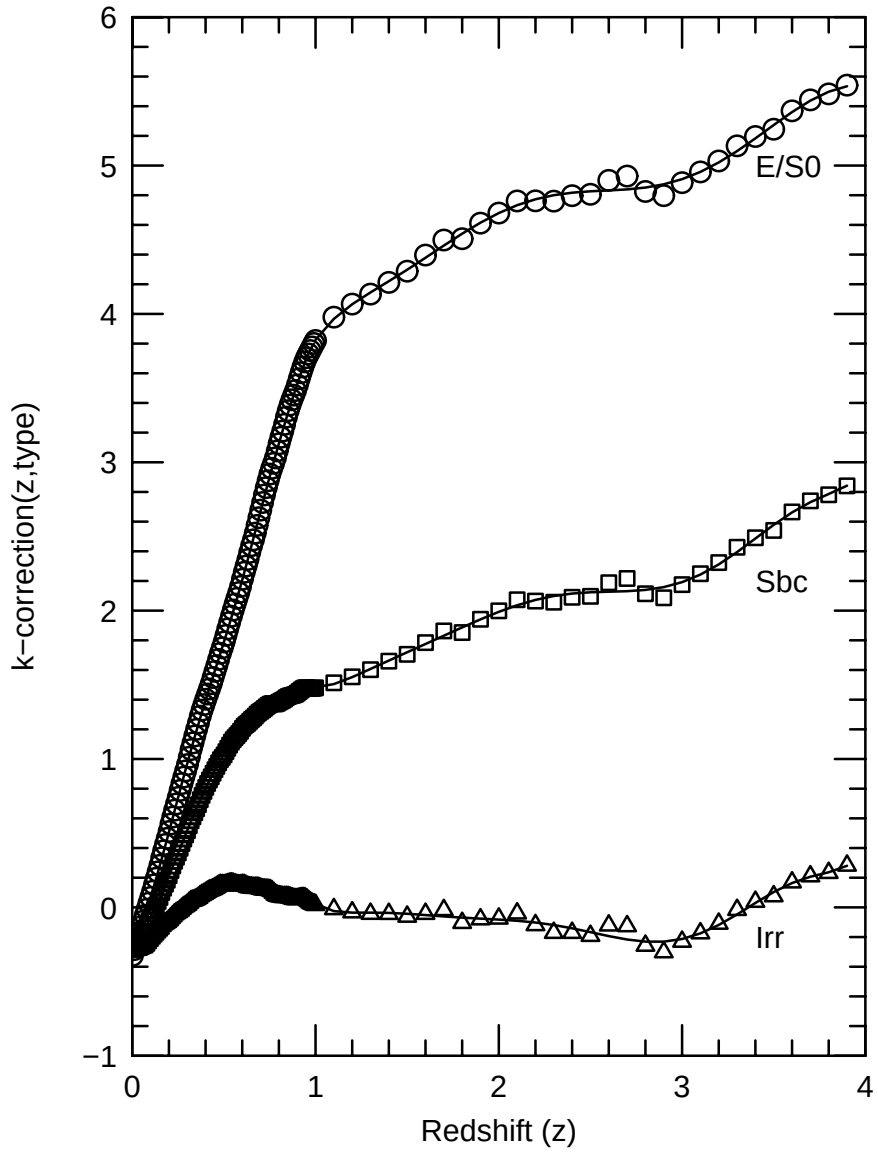

Figure 15.1: K-corrections as a function of redshift for E/S0, Sbc and Irr template SED's. These are computed using Equation 15.2. Also shown are the polynomial fits to these functions, which are evaluated using the coefficients given in Table 15.1. Note that these k-corrections are specific to the bands used in this work, which are to compute B-band absolute magnitudes from observed b_J-band apparent magnitudes.

al. 1991) galaxies with $B \lesssim 15$ mag, 0.235 for the MGC(Liske et al. 2002) galaxies with $B \lesssim 18$ mag, and 0.278 for the Nearby Field Galaxy Survey (NFGS; Jansen et al. 2000), which was selected so as to mimic a volume limited sample of nearby galaxies. It is therefore concluded that 25% of what Marzke et al. (1998) calls spirals belong in our Sd/Irr class, and only 75% of the spirals belong in our Sabc class. Based on these studies, we compute the number counts of E/S0's using the SSRS2 LF for E/S0's directly along with the k-corrections for E/S0's. For Sabc's, we compute the number counts from the SSRS2 spiral LF using the k-correction computed from a typical Sbc galaxy template SED, and then multiply the resulting model number counts by 0.75 in order to get our model for the Sabc's. While this corrects for the total number of galaxies in each class, it implicitly assumes that all spirals ($1 \leq T \leq 9$) share the same shaped LF, *e.g.*, Sa's have the same shaped distribution of luminosity as Sd's. Whether or not this is true is currently unknown, but this is a reasonable starting point, until such a time as a more detailed type-dependent LF can be measured. For our Sd/Irr model (which is technically for Scd-Irr), we compute a model based on the SSRS2 Irr LF, with k-corrections computed using the Irr galaxy spectrum and adding 0.25 times the spiral model

$$N_{Sd/Irr}(m) = N_{Irr}(m) + 0.25 \times N_{spiral}(m) \tag{15.3}$$

This results in model counts for the late-types which provide the proper combination of late-type spirals and irregulars. An alternative approach is to only adjust ϕ^* for

the two types, but this would clearly cause the latest-type model to either improperly represent the brighter galaxies that belong to that class, or if this renormalization is too large, it would mask out the need for evolution to explain the faint counts. The major result of the present method is to increase the number of model predicted galaxies at the bright-end of the late-type model.

CHAPTER 16

Results

16.1 The Bright End: $B \lesssim 18$ mag

Plotting these models over the extensive data here shows some very interesting new results that could never have been seen without combining the HST and ground-based surveys. Ignoring evolution for the moment, it would seem that renormalizing any of the models locally (*i.e.*, at $b_J \simeq 18$ mag) is not required by the data. This is somewhat surprising, given that the HST data alone seemed to indicate this was necessary (Cohen et al. 2003). There are at least three issues that may have helped in getting these models to match up at $b_J \simeq 18$ mag. First, the fact that we justifiably have moved 25% of the spiral counts model over to the late-types is most likely the dominant factor. Inspecting the LF's of Marzke et al. (1998), it is clear that the shape parameters, ϕ^* and α, of the spirals are closely matched to the parameters of the *total* LF for all types. Therefore, moving this fraction of the spirals over to the late-types has increased the bright-end counts, and had a minor impact on the faint-end of the counts. This has all but eliminated the need for renormalizing the late-type models as recently indicated in Cohen et al. (2003).

Also important is the use of a consistent photometric system. We have opted to convert all counts and all models to the b_J Vega system, since this system is closest to

our HST F450W system as descibed in Cohen et al. (2003). All bright-end data was actually taken in Johnson-B, and therefore was converted to b_J as explained in the observations section. Lastly, we also computed our own k-corrections, which allowed the flexibilty to use a LF measured in the B-band and to compute a model in the b_J band. In a future paper, we will show that the same method successfully reproduces the I-band counts which provides us with confidence in the method of computation. The most important result is that we have shown that these models do in fact match up at the bright end, which provides the strongest evidence to date that this method of predicting the faint counts using the observed *local* LF is warranted.

16.2 The Faint End: $B \gtrsim 18$ mag

Now that we can show for the first time that the galaxy counts as a function of morphological types match up with the local LF at the bright end, and that there is no need to renormalize any of the models, we can for the first time, say that the excess of faint blue galaxies is not due to a local hole (or under-density) or galaxies missing in the local surveys due to surface-brightness or other selection effects. It would seem that evolution is the only logical way to explain the faint-end excess of the counts over the levels predicted by the models.

In Fig. 14.1, we show a variety of models with luminosity evolution incorporated by allowing L^* to be a function of redshift. The strongest statement that can be made is that the no-evolution models do reproduce the bright-end counts, but do not

reproduce the faint-end counts. It turns out that given the data and models used here, $\beta = 2$ seems to provide a reasonable model to the faint-end counts of all types. If luminosity evolution is the only factor to consider, then this raises the obvious question of whether it makes sense for all types to evolve in the same way. If galaxy interactions cause morphological type migration, and merging were higher in the past, then one might not expect the same amount of simple luminosity evolution for the three basic types of galaxies studied here, and perhaps some form of number-density evolution (perhaps as a function of morphological type) would also seem appropriate. In fact, the Sabc $\beta = 1$ model seems to fit the data for $B \lesssim 24 - 25$ mag, but the $\beta = 2$ model fits the fainter $B \gtrsim 24 - 25$ mag data. The CFRS (Lilly et al. 1998) found $\beta = 1.4$ for $z < 1$, and since the median redshift for $B \gtrsim 25$ mag is $z \simeq 1.5$, this jump in the observed Sabc number counts could be a sign of an increased merger rate at the higher redshifts.

CHAPTER 17

Discussion

We have presented data that for the first time is able constrain the models of galaxy counts over a broad flux range $15 \lesssim b_J \lesssim 27$ mag by combining the deepest HST studies with our own work on data from three publicly available wide-field ground-based surveys. The most important issue is that we have demonstrated that the type of simple models presented here can, in fact, properly reproduce the counts of bright galaxies of all types. If this bright-end data is representative of the Universe as a whole, then this validates using models of this variety to attempt to further study the morphologies of faint galaxies and their evolution. This nullifies the need to make the ad-hoc renormalization that was cautiously proposed in the past, although it was perfectly understandable based on the data available at the time (Driver, Windhorst & Griffiths 1995; Cohen et al. 2003).

As far as the faint galaxies are concerned, we have shown that our $\beta = 2$ model provides a reasonable, though not perfect, fit to the HST counts as a function of type. We have only considered simple evolution of L^*, though it is highly likely that merging (*i.e.*, number density evolution) played a role in the history of galaxy evolution (see e.g. Cohen et al. 2003). These interactions could presumably affect both the morphological type of a galaxy at a given epoch and therefore also the relative

number of each type. Also, evident from our data is the poor understanding of the observed counts of E/S0 galaxies for $B \gtrsim 24.5$ mag. The large error bars are due to the small number of E/S0's in the small WFPC2 field of view, coupled with the large, apparently cosmic, scatter associated with these small number statistics in only three deep fields. The combination of area and depth utilized by the upcoming *HST GOODS* survey should provide the data to reduce these error bars in the faint E/S0 counts in the flux range of $B \simeq 24 - 26$ mag, once that survey has been completed. The photometric redshifts and extensive spectroscopic follow-up should allow for the redshift and number count distributions to be simultaneously fit, therefore providing the strongest constraints to distant galaxy evolution to date. The *HST* Ultra Deep Field will go 1.5–2 mag fainter than the HDF–N in the I-band, and may well provide important information on the ability to classify faint galaxies, if the deeper images begin to show more of the outer parts of the galaxies that have been hidden by cosmological surface-brightness dimming in even the deepest images to date.

One of the most difficult things in gathering the data for this paper was not object detection, but rather measuring the flux of those objects once they are found via the automatic source detector, SExtractor. An important step in our process was to review the photometry for each object by determining whether the outer isophote that was automatically derived was appropriate for that galaxy. This was a bigger issue with the brighter galaxies (for both the *HST* and ground-based observations), where we often had to set this outer isophote manually. This problem was most prevalent

for the late-type galaxies which are asymmetric and usually "blobby" or irregular. The source of this problem is that it is difficult to set an ideal deblending threshold over a large flux range and any centering algorithm will have trouble with these types of objects, especially if they are clumpy, asymmetric and have low-SB extensions. In other words, without this manual step, we would have underestimated the magnitudes of even the brighter galaxies, though not necessarily in a systematic way. Had a similar problem occured in measuring the fluxes in a redshift survey, this would cause the galaxies (and hence M^*) to be too faint. This would push the models to the right in our plots, an effect which is countered by a potential renormalization upwards for the late-types. One could question if this will be addressed by the next generation CCD based redshift surveys. This would require that both the spectroscopic selection not be biased against low-SB galaxies and that special care be taken to measure their fluxes accurately in the CCD imaging portion of the survey. There is an indication that this will not be fixed up in the SDSS (Nakamura et al. 2003). Nakamura et al. (2003) have provided r^* type-dependent LF's for a sample of visually classified galaxies from the SDSS, however, their fit to the late-type LF is based on only ten galaxies and is far too uncertain to include here. They give the reason for the relatively small number of late-types (10 out of 1500 galaxies) in their sample as a bias against both good photometry and selection for spectroscopic follow-up for low-SB galaxies in the SDSS pipeline. This would seem to restrict the usefulness of using future SDSS data to compute fully type-dependent luminosity functions which could improve upon

the study of the faint galaxy counts as a function of morphological type. Since the late-types dominate the counts on the faintest galaxies, a complete census of their nearby counterparts is needed to fully understand them.

CHAPTER 18

Acknowledgements for Part III

We would like to thank Simon Driver and Joe Liske for sharing their MGC data with us in advance of publication and for initiating the collaboration on the morphological aspects of this data. This research was funded by NASA grants GO.5985.01.94A, GO.6609.01.95A, AR.6385.01.95A, AR.7534.02.96A & AR.9528.01A (to RAW & SCO) from STScI, which is operated by AURA, Inc., under NASA contract NAS5-26555. This work made use of images and/or data products provided by the NOAO Deep Wide-Field Survey (Jannuzi and Dey 1999), which is supported by the National Optical Astronomy Observatory (NOAO). This research also draws upon data provided by Tony Tyson (Deep Lens Survey) as distributed by the NOAO Science Archive. NOAO is operated by AURA, Inc., under a cooperative agreement with the National Science Foundation.

PART IV

Conclusions

CHAPTER 19

Overview

In this final section, a summary of results for the B-band galaxy counts as a function of morphological type is presented. This is followed by a description of the prospects for improving both the models and the data, as well as continuing similar studies in other bands. It is shown that potential improvements in the galaxy count data are on the horizon from recently approved Hubble Space Telescope (*HST*) wide-field surveys (degree scale) complemented by the upcoming *HST/ACS* Ultra-Deep Survey. The prospects of improving the morphologically divided local luminosity functions (LF's) are perhaps not as good, as the SDSS spectroscopic survey is potentially biased against late-type galaxies.

CHAPTER 20

Summary Of Results

A large volume of astronomical data from many different sources has been put together to create the best possible study of the B-band galaxy counts as a function of morphological type over a large dynamic range in flux. The main goal was to provide a foundation to understand the counts of the faintest galaxies that have been observed with the Hubble Space Telescope (HST). In fact, the investigation progressed from analyzing the faintest galaxies for which morphological details have been seen in the Hubble Deep Field North (HDF–N, Williams et al. 1996), to the brighter work in the 30 field HST WFPC2 B-band Parallel Survey (BBPS, Cohen et al. 2003), and finally to studying the morphological distributions of even brighter galaxies that could be observed from the ground. This is the opposite of what is normally done in astronomy, where one is usually trying to push to the faintest limits that the current technology will allow. In this work, the focus has always been to do the "easier" parts correctly to provide a stronger foundation for understanding the more "difficult" measurements.

This work started after it was seen that the galaxies responsible for the faint blue galaxy excess were those of the latest types (Driver et al. 1995a; Driver, Windhorst & Griffiths 1995; Glazebrook et al. 1995; Odewahn et al. 1996). This excess occurs

because the model for the latest types is well below the observed late-type galaxy counts, and this descrepancy was large enough to make the model for the *total* counts fall below the observed counts at the faint end. This raised the question of whether there was a large difference between the Universe nearby ($z \lesssim 0.1-0.2$) and the Universe at high redshift. Is this a strong indication that the latest types are undergoing evolution in their luminosities and/or space density? The fundamental problem in being able to draw this conclusion was that the counts as a function of type had yet to be studied for *brighter* galaxies ($B \lesssim 23-24$ mag). At what flux-level do the counts and models diverge when the morphological information is taken into account? The late-type models appeared to be well below the data at $B = 25$ mag, but is this also true at $B = 18$ mag where the median redshift is $z \lesssim 0.1-0.2$, and hence evolutionary effects should be minor and local large-scale structure should not bias the counts?

In order to answer these questions, the HST B-band Parallel Survey was undertaken. This was the first HST survey to cover many WFPC2 Fields in the B-band to study galaxy morphology. Thirty fields were observed the F450W filter to measure the b_J-band magnitudes, and to select objects in a similar manner to the existing local surveys. Shorter exposure I-band images were also taken in order to provide superior images for galaxy classification (due to both image quality and possible effects from bandpass shifting). These galaxies were all classified using the same artificial neural networks as were developed for the HDF-N (Odewahn et al. 1996). In the end, these observations provided galaxy counts as a function of morphological type over

the range $19 \lesssim b_J \lesssim 24$ mag.

These counts suggested moderate evolution for the E/S0 and Sabc classes, and that the late-type models needed to be multiplied upwards by some factor to get the bright-end predictions to match the available data, and then also still required luminosity evolution to fit the faintest observed counts. This renormalization had been suggested before (Driver, Windhorst & Griffiths 1995), but this was the first data that extended far enough to the bright-end to give the idea some real basis. Applying this factor is effectively saying that these galaxies were not properly or completely included in local surveys, either because they were missed or simply don't exist. Even with the significant areal coverage of the BBPS data, there was still clearly a remaining uncertainty that the counts needed to be extended to even brighter magnitudes, because our HST statistics were poor for $B \lesssim 20$ mag. Extrapolating the BBPS count data, it was concluded that this would be impractical with the small field of view of the HST WFPC2, and that several hundred HST fields would be required to see a statistical sample of $B = 18$ mag galaxies with types in the range of Sd-Irr.

The next idea was to consider if this flux range could be imaged well enough from the ground, where wide-field imagers (*i.e.*, $0.5^\circ - 1.0^\circ$ field of view) are now becoming common. The limiting factor of such ground-based images is obviously atmospheric seeing, which usually limits the spatial resolution to about $0.5 - 1.0$ arcsecond. Based on our measurements, and on an extrapolation of our models of the size distributions

of our HST galaxies, it seemed that it would be possible to do this imaging from the ground, especially with claims of ground-based telescopes getting subarcsecond seeing on a regular basis. The indication from our work was that at $B = 18$ mag, the sizes of galaxies would be on the order of one arcsecond, and so this ground-based imaging was worth pursuing. Some tests were performed on ground-based imaging data that we had from other projects as well. It was concluded that all that was needed was several square degrees of deep ground-based imaging data (to see the outer parts of the galaxies) with decent seeing.

At about the same time, several imaging surveys were being conducted as part of a new National Optical Astronomy Obervatory (NOAO) Survey program, which asked people to propose large survey-type projects under the proviso that these data would be released to the astronomical community on a timely basis and in a useful form to maximize the scientific return. We utilized the data from two of these surveys. The first survey to release their data was 1.5 square degrees from the NOAO Deep Wide Field survey (NDWFS, Jannuzi & Dey 1999), whose stated purpose was a multiwavelength study to select interesting targets for follow-up studies on the recently completed 8-meter Gemini Telescopes. We then found 2.4 square degrees of data suited to our purposes from the Deep Lens Survey (DLS, Wittman et al. 2002). This is also an NOAO survey program, and its central objective is to locate and study weak gravitational lensing signatures to learn more about the mass distribution in the Universe. We were also fortunate to be affiliated with the Millenium Galaxy Catalog

(MGC, Liske et al. 2002), which was designed to be a 30 square degree B-band CCD based galaxy survey that also goes very deep, and has measured redshifts from the 2dF galaxy redshift survey (Colless et al. 2001).

With these three surveys, we were able to measure and visually classify the galaxies that could provide the desired galaxy counts as a function of type at brighter flux levels. The results were galaxy counts that covered the range of $15 \lesssim b_J \lesssim 18$ mag. From all these surveys, galaxies could be measured to much fainter flux levels, but for our purposes, the faint limit is a classification limit due to the sizes of the observed galaxies being about the same as the seeing disk. The data does not quite overlap the flux range of the HST data, but it does at least tend to show similar trends that indicate the the counts would line up nicely if they did. The strongest statement that can be made is that the ground-based and HST data presented here are not inconsistent with eachother.

This new ground-based data provided the impetus to go back and compute new count models. A self-check was made to make sure that all data was on the same photometric system, which was well understood. We chose to convert to the ground-based data to the HST F450W system which is equivalent to the photographic b_J system (Kron 1980) and the b_J CCD system (Tyson 1988). Once this issue was settled, k-corrections were computed using template SED's that had proven quite successful in photometric redshift studies (Fernández-Soto, Lanzetta & Yahill 1999). Using these k-corrections, new galaxy count models were computed with the type-

dependent luminosity functions of Marzke et al. (1998), where careful attention was paid to ensure that the galaxy type ranges were the same for both the models and the data.

This new data and the new models, when combined with the HST data showed some interesting results. The primary one is that no renormalization of any of the models is required. All the models fit reasonably well at the bright end $B \lesssim 18$ mag. Renormalization is not ruled out, but there is no indication from the current data that it is necessary either. It appears that, at these brighter magnitudes, the models predict the observed counts rather well. At the faint end, the observed data is still well above the no-evolution prediction. We used a simple parameterization of luminosity evolution, where we allowed the characterisitic luminosity of the LF, L^*, to be a function of redshift. Our $\beta = 2$ luminosity evolution model seems to fit all types and the total counts reasonably well, although there is still an excess of late-types compared to this model, possibly because merging was not included in the models. The Sabc $\beta = 1$ model seems to fit the data for $B \lesssim 24 - 25$ mag, but the $\beta = 2$ model fits the fainter $B \gtrsim 24 - 25$ mag data. The CFRS (Lilly et al. 1998) found $\beta = 1.4$ for $z < 1$, and since the median redshift for $B \gtrsim 25$ mag is $z \simeq 1.5$, this jump in the observed Sabc number counts could be a sign of an increased merger rate at the higher redshifts. It is also clear that the data in the intermediate flux range needs to be improved. As discussed in the next section, this will require both a several square degree ground-based survey with seeing of $0\farcs5 - 0\farcs8$ FWHM and an

HST survey covering a smaller area, where both have the correct filter selection for the present purpose.

CHAPTER 21

Future Work

21.1 Improving The Models

The first results from the Wilkinson Microwave Anistropy Probe (WMAP, Spergel et al. 2003) have provided the strongest constraints to date on many of the cosmological parameters, two of which, mainly Ω_M and Ω_Λ, are fundamental in modeling the galaxy counts in the manner presented in this work. These parameters, known as the matter density and cosmological constant respectively, define the geometry of the Universe. Also, knowing the age of the Universe, along with the Hubble constant, H_o, allows for the age of the Universe to be known at any given redshift. Another free parameter is the assumed redshift of galaxy formation, z_f. The observation of the nearly complete Gunn-Peterson trough in the spectra of $z \simeq 6.28 - 6.43$ quasars (Fan et al. 2002) demonstrates that the reionization epoch ended at $z \approx 6$, and therefore that the first galaxies must have formed at around this cosmic epoch.

21.1.1 Local Luminosity Functions

In order to determine the type dependent LF's, a large redshift survey is required along with decent images from which we can to both classify and measure the total fluxes of these galaxies. The observing and data processing effort required to produce

the two sets of LF's used in this work (Marzke et al. 1994, 1998) is astounding. A possible problem of these studies was the use of the photographic observations as their finder survey that defined the object catalogs. Photographic data are known to have significant surface-brightness sensitivity, dynamic range and fundamental calibration issues. The fact that they produce reasonable results in the current study is a vindication of the effort that was put into understanding and minimizing these issues. Still, the 0.3 mag RMS uncertainty in the fluxes from these surveys (Marzke et al. 1998) is unsettling, and the need for high quality wide area ground-based CCD based imaging surveys is obvious.

The SDSS (Gunn et al. 1998) is an all-sky CCD survey in five bands, *ugriz*, coupled with spectroscopic measurements for many more galaxies than were possible in the studies discussed above. At first glance, this data seems optimal to determine the optical local LF as a function of type. A first attempt on the preliminary data has been carried out by Nakamura et al. (2003), who use visual classifications and measured SDSS redshifts to compute these quantities. Unfortunately, there is a glaring problem specifically related to the determination of the late-type LF in the SDSS. In their sample of $\approx$ 1500 bright galaxies, only 10 were both of late-type and of sufficient photometric and spectroscopic quality to be included in the LF computation. There are several issues at work here. First is that local late-type galaxies are faint, and therefore possibly systematically omitted from a magnitude limited survey. This is also seen in the steep LF for these late-types (Marzke et al. 1998). A second problem

is that since these objects, by definition, have irregular shapes and are clumpy, they tend to be improperly measured by automated object finding routines. Thirdly, they are the lowest surface-brightness galaxies, which makes their spectroscopic follow up also difficult. In the words of Nakamura et al. (2003), "...the spectroscopic target selection is biased against low surface brightness galaxies..." in the SDSS. In essence, everything about these galaxies causes them to have the strongest (anti-) selection bias. In contrast, these late-type galaxies appear to be the dominant type in the faintest HST studies. Therefore, this selection bias may restrict the usefulness of using the SDSS type-dependent LF's to understand the distant Universe.

The MGC (Liske et al. 2002), whose B-band CCD imaging data was used in our work, also has measured redshifts, because it lies in a region of sky covered by the Two Degree Field Galaxy Redshift Survey (2dFGRS, Colless et al. 2001). In fact, a primary goal of the MGC is to study these type-dependent counts and LF's. The MGC should be less biased against late-type galaxies, because it has both a better surface-brightness threshold and it is complete to about $B \lesssim 24$ mag for direct imaging, which is about 3 mag fainter than the SDSS imaging data. It is also B-band selected, which helps to not exclude late-type galaxies which are generally blue. There are, however, issues for the MGC as well. As with any ground-based survey, the seeing varies from $1\farcs00$ to $1\farcs95$ over the 144 CCD frames that it took to cover $\simeq$ 30 square degrees (Liske et al. 2002). This has presented problems in applying machine based classification algorithms which necessarily depend on the number of

independent resolution elements as discussed in Odewahn et al. (2002). The MGC type-dependent LF has yet to be determined, because we are awaiting an automated classifier which will account for the variable seeing in their 144 data frames (S. Driver, private communication).

21.1.2 Evolutionary and K–Corrections

These corrections require some assumptions about the SED's of the different types of galaxies. We opted to use a single representative SED for each of the three types of galaxies we considered, which were based on observations that had enough UV coverage to be useful. We also chose a simplistic method to parameterize the evolutionary corrections. Now that the cosmological parameters are more or less known from WMAP, the use of synthesized SED's should be reconsidered. These model SED's require the age of the galaxy to be specified, which is important because the evolutionary correction is a function of redshift and hence age (Tinsley 1970). With the cosmology now known, age and redshift can be easily and uniquely related.

Also, much has been learned about both hot and cool stars, and this should be incorporated into the galaxy spectral evolutionary sythesis models. This is especially important for the youngest SED's where hot stars dominate.

Another improvement should be to use intelligent estimates of the range of metallicites, formation redshifts and type-ratios to use the LF's as distribution functions in a Monte-Carlo computation, instead of in the simple model computation used here.

This could also be improved by incorporating a Bayesian approach to determine which combination of input parameters provides the best fit to the data, as well as helping to provide an estimate of the uncertainty in the resulting model parameters.

21.2 Improving The Data

There are several exciting prospects for obtaining more data to help reduce the noise in the number counts. Much of this data will be made readily available in the spirit of archiving and sharing astronomical survey information.

21.2.1 The Bright End

The ground-based data presented here provided strong evidence that the method of using local surveys to understand distant ones can indeed provide useful information. The was especially true for the MGC, which covered the most area, and therefore provided the best statistics. The one missing link is data that would overlap both the MGC and the HST studies. It is clear that what we need is a B-band survey which covers sufficient area (several square degrees) with excellent seeing in the range of $0\farcs4 - 0\farcs8$. This is very possible with the newest wide-field imagers at locations where seeing of this quality can be expected. The prime locations would be Magellan and the MMT, which are both 6.5-meter class telescopes that will have wide-field imagers (FoV$\approx$ 0.5 $\times$ 0.5 deg). Magellan will typically have better seeing than the MMT, and so is a better candidate for this purpose. Performing a survey of this nature in

multiple bands will allow for interesting objects to be selected for future studies, and will help to maximize the scientific usefulness of such a survey.

Also of note is the HST Cosmic Evolution Survey (COSMOS, PI: Scoville, PROPID: 9822), a large HST Legacy Survey that was approved for Cycle 12 in April 2003. This survey will employ the Advanced Camera for Surveys (ACS) and cover about two square degrees with HST exposures in the I-band (F814W) filter. Based on our data and models, this survey has the potential to provide the necessary information of the galaxy counts as a function of morphological type, that should easily bridge the gap between our ground-based and HST surveys. It should also be pointed out that this will be a huge data set, because it will take many ACS exposures to cover this much area. This data will probably will be superior to a ground-based survey, because the resolution will be superior, and the HST data also has the advantage of having a more homogeneous quality than is possible from the ground.

21.2.2 The Faint End

The faint-end of the galaxy counts currently has only three deep fields to date, which provide excellent images for $B \lesssim 27$ mag for object classification. These fields are far from perfect for statistical surveys, as is abundantly clear from the lack of good statistics for the E/S0's for $B \gtrsim 24$ mag. There are two contributing factors to this. First, the models predict a small number of ellipticals per WFPC2 field at these magnitudes compared to other galaxy types, and therefore field-to-field variations will

be most prevalent for this type. The second problem is that these fields are far from randomly selected. The HDF–N was selected to be devoid of bright radio sources (Williams et al. 1996) which biases it against the earlier type galaxies at $z \simeq 1-2$ that would host these sources. The 53W002 field was chosen because it had a weak radio source at $z = 2.4$, named 53W002, as well as a possible cluster or group at that redshift (Pascarelle et al. 1996). Given the relative scarcity of fainter E/S0's, it would be prudent to observe many "deep" fields to get a true statistical understanding of their nature. The question really then becomes how deep does one really need to go to solve this problem?

The amount of valuable HST time required for the HDF's (about ten days worth for the HDF–N Williams et al. (1996)) makes it a costly problem. The current deep HST fields go about two magnitudes deeper than the flux level at which we are able to classify the galaxies. The new imager on HST, the ACS, has a wider field-of-view and better sensitivity, and is about ten times more efficient than WFPC2 for broad-band imaging at the redder wavelengths. There are several projects underway that use this new wide-field HST imaging capability to obtain useful data for our purposes.

The first is the Great Observatories Origins Deep Survey (GOODS, PI: Giavalisco, PROPID: 9425). This is an ambitious project that will provide data from three of NASA's Great Observatories: the HST, the Chandra X-ray Observatory, and the Space Infrared Telescope Facility (SIRTF), as well as many ground-based observatories. The HST portion covers two 10×15 arcminute fields to near-HDF depth in four

optical bands. This is a public survey, and the first complete data release is scheduled for 2003 May 6. This data has the potential to really improve the statistics over the range of $19 \lesssim b_J \lesssim 26 - 27$ mag as far as morphological information is concerned.

Also in the works is the HST Ultra Deep Field (UDF), which will use 410 orbits of HST Director's Time to image a single ACS field (within the GOODS area) to unprecidented depth in 4 filters. Data for this survey will begin being taken in August of 2003, and may continue over the course of two years. It is unclear that this deep data will allow for classifications to be pushed to fainter magnitudes because of the small object sizes and the fundamental limit of the HST sky-background (Cohen et al. 2003). However, the UDF is certainly a worthwhile pursuit, because one never knows what is out there, and there are many other uses of his deep data besides galaxy morphology. Since this data is within the southern GOODS field, it will at least allow a comparison of the measured structural parameters from the 3-5 orbit GOODS data to the > 100 orbit per filter UDF data. The understanding of the way that the improved signal-to-noise ratio affects these measurements is fundamental to improving computer-based galaxy classifications to fainter limits. The next few years will be an exciting time for faint galaxy research, especially with all this new data being made publicly available to the astronomical commmunity on very short time scales.

21.2.3 Comparison To Other Bands

We have studied the counts in the B-band, mainly because this has been the band used historically, dating back to the era of photographic surveys. A study of this type is equally well suited to other passbands, because the k-correction is really the only item that is required to compute the conversion between filters. The major difference between the counts in different bands is that the intrinsic colors of the galaxies cause different selection effects in these different bands. This is manifested in the decreasing slope of the faint counts as one goes to redder bands (e.g., Tyson 1988).

Since all of our HST fields were also observed in the I-band, and since we have used this I-band for more reliable classifications, it should be fairly straightforward to compute galaxy counts as a function of type in the I-band. All the new HST surveys above will also provide I-band data, and so this situation will improve in the very near future. The new ACS z-band (F850LP) also presents exciting potential. This is a band that has not been widely used in the past, and therefore gives the opportunity to study new aspects of distant galaxies. Deep imaging in this band is really only possible with HST, because the Earth's atmosphere has many emission lines in this region, which results in a high background from the ground. This band is also as close to the infrared J-band as one can observe on an "optical" CCD detector before one hits the silicon cut-off at 1.03 microns. A deep understanding of the properties of galaxies in this band will be useful, since the successor to HST, the James Webb

Space Telescope (JWST, formerly known as the Next Generation Space Telescope or NGST), will be primarily an infrared observatory, and knowledge of galaxy properties at this wavelength can help to guide the design specifications of the JWST.

CHAPTER 22

Closing Remarks

This work has made heavy use of public surveys, sponsored both by NOAO and HST/STScI. The idea of making both new and old data publicly available is perhaps one of the most important advances in astronomy. Historically, people obtained their data and waited to share it until they could publish their results, if ever. We used the data from two NOAO Survey programs for investigations that were much different from the intentions of the original proposers. This saved money, and especially time and resources, in that we would have had to go and take the data ourselves and then process it. As time on the 4-meter class telescopes is hard to get, it may have taken years to get enough of it to gather the data we needed.

We have learned that besides making the data itself public (in this case that means calibrated FITS images), it is necessary to have good documentation on the details of the calibrations and reduction methods, along with image quality such as seeing and depth. The fundamental aspects that need to be supplied by the archiver are the photometric filter used, the photometric system it has been calibrated to (where the more details supplied, the better), as well as astrometric information such as images with full World Coordinate System keywords specified in the header. It should also be pointed out that distributing catalogs without the original images has a *limited*

use. We needed the *actual images* because we wanted to measure quantities with our own tools, which could not have been done otherwise. Comparing the distributed catalogs with our own also allows for consistency checks and evaluation of errors, and can even lead to the archival researcher finding errors that the distributor may have missed.

Perhaps the best recent example of sharing has been the HDF–N (Williams et al. 1996). This one field, which was observed with HST Director's Discretionary Time, was made public immediately. This led to almost countless investigations of this single field, and has promoted significant science-driven competition.

Also of interest is the vast increase in the available computational power throughout the course of this work. The computer that this work was started on could not have handled the NOAO survey data. Our WFPC2 stacking routine, *stcombine*, took more than 20 minutes to run on our 166 MHz DEC Alpha in 1996 when the code was developed. Today it will run in $2-3$ minutes on our 1.5 GHz AMD Athlon-based machines. Each of the 11 fields that we used from the two NOAO surveys were from an $8k \times 8k$ pixel CCD camera, and the size of each image file was $300-400$ megabytes. These images needed all of the 1.5 GHz processor and 1.5 gigabytes of memory, as well as a lot of disk space to process, and they pushed this modern computer to its limits.

REFERENCES

Abraham, R. G., van den Bergh, S., Glazebrook, K., Ellis, R. E., Santiago, B. X., Surma, P., & Griffiths, R. E. 1996, ApJS, 107, 1

Abraham, R. G., Tanvir, N. R., Santiago, B. X., Ellis, R. E., Glazebrook, K., & van den Bergh, S. 1996, MNRAS, 279, L47

Abraham, R. G., Ellis, R. S., Fabian, A. C., Tanvir, N. R., & Glazebrook, K. 1999, MNRAS, 303, 641

Babul, A., & Ferguson, H. C. 1996, ApJ, 458, 100

Bahcall, J., & Soneira, R. M. 1981, ApJS, 47, 357

Barnes, J. E., & Hernquist, L. 1996, ApJ, 471, 115

Bazell, D. 2000, MNRAS, 316, 519

Bertin, E., & Arnouts, S. 1996, AJ, 117, 393

Biretta, J. A., et al. 2000, Wide Field Camera 2 Instrument Handbook, Version 5.0 (Baltimore: STScI)

Blanton, M. R., et al. 2001, AJ, 121, 2358

Bouwens, R., Broadhurst, T., & Silk, J. 1998a, ApJ, 506, 557

Bouwens, R., Broadhurst, T., & Silk, J. 1998b, ApJ, 506, 579

Brinchmann, J., et al. 1998, ApJ, 499, 112

Broadhurst, T. J., Ellis, R. S., & Shanks, T. 1988, MNRAS, 235, 827

Brown, G. S., & Tinsley, B. M. 1974, ApJ, 194, 555

Burg, C. A., Windhorst, R. A., Odewahn, S. C., de Jong, R. S., & Frogel, J. A. 1997, in AIP Conf. Proc. 408, The Ultraviolet Universe at Low and High Redshift: Probing the Progress of Galaxy Evolution, ed. W. H. Waller, M. N. Fanelli, J. E. Hollis, & A. C. Danks (New York: AIP Press), 434

Burkey, J. M., Keel, W. C., Windhorst, R. A., & Franklin, B. E. 1994, ApJ, 429, L13

Burstein, D., & Heiles, C. 1982, AJ, 87, 1165

Carrol, S. M., Press, W. H., & Turner, E. L. 1990, ARA&A, 30, 499

Casertano, S., Ratnatunga, K. U., Griffiths, R. E., Im, M., Neuschaefer, L. W., Ostrander, E. J., & Windhorst, R. A. 1995, ApJ, 453, 599

Colless, M., et al. 2001, MNRAS, 328, 1039

Cohen, J. G., Hogg, D. W., Blandford, R., Cowie, L. L., Hu, E., Songaila, A., Shopbell, P., & Richberg, K. 2000, ApJ, 538, 29

Cohen, S. H., Windhorst, R. A., Odewahn, S. C., Chiarenza, C. A.,& Driver, S. P. 2003, AJ, 125, 1762

Coleman, G. D., Wu, C. C., & Weedman, D. W. 1980, ApJS, 43, 393

Davis, M., Huchra, J., Latham, D. W., & Tonry, J. 1982, ApJ, 253, 423

de Lapparent, V., Geller, M. J., & Huchra, J. P. 1986, ApJ, 302, L1

de Vaucouleurs, G. 1959, Handbuch der Physik, 53, 311

de Vaucouleurs, G., de Vaucouleurs, A., Corwin, H. G., Buta, R. J., Paturel, G. Fouque, P. 1991, Third Reference Catalogue of Bright Galaxies (New York:Springer)(RC3)

Driver, S. P. 1999, ApJ, 526, L69

Driver, S. P., Couch, W. J., Phillipps, S., & Windhorst, R. A. 1996, ApJ, 466, L05

Driver, S. P., Fernandez-Soto, A., Couch, W. J., Odewahn, S. C., Windhorst, R. A., Phillips, S., Lanzetta, K., & Yahil, A. 1998, ApJ, 496, L93

Driver, S. P., Windhorst, R. A., Ostrander, E. J., Keel, W. C., Griffiths, R. E., & Ratnatunga, K. U. 1995a, ApJ, 449, L23

Driver, S. P., Windhorst, R. A., & Griffiths, R. E. 1995, ApJ, 453, 48

Ellis, R. E. 1997, ARA&A, 35, 389

Fan, X., Narayanan, V. K., Strauss, M. A., White, R. L., Becker, R. H., Pentericci, L. & Rix, H. 2002, AJ, 123, 1247

Ferguson, H. C., & Babul, A. 1998, MNRAS, 296, 585

Fernández-Soto, A., Lanzetta, K. M., & Yahil, A 1999, ApJ, 513, 34

Flynn, C., Gould, A., & Bahcall, J. N. 1996, ApJ, 466, L55

Gardner, J. P 1998, PASP, 110, 291

Giallongo, E., Menci, N., Poli, F., D'Odorico, S., & Fontana A. 2000, ApJ, 530, 73

Giavalisco, M., Livio, M., Bohlin, R. C., Macchetto, F. D., & Stecher, T. P. 1996, AJ, 112, 369

Glazebrook, K., Ellis, R. E., Santiago, B., & Griffiths, R. E. 1995, MNRAS, 275, L19

Glazebrook, K., Abraham, R. G., Santiago, B., Ellis, R. E., & Griffiths, R. E. 1998, MNRAS, 297, 885

Gunn, J. E., et al. 1998, AJ, 116, 3040

Harris, W. E. 1986, AJ, 91, 822

He, P., & Zhang, Y.-Z. 1998, ApJ, 511, 574

Hibbard, J. E., & van Gorkom, J. H. 1996, AJ, 111, 655

Holtzman, J. A., Burrows, C. J., Casertano, S., Hester, J. J., Trauger, J. T., Watson, A. M., & Worthey, G. 1995, PASP, 107, 1065

Hubble, E. P. 1922, ApJ, 56, 162

Hubble, E. P. 1936, The Realm Of The Nebulae (New Haven: Yale University Press)

Im, M., Griffiths, R. E., Ratnatunga, K. U., & Sarajedini, V. L. 1996, ApJ, 461, L79

Im, M., Griffiths, R. E., Naim, A., Ratnatunga, K. U., Roche, N., Green, R. F., & Sarajedini, V. L. 1999, ApJ, 510, 82

Jannuzi, B. T., & Dey, A. 1999, in ASP Conf. Ser. 191, Photometric Redshifts and the Detection of High Redshift Galaxies, ed. R. Weymann, L. Storrie-Lombardi, M. Sawicki, & R. Brunner (San Francisco: ASP), 111

Jansen, R. A., Franx, M., Fabricant, D., & Caldwell, N. 2000, ApJS, 126, 271

Jimenez, R., Friaca, A. C. S., Dunlop, J. S., Terlevich, R. J., Peacock, J. A., & Nolan, L. A. 1999, MNRAS, 305, L16

Kauffmann, G., Charlot, S., & White, S. D. M. 1996, MNRAS, 283, L117

Kinney, A. L., Calzetti, D., Bohlin, R. C., McQuade, K., Storchi-Bergmann, T., & Schmitt, H. R. 1996, ApJ, 467, 38

Koo, D. C., Guzmán, R., Faber, S. M., Illingworth, G. D., Bershady, M. A., Kron, R. G., & Takamiya, M. 1995, ApJ, 440, L49

Koo, D. C., & Kron, R. G. 1992, ARA&A, 30, 613

Kron, R. G. 1980, ApJS, 43, 305

Kron, R.G., Koo, D. C. & Windhorst, R. A. 1985, å, 146, 38

Kuchinski, L. E., et al. 2000, ApJS, 131, 441

Landsman, W. B. 2003, in ASP Conf. Ser. 52, Astronomical Data Analysis Software and Systems II, ed. R. J. Hanisch, R. J. V. Brissenden, & J. Barnes (San Francisco: ASP), 246

Le Fèvre, O., et al. 2000, MNRAS, 311, 565

Lilly, S. J., Le Fèvre, O., Crampton, D., Hammer, F., & Tresse, L. 1995a, ApJ, 455, 50

Lilly, S. J., Tresse, L., Hammer, F., Crampton, D., & Le Fèvre, O. 1995b, ApJ, 455, 108

Lilly, S. J., et al. 1998, ApJ, 500, 75

Liske, J., Lemon, D. J., Driver, S. P., Cross, N. J. G., & Couch, W. J. 2002, preprint (astro-ph/0207555)

Loveday, J., Peterson, B. A., Efstathiou, G., & Maddox, S. J. 1992, ApJ, 390, 338

Loveday, J., Peterson, B. A., Maddox, S. J., & Efstathiou, G. 1996, ApJS, 107, 201

Maddox, S. J., Sutherland, W. J., Efstathiou, G., Loveday, J., & Peterson, B. A. 1990, MNRAS, 247, 1

Marcum, P. M., et al. 2001, ApJS, 132,129

Marleau, F. R., & Simard, L. 1998, ApJ, 507, 600

Marzke, R. O., Geller, M. J., Huchra, J. P., & Corwin, H. G. 1994, AJ, 108, 437

Marzke, R. O., Da Costa, L. N., Pellegrini, P. S., Willmer, C. N. A. & Geller, M. J. 1998, AJ, 503, 617

Méndez, R. A., & Guzmán, R. 1998, A&A, 333, 106

Metcalfe, N., Fong, R., Shanks, T. 1995, MNRAS, 274, 769

Metcalfe, N., Shanks, T., Campos, A., Fong, R, & Gardner, J. P. 1996, Nature, 383, 236

Naim, A., et al. 1995, MNRAS, 274, 1107

Neuschaefer, L. W., Im, M., Ratnatunga, K. U., Griffiths, R. E., & Casertano, S. 1997, ApJ, 480, 59

Nakamura, O. et al. 2003, AJ, 125, 1682

Neuschaefer, L. W., & Windhorst, R. A. 1995, ApJS, 96, 371

Navarro, J. F., Frenk, C. S., & White, S. D. M. 1996, MNRAS, 275, 56

Odewahn, S. C. 1995, PASP, 107, 770

Odewahn, S. C., Windhorst, R. A., Driver, S. P., & Keel, W. C. 1996, ApJ, 472, L13

Odewahn, S. C., Burstein, D., & Windhorst, R. A. 1997, AJ, 114, 2219

Odewahn, S. C. 1997, Annals of the New York Academy of Sciences, v. 808, pg. 184, "Nonlinear Signal and Image Analysis," eds. J. R. Buchler, & H. Kandrup

Odewahn, S. C., Cohen, S. H., Windhorst, R. A., & Philip, N. S. 2002, ApJ, 568, 539

Pascarelle, S. M., Windhorst, R. A., Keel, W. C., & Odewahn, S. C. 1996, Nature, 383, 45

Pascarelle, S. M., Windhorst, R. A., & Keel, W. C. 1998, AJ, 116, 2659

Poggiantti, B. M. 1997, A&AS, 122, 399

Pozzetti, L., Bruzual, A. G., & Zamorani, G. 1996, MNRAS, 281, 953

Ratnatunga, K. U., Griffiths, R. E., & Ostrander, E. J. 1999, AJ, 118, 86

Roberts, M. S., & Haynes, M. 1994, ARA&A, 32, 115

Roche, N., Ratnatunga, K., Griffiths, R. E., Im, M., & Neuschaefer, L. 1996, MNRAS, 282, 1247

Roche, N., Ratnatunga, K., Griffiths, R. E., & Im, M. 1997, MNRAS, 288, 220

Schade, D., et al. 1999, ApJ, 525, 31

Schlegel, D. J., Finkbeiner, D. P., & Davis, M. 1998, ApJ, 500, 525

Schmidtke, P. C., Windhorst, R. A., Mutz, S. B., Pascarelle, S. M., & Franklin, B. E. 1997, AJ, 113, 569

Spergel, D. N., et al. 2003, preprint (astro-ph/0302209)

Tinsley, B. M. 1974, Ap&SS, 6, 344

Tyson, J. A. 1988, AJ, 96,1

Valdes, F. 1982, Proc. SPIE, 331, 465

van den Bergh, S., Abraham, R. G., Ellis, R. E., Tanvir, N. R., Santiago, B. X., & Glazebrook, K. 1996, AJ, 112, 359

van Dokkum, P. G., Franx, M., Fabricant, D., Illingworth, G. D., & Kelson, D. D. 2000, ApJ, 541, 95

Williams, R. E., et al. 1996, AJ, 112, 1335

Windhorst, R. A., Franklin, B. E., & Neuschaefer, L. W. 1994, PASP, 106, 798

Windhorst, R. A., van Heerde, G. M., & Katgert, P. 1984, A&AS, 58, 1

Windhorst, R. A., Miley, G. K., Owen, F. N., Kron, R. G., & Koo, D. C. 1985, ApJ, 289, 494

Windhorst, R. A., Gordon, J. M., Pascarelle, S. M., Schmidtke, P. C., Keel, W. C., Burkey, J. M., & Dunlop, J. S. 1994, ApJ, 435, 577

Windhorst, R. A., Keel, W. C., & Pascarelle, S. M. 1998, ApJ, 494, L27

Windhorst, R. A., et al. 2002, ApJS, 143, 113

Wittman, D., et al. 2002, preprint (astro-ph/0210118)

Yasuda, N., et al. 2001, AJ, 122, 1104

Yee, H. K. C., Ellingson, E., & Carlberg, R. G. 1996, ApJS, 102, 269

Yee, H. K. C., et al. 2000, ApJS, 129, 475

Zucca, E., et al. 1997, A&A, 326, 477